

LOW TEMPERATURE ALKANE ACTIVATION OVER ZEOLITES

Johannis A.Z. Pieterse

Leden van de promotiecommissie:

Voorzitter/Secretaris:	Prof.dr. W.E. van der Linden (Universiteit Twente)
Promotor:	Prof.dr. J.A. Lercher (Technische Universiteit München)
Asistent promotor:	Dr. K. Seshan (Universiteit Twente)
Leden:	Prof.dr. J.A. Moulijn (Technische Universiteit Delft) Prof. dr. K. P. de Jong (Universiteit Utrecht) Prof.dr.ir. W. Briels (Universiteit Twente) Prof.dr.ir. L. Lefferts (Universiteit Twente)
Deskundige:	Dr. M.J.G. Janssen (Exxon Chemical)

This work was performed under auspices of NIOK, the Netherlands Institute for Catalysis Research and PIT, Process technology Institute Twente.

This publication has been supported financially by

SON (Dutch Foundation for Chemical Research)

NWO (Dutch Organization for Scientific Research)

ISBN 90-365-1408-8

© Johannis A.Z. Pieterse, Enschede, The Netherlands

Printed by Print Partners Ipskamp, Enschede, The Netherlands

LOW TEMPERATURE ALKANE ACTIVATION OVER ZEOLITES

PROEFSCHRIFT

ter verkrijging van
de graad van doctor aan de Universiteit Twente,
op gezag van de rector magnificus,
prof.dr. F.A. van Vught,
volgens het besluit van het College voor Promoties
in het openbaar te verdedigen
op donderdag 13 januari 2000 te 15:00 uur.

door
Johannis Alouisius Zacharias Pieterse
geboren op 7 februari 1970
te Oostflakkee

Dit proefschrift is goedgekeurd door de promotor
prof.dr. J.A. Lercher en de assistent promotor Dr. K. Seshan.

To the memories of my mother Elizabeth

Acknowledgment

As this section of this thesis will be for many of you by far the most popular one, I will give it some depth. The very first day I got off at the bus stop in the not-too-appealing-far-east-located place called Enschede, I hesitatingly wandered to the CT building. Being horrified by the view of the buildings dark and sinister outlook, I desperately sought for the answer whether this really could be just fine for the next 4 years. The answer is that it was very fine. Some tough periods were rather associated with the complexity of the work than with the city it self or with the social life at and around the university. With respect to the latter I mostly enjoyed the diversity of people of different nationality. These people offered me an unique opportunity to put a glimpse on their culture and general customs and habits. My conclusion is that for some of them the Dutch efficiency may not always be reached, they certainly may take the lead what comes to spontaneity and humanity though. After 4 years I am very happy to conclude that these people played an important role in my life. To thank a few of them, Gerhard for your encouragement to leave half of our monthly salary to cafe de Geus in our first years and for lots of other social activities, as well as nice (pseudo-) scientific conversations, Edu and Cristobal for some great vacation time and for polluting my mail box with senseless, enjoyable email though, Axel and Saskia & Victor and Sheila for their valuable therapeutical skills and the Volkskrant, Juri for thorough smoke-invoked disinfection of our mutual residence, Gautam for pointing out that you can always do more, László D. for the solid bass tunes either form his guitar or late night laundry, Marco for 'in-depth' discussions, Fiona, the TWAIO board, the OR and the (kl)ioio's of CT for their support during a crusade, held in behalf of the OIO's fringe benefits, Laurent for a nice and educational EXAFS trip to the USA although the tradition to wake up at 2 am was easily sworn off, Sergio for his gorgeous smile, for Santana during the Battle of Utrecht and lots of other music, Toshi for a very interesting share of the same front door, Martijn for reminding me my scientific roots in Leiden, Jenô for his crazy purchases and funny complaints and László L. for proving that this attitude should not be simply extrapolated to the whole Rumanian civilization, Yingjie for reproducing outstanding sulfur induced isomerization activity and mirroring my own sulfur induced paleness, Florian for hands-on training on the tricky balance, Harry and Andre for carrying on the solution for numerous of my 'green' problems, Bert for his ready-for-action help with lots of experimental issues, Karin and Vilmos for kind assistance with the inevitable laboratory work, Cis for help with the administration and cheer-up smiles, the ladies Edyta, Itziar, Peppi and Montse for remembering me my own student time, the people in Munchen for their kind welcome during my stays at TUM, in Utrecht, senôr Bok for his lively presence at nearly any of the congresses I ever attended (and his detailed review on the ones I did not attend) and, as a consequence of the congress late-night discussions, our fruitful collaboration in the last months of this PhD work, Patricia (Kooyman) for critical reviewing chapter 6 and lots of HREM work. Dear colleagues and friends, I thank you very much for this unforgettable period.

I would like to thank my promotor, Prof. dr. J.A. Lercher for offering me to work on this intriguing project and for his insights and sharp criticism, which definitely added very much to the work. Johannes, your efforts to change my suicidal skiing technique are also highly appreciated.

I thank Dr. K. Seshan for discussions, his valuable calmness in hectic periods and for putting me up with milestones which certainly helped me finishing off in time.

I also owe thanks to SON, NWO and the KNCV for financial support enabling me to present my work on (inter)national conferences.

Jan, Wil en Francien, hartelijk bedankt voor jullie geweldige steun en geduld door de jaren heen. Arja, dank je wel voor een geweldige tijd ook buiten de universiteit (Mina rakastan sinua soma naiseni!).

*Jean-Pierre,
December 1999*

Table of Contents

1.	Introduction.....	1
2.	Experimental.....	19
3.	An IR spectroscopic and isotope tracer study of site-controlled H/D exchange over zeolites MFI and BEA.....	29
4.	On the role of adsorption effects for the enhanced activity of dealuminated mordenite catalysts in the conversion of Light Alkanes.....	47
5.	Improving the stability of H-Mordenite for <i>n</i> -butane isomerization.....	73
6.	Sulfur tolerant catalysts based on mordenite for the hydroisomerization of <i>n</i> -butane.....	91
7.	Sorption and ordering of dibranched alkanes on medium pore zeolites Ferrierite and TON.....	111
8.	Structure-activity correlations for TON, FER and MOR in the hydroisomerization of <i>n</i> -butane.....	129
9.	Summary/Samenvatting.....	151

Introduction

General Introduction

The development of new and effective refining processes aims at meeting the increasing demands for fuels. Crucial for the improvement of yield and selectivities is the development of a thorough understanding of the physical and chemical processes underlying the catalytic reactions. As a result, substantial progress in the understanding of sorption and activation of alkanes was seen over the last years. This is related to new theoretical and experimental tools becoming available leading to a more quantitative description of the elementary steps in the ordering of alkanes in molecular sieves and their chemical interaction with the acid site. Nevertheless, general consensus regarding the specific mechanistic details is not yet reached. Also, owing to the structural complexity and diversity of molecular sieves (zeolites) a significant incentive exist to develop structure-activity relations that could lead to understanding on structure decisive alkane activation.

The work presented in this thesis is part of a larger effort to obtain knowledge on alkane activation and reaction over zeolites, especially concerning the processes at low temperatures (< 773 K). Research was dedicated to bottlenecks in literature and specific demands of the refinery industry, in particular on isomerization processes dedicated to the production of methyl *tert*-butyl ether (in 1998 the world demand for MTBE was estimated to be $1.2 \cdot 10^7$ t/y [1]). In this introductory chapter, some issues in hydrocarbon processing, e.g. alkane sorption, activation and reactions in relation to zeolite molecular sieves is reviewed.

1.1 Hydrocarbon processing

Hydrocarbon refining aims at the most effective exploitation of crude oil with respect to the requirements for engine fuels and petrochemistry [2]. A large variety of chemical processes bases on the products formed in crude oil refining processes.

Crude oil consists of a large diversity of hydrocarbons, including aliphatic, alicyclic and aromatic compounds as well as hetero-compounds (containing predominantly sulfur but also nitrogen and oxygen [3]). The heterogeneity of the feedstock requires separation and upgrading. The major (upgrading) refining processes are cracking, reforming, isomerization and alkylation. Hydrocarbon cracking, i.e. carbon-carbon bond cleavage, reduces the size of large hydrocarbon

molecules and thus, makes fractionation of residues for engine fuels. Reforming converts gasoline-range molecules without changing their carbon numbers. It branches side chains and aromatizes the feed. Alkylation is the reaction of alkanes with olefines, one of the most promising (recycle) routes for the manufacture of high octane gasoline.

Paraffin isomerization branches the chains of linear hydrocarbons. Beside aromatization the latter process enhances the octane number. Due to the introduction of the Clean Air Act Amendments of 1990 in the USA and similar legislation in other countries oxygenates (e.g. MTBE, TAME) are currently favoured as octane boosters for engine fuels in order to replace

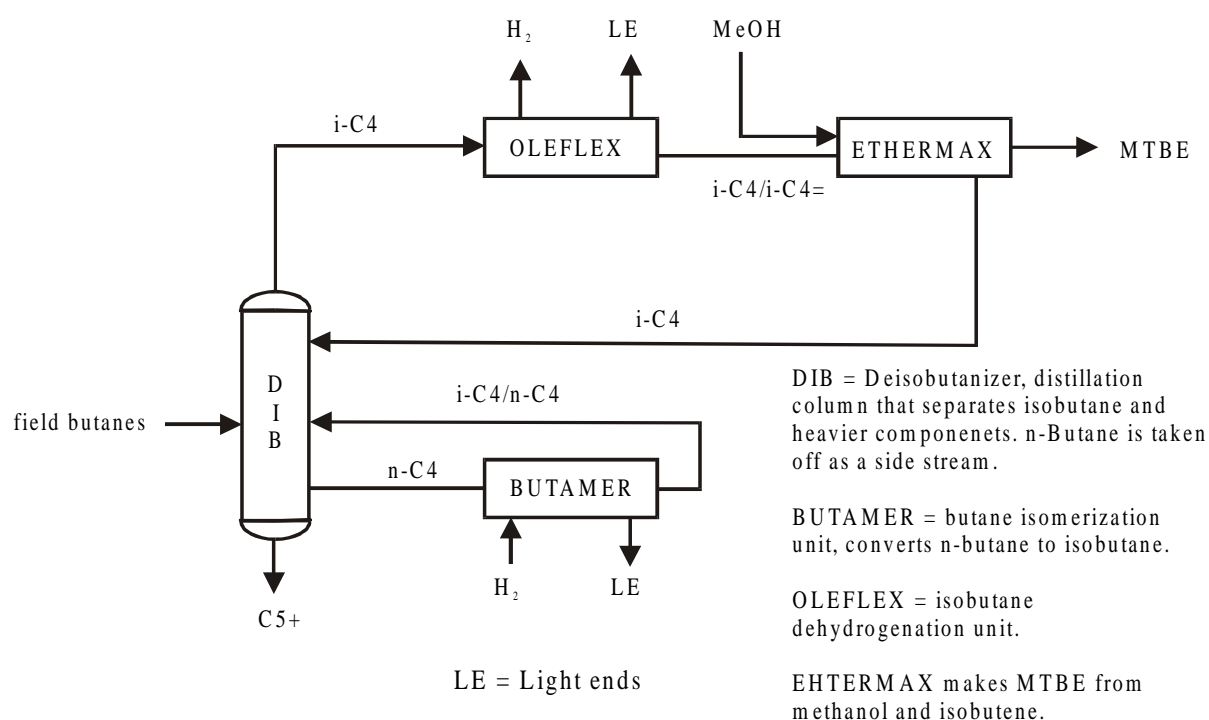


Figure 1. Scheme of the UOP process for producing MTBE from butane

tetraethyl-lead. MTBE can be formed from an alkane feed. As an example, UOP uses a combination of the BUTAMER and the OLEFLEX process to produce isobutene (and ultimately MTBE *via* etherification) from *n*-butane. A generalized process scheme is shown in Figure 1.

An alternative as part of the MTBE synthesis is e.g. the direct isomerization of *n*-butene to isobutene [4], which however, suffers on limited resources of butenes. One step further, the (oxidative) dehydroisomerization from *n*-butane to isobutene might be even more interesting but is severely restricted by thermodynamics [5].

Before world war II, the catalyst used for paraffin isomerization was anhydrous

aluminium chloride. Significant amounts of hydrochloric acid had to be used to obtain the required level of acidity leading to corrosion and environmental problems [6]. After 1950, bifunctional catalysts consisting of a metal function and chlorided alumina as acid component were used. Zeolites were introduced by the Shell HYSOMER process in which Mordenite was used as catalyst. Zeolites are crystalline, microporous aluminosilicates. Approximately 50 natural zeolites are known [7] and more than 150 synthetic types have been reported [8]. Their lattice consists of tetrahedrally oxygen coordinated Si^{4+} and Al^{3+} ions. The latter introduce negative charge to the crystalline structure, which is compensated by metal cations or protons. Compensation of this charge by protons generates Brønsted acid sites. Their location and their acid strength, and therefore their impact on catalytic reactions largely depends on the structure of the zeolite. Because the pore dimensions of the channel structure in zeolites fall in the range of the kinetic radii of many hydrocarbons, these materials were also denoted as *molecular sieves*. The idea of molecular sieving (size exclusion) led to the concept of shape selectivity, which is one of the striking advantages zeolites offer.

Although the technology based on Mordenite requires somewhat higher temperatures of operation (about 100 K) than demanded with the HCl based catalysts the fact that mordenites do not cause problems concerning waste disposal and corrosion makes it superior in a time of severe legislative policies. Apart from this, the use of zeolites offered the possibility of integrating isomerization and the separation section needed for the purpose of recirculation of the unreacted *n*-paraffine. Moreover, crude oils can contain up to 6 wt% sulfur containing compounds like thiols, thiophene and hydrogen sulfide [3]. Preliminary studies with Pt/Mordenite and sulfur containing *n*-pentane feed indicated a sulfur tolerance that may eventually allow the simultaneous presence of these compounds in an industrial plant [9]. Chapter 6 of this thesis deals with sulfur tolerance of bifunctional hydroisomerization catalysts based on Mordenite.

1.2 Acid properties of zeolites

1.2.1 Brønsted acid sites

Pure siliceous zeolites are electrically neutral. By replacing silicon (tetrahedrally coordinated with oxygen atoms) having a formal charge of 4^+ in the zeolite lattice with aluminium (formal charge 3^+) a negatively charged tetrahedron is created. Among others (NH_4^+

and alkali cations like Na^+ , K^+ etc.) the counterion H^+ compensates this negative charge. The protons are formally assigned to be bonded to the bridging oxygen of an Si-O-Al bond to form hydroxyl groups that act as strong Brønsted acids at the solid/gas interface. Brønsted acid sites will have acid strength, which depends on their environment, i.e. depending on chemical composition and the structure of the zeolite [10]. The local environment of the acid site in a molecular sieve is determined by the structure, i.e. the coordination of the TO_4 tetrahedra in the framework (topology). This leads to different amounts of topologically inequivalent T sites, i.e. sites in tetrahedral position. In this way, LTL zeolites would have two, MOR four and MFI twelve non equivalent T sites [8], while FAU structures have no inequivalent T sites. These different tetrahedral positions differ in T-O-T bond angles and T-O bond lengths [11,12]. Quantumchemical calculations indicated that the O-H bond length and the deprotonation energy depend upon the bond lengths of Al-O and Si-O and the corresponding Al-O-Si and Si-O-Si angles [12, 13]. Redondo and Hay [12] showed this for the 12 different acid site positions of H-MFI with semiempirical quantum chemical methods. Thus, different T-O-T angles for the topologically different sites and different deprotonation energies lead to different acid strengths. These results are supported by *ab initio* calculations of Kramer and van Santen [14], who calculated proton affinities for FAU and MFI structures and also found different protonation energies for topologically different sites.

1.2.2 Lewis acid sites

Lewis acid sites (electron pair acceptor sites) are related to the formation of positively charged oxide clusters or ions within the porous structures of the zeolites. These species are typically alumina or silica/alumina, formed by extraction of aluminum from the lattice, or metal ions exchanged for the protons of acid sites. Depending on the nature of the metal cation, these may contain hydroxyl groups (by partial hydrolysis of water). Note, that these metal cations together with the adjacent framework oxygens will act as Lewis acid/base pair and may polarize bonds in reacting molecules. The former type of Lewis acidity, i.e. aluminum oxide clusters containing alumina in octahedral and tetrahedral coordination will usually be a stronger Lewis acid than exchangeable metal cations (“true” Lewis acids) [15]. These entities are typically extracted out of the zeolite lattice by steam treatment at higher temperatures and form oxohydroxides or oligomeric species [16], which can be charged or neutral. Extra framework

alumina/silica (EFAL) species can either block an active site by exchanging for a proton, enhance the acidity by interacting with a Brønsted acid site [17] or block the access to micropores by forming voluminous oligomeric species. Due to the formation of such different species the influence on the catalytic behavior of a zeolite catalyst is very diverse varying from enhancing to weakening the strength of Brønsted acid sites.

However, Lewis acid sites cannot only modify the Brønsted acid sites. These species will also act themselves in various ways in the molecular sieve catalysts. Nearby molecules may become polarized, possibly enhancing their chemical reactivity [17, 18]. For already polar molecules this polarization could also be sufficient to catalyze a chemical transformation (e.g. in the reaction of alcohols) [19]. Lewis acid sites are acting also as hydride (or anion) receptors in a variety of reactions. Thus, in most cases the character of an acid-base pair site will be more pronounced in the case of Lewis than in the case of Brønsted acid sites [20]. The impact of steam dealumination is studied in chapter 3 and 4.

1.2.3 Concentration of acid sites

Due to the instability of the Al-O-Al bond, not more than half of all silicon atoms can be replaced by aluminum in a molecular sieve material (Loewenstein's rule). Therefore, the lowest Si/Al ratio possible is unity. In this configuration zeolitic structures have one Al site surrounded by 4 Si atoms as nearest neighbors and various amounts of Al atoms as next nearest neighbors (NNN) depending on the zeolite, such as 9 in the FAU or 12 in the MFI structure [8]. Various models, as reviewed by Barthomeuf [10] relate the acid strength of an active site to the amount of Al atoms in the NNN layer. The strongest acid sites are connected to sites with no Al atoms in the second layer, i.e. with zero NNN. The model considers also the second to the fifth layer around the Al site to include overall effects in a zeolite structure [10]. This model was shown to correlate well with theoretical calculations performed by Mortier's group [21]. Both models suggest that acid strength is the highest with low amounts of neighboring Al atoms, i.e. isolated Al atoms. The limiting concentration of Al atoms lies between 23 and 40 Al atoms per unit cell (Si/Al ratios of 7.3 to 3.8), depending on the structure and the model applied. These results show that the acid site concentration, which depends on the amount of aluminum in the zeolitic material, also influences the acid site strength of a particular site. Thus, the acid strength of a Brønsted site depends on its local geometry, i.e. the T-O bonds and T-O-T angles (the structure

of the zeolite) and the concentration of aluminum in the zeolite.

1.3 Adsorption of hydrocarbons in zeolites

In the following paragraphs, the most important findings regarding the first steps involved in catalytic chemistry, i.e. alkane sorption and proton transfer, will be discussed.

1.3.1 Structural and energetic aspects of alkane adsorption

Being a key step in the alkane activation, sorption of alkanes has been directly (studies dedicated to adsorption) and indirectly (deductions from catalytic conversions) addressed. It is commonly accepted that alkanes are primarily bound by dispersive interactions to the molecular sieve walls, independent of the presence or absence of Brønsted or Lewis acids sites [22]. This leads to a generally weak perturbation of the alkane C-H bonds that has been experimentally observed by IR spectroscopy [23, 24].

The energy of interaction (e.g. represented by the heat of adsorption) between alkanes and molecular sieves increases with the number of carbon atoms of the adsorbate. For molecular sieves, that constrain sorbate-sorbate interactions, this increase is a linear function of the number of carbon atoms, for structurally related alkanes. For *n*-alkanes (from ethane to *n*-hexadecane), this has been reported independently by three groups over the last 4 years [22, 23, 25]. The stronger heat of adsorption is always accompanied by a lower entropy in the sorbed state indicating that a marked compensation effect exists [23, 25]. The increase in the heat of adsorption with increasing carbon number does not depend upon the presence of acid sites in the zeolite (as seen in the comparison of the heats of sorption of linear alkanes on silicalite and H-MFI [26]) underlining the relatively low importance of acid sites for the overall energetics of sorption.

The observed heat of adsorption of a particular hydrocarbon and the increase of the heat of sorption per carbon atom depends upon the nature of the zeolite. When comparing to the minimum pore radius of the molecular sieve main channels [24], however, it seems to increase first with decreasing minimum pore radius and then to fall again at 0.4 and 0.5 nm minimum pore diameter, i.e. as the pores become too small and repulsive forces (less favourable intermolecular potential) dominate [27]. This is well documented for all silica zeolites such as MFI, MOR, FAU,

RHO, LTA, and FER by configurational biased Monte Carlo simulations [22, 27]. Experimentally, values of the heat of adsorption of approximately 6 kJ/mol per carbon atom for FAU and 10 kJ/mol for H-MFI were reported [23]. The theoretically predicted and the measured values are generally in good agreement [23, 25, 27].

Molecular sieves, containing a larger main channel and smaller side pockets (connecting channels) such as mordenite, induce additional complexity regarding the location of the alkanes in the pores. Alkanes, with the exception of methane, do not enter the side pockets of mordenite [23, 24, 28] and, thus, do not utilize the acid sites located there.

Localized sorption on acid sites is energetically preferred at low coverage as seen from IR spectroscopy [23] and the linear correlation of Henry constants of sorption with Brønsted acid site concentration for a given zeolite [29]. The interaction between the apolar alkane and the zeolite acid site occurs *via* dipole induced hydrogen bonding that contributes an almost constant energy independent of the number of alkane carbon atoms. This hydrogen bonding involves induction of polarity in the alkane by the proton of the hydroxyl group in the zeolite. This interaction increases with the polarizability of the C-H bond and the acid strength of the bridging hydroxyl group and is e.g. manifested by increasing perturbations of the OH stretching frequency as the size of the alkane increases [23]. The contribution of these variations to the overall sorption enthalpy are, however, very small (approximately 1 kJ/mol [26]). Interactions between molecules may lead to a further stabilization, whenever the pores/cavities are large enough to accommodate more than one molecule, as seen from the increase of enthalpy of sorption with alkane loading for FAU and AFI structures [24]. Intermolecular interactions also seem to play a role for adsorption in the pores of an all silica MFI. Heats of adsorption for the *n*- and single branched alkanes (2-methyl or 3-methylpentane) were independent of the coverage, but for 2,2 dimethylpentane, methyl cyclopentane and cyclohexane the heat of adsorption increased with the coverage [30]. This suggests that only these bulkier molecules populate the channel intersection that allow intermolecular interactions. Support for this interpretation is obtained by earlier molecular modeling [31]. It is interesting to note that Eder [24] found evidence for adlineation of two *n*-alkanes (not for iso-alkanes) at the acid site of MFI which is only likely to occur at the intersection of the MFI channels.

The chemical composition of molecular sieves has been assumed to strongly influence the interaction with alkanes [23, 25, 26, 28, 30]. In contrast, Eder and Lercher [32] showed for

an aluminum phosphate and an all silica form of the AFI structure that the different chemical composition and, thus, the different polarity of the lattice did not influence the sorption enthalpies and entropies of alkanes. Thus, the chemical composition is rather important from the viewpoint of localized sorption: the concentration of reactant molecules inside the pores can be varied by modifying the chemical composition, i.e. the concentration of acid sites.

Highly ordered structures of alkanes in zeolites have now been well demonstrated for at least two molecular sieves, MFI and FER. First, this was theoretically predicted by Smit *et al.*[33], and was subsequently verified experimentally by Eder [24] and van Well [34]. Experimental evidence (a kink or step in the adsorption isotherm) indicates that ordering occurs at a loading when intermolecular repulsion becomes critical, i.e. when the physical presence of one molecule at a particular position hinders the adsorption of another. It is, thus, confined to molecules that match the micro dimensions of (intersecting) channel structures. With MFI, the most pronounced ordering occurred for hexane and heptane, while it was butane and pentane with FER [24, 33, 35]. For molecules with a smaller size, ordering does not lead to an improved packing (so that a higher volume of sorbate can be accommodated), for larger molecules it does not help to avoid mutual sorption constraints exerted by the sorbate (leading to a lower total uptake).

1.3.2 Relation between adsorption effects and the kinetics of alkane conversion

In the pores of zeolites, the reactants may suffer an electronic confinement, which will become more important when the size of the guest molecule matches the size of the cavities. Then, owing to the partial covalent character of zeolites [36 and references therein], electrons are not localized on the framework atoms but are partially delocalized through the bulk. In these conditions the electron density of the orbitals of the guest molecules suddenly drops to nearly zero when they reach the walls of the zeolites as a consequence of the short-range repulsive interaction with the delocalized electronic clouds of the lattice. This implies that a contraction of the orbitals of the guest molecules will occur, with the corresponding changes in their energy levels. The implications of this electronic confinement for chemical reactivity are obvious if one considers that those changes in the energy levels of the guest molecule could imply a preactivation of the molecule.

The relation between kinetics and thermodynamics of sorption can easily be understood

form the functional relation developed by Temkin [37]. Combining the Power Rate Law formalism and the Clausius-Clapeyron equation he obtained

$$E_{app} = E_t + \sum n_i \Delta H_i \quad (1)$$

relating the activation energy, the order n_i and the adsorption enthalpy. Experimental approaches demonstrate that cracking of alkanes obeys this equation and is primarily governed by adsorption of the alkane. For light n -alkanes Narbeshuber *et al.* [38] show that the decrease in the apparent activation energy of protolytic cracking with increasing alkane chain length is compensated for by the increase in heat of adsorption leading to a constant true energy of activation independent of the carbon chain length. Thus, the higher reactivity of larger hydrocarbons is due to their higher abundance in the molecular sieve pores and not to their intrinsically higher reactivity. Wei [25] shows that this leads to negative apparent activation energies for alkanes larger than n -hexadecane.

1.4 Activation of alkanes by proton transfer or hydride abstraction

Activation of alkanes to carbonium (addition of a proton) or carbenium ions (hydride abstraction) is strongly endothermic. Thus, their concentration in molecular sieve pores will be low under all practical conditions.

Many theoretical studies were devoted on answering the question whether the carbonium ions and carbenium ions could exist only as transitions states. The approach is usually to use model clusters simulating the bridging hydroxyl group between a Si-O₄ and an Al-O₄ tetrahedron. Hydrogen (deuterium) exchange between such an acidic cluster and methane (the reversible protonation of methane), occurs *via* a carbonium ion in the transition state [39], as suggested by density functional theory [40]. During the exchange a symmetric transfer of the proton from and to the zeolite and the methane molecule occurs. Two oxygen atoms of the zeolite (attached to Al) are involved, one in accepting the proton (acting as base), the other in donating the proton (acting as acid). *Ab initio* calculations by Kramer and van Santen [41] confirmed this view reporting the rate of exchange to be solely determined by the difference in acid/base strength between the two oxygen sites involved in the process and not upon the intrinsic acidity of the zeolite. Hartree-

Fock type quantum-chemical calculations indicate that the transition states and the surface chemistry of these reactions depend on the sign of the bond polarization [42, 43]. Protolytic attack of the C-H bond results in the heterolytic splitting of this bond with abstraction of a hydride ion. The transition state for this reaction step resembles a carbenium ion and the reaction leads to one molecule of hydrogen and the formation of a surface alkoxy group. Only when a proton is split off from the paraffin, hydrogen exchange is observed as discussed above. Recently, Schoofs *et al.* [44] experimentally found activation energies for H/D exchange with methane on MFI and FAU similar to the ones found with *ab initio* calculations of Kramer and Van Santen [41]. No consensus, however, was reached on the proposal of Kramer *et al.* [39] on the concerted reaction mechanism of H/D exchange, as a kinetic isotope effect was evident. Lee *et al.* [45] supported the concerted mechanism upon probing light alkanes on FER.

Blaszkowski *et al.* [46] determined, using density functional theory, the energy barriers of ethane conversion to be 118 kJ/mol for hydrogen exchange, 202 kJ/mol for hydride transfer, 292 kJ/mol for cracking and finally 297 kJ/mol for dehydrogenation. Considering the different heat of adsorption, the calculations are in remarkably good agreement with the data of Narbeshuber *et al.* [47] for hydrogen deuterium exchange of perdeuterated *n*-butane. However, the two latter energies of activation (dehydrogenation and cracking) are significantly higher than those reported experimentally.

The nature of carbenium ions is usually studied using the same theoretical approaches as discussed above and experimentally using NMR and IR spectroscopy. Kazanski *et al.* [42, 43] used diffuse reflectance IR spectroscopy to establish the covalent character of the ground state of the zeolite hydroxyl groups. Interaction of these acidic hydroxyl groups with olefins leads to the formation of covalent surface alkoxides. Note that this is in perfect agreement with earlier studies of Farneth *et al.* [48] on the formation of alkoxy groups by reacting alcohols with zeolite hydroxyl groups using ^{13}C NMR spectroscopy. Further support was provided by Stepanov *et al.* [49, 50] by IR and NMR, who shows that the proton has been transferred from the solid to the sorbate, but that the alkylsilyl ethers are the most abundant species. The (adsorbed) carbenium ions are, thus, the energetically excited transition states formed from these covalent precursors. The Brønsted acid part protonates the adsorbed alkene forming a carbenium, while its strong interaction with the neighboring basic oxygen converts it into the more stable covalently bound alkoxy group.

Carbonium or carbenium ions involved in the reactions exist only as transition states. The calculations indicate that the stable species involved in hydrogen exchange are rather covalent.

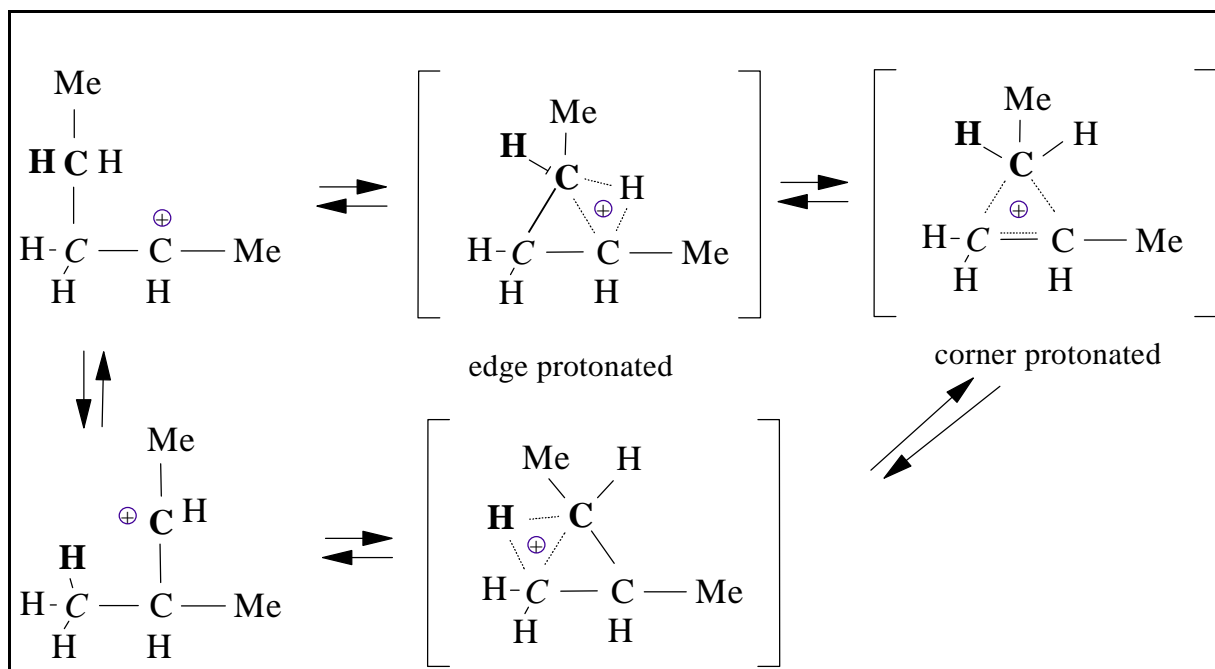


Figure 2. Cyclopropyl carbenium ion rearrangements.

The species in the transition state resemble a carbonium ion for the hydrogen exchange reaction and carbenium ions for cracking and dehydrogenation. Common to all these models is the fact that alkane activation involves the simultaneous interaction of the alkane with the acid hydroxyl group and a neighboring basic oxygen atom which leads finally to cleavage into a saturated fragment and a covalently bound alkoxide. This suggests carbenium and carbonium chemistry in terms of nucleophilic/electrophilic substitutions with an important role for proton accepting and proton donating sites.

It is important to note that the concept of carbonium ion chemistry on zeolites is usually correlated to conditions at which monomolecular cracking prevails [47]. The formation of these species at low temperatures, however, was addressed for the H/D exchange with isopentane over HY, by Mota *et al.* [51]. Sommer *et al.* [53], however, has proposed the H/D exchange of isobutane over sulfated zirconia, H-Y, H-ZSM-5 and Beta zeolites, to occur (at temperatures as low as 373 K) *via* the formation of alkenes as reaction intermediates. Both mechanism of H/D exchange with isobutane are further explored in chapter 3.

1.5 Isomerization of paraffines

Studies on alkane reactions at low reaction temperatures inherently include thermodynamically favored isomerisation. General consensus on the operating reaction routes is not always easily reached. Especially mechanisms of isomerisation of butane (and butenes) are actively debated currently. In general, two mechanisms of isomerization can be distinguished, namely, Type A and B, which occur *via* non-branching and branching methyl rearrangements, respectively [53]. If branching rearrangements occurred *via* hydride and alkyl shifts they would necessarily include primary carbenium ions. This is not likely due to the unfavorable energetics for formation of these species (claimed to have 100 kJ/mol higher true energy of activation [54]). In order to avoid this, isomerization of alkanes larger than C₄ is generally accepted to include branching via cyclopropyl carbenium ions (Fig. 2). It is important to note that *n*-butane still cannot isomerize *via* the mechanism in figure 2 without formation of primary carbenium ion. A bimolecular pathway was therefore proposed and experimentally confirmed [55- 57]. A detailed overall mechanistic scheme for this reaction route is provided in chapter 5. In this model, butene species (either formed by hydride abstraction on lewis acid sites [58] or present as impurities in the feed) are thought being protonated at Brønsted acid sites. The so-formed butoxy species (in

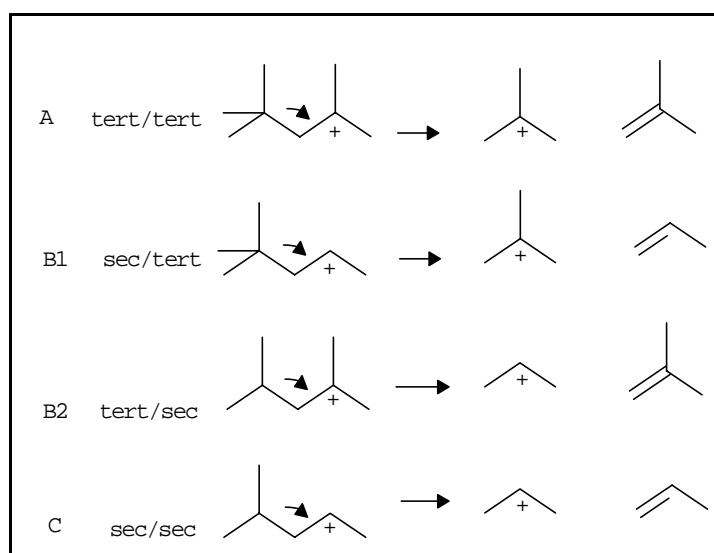


Figure 3. Possible modes of β -scission

the ground state) react with incoming butene to form C₈ alkoxyde species. The cracking of C₈ carbenium ions (in the transition state) occurs through β -scission. There exist five modes of β -

scission, denoted as A, B₁, B₂, C and D [59]. The distinction between the mechanism is based on the position of the side chains relative to the charged atom. These specific configurations are α,γ,γ -tribranching, γ,γ -dibranching, α,γ -dibranching and γ -monobranching for β -scissions of types A, B₁, B₂ and C, respectively. Type D β -scissions convert unbranched ions. The rate of the β -scission reactions decreases in the order: A >> B₁, B₂ > C >> D. The different modes of β -scission are depicted in figure 3.

Isomerization of *n*-alkanes over pure and/or Pt modified Mordenite zeolites have been reported by different groups [56, 60, 61]. Sachtler and co-workers [61] compared isomerization of lower alkanes over two, apparently, bifunctional catalysts (Pt/H-Mor and Pt/ZrO₂-SO₄) with similar concentrations of metal and acid sites and similar strengths of Brønsted acid sites. The catalytic performance and the kinetic parameters were found to significantly differ for these systems. Under conditions where *n*-butane isomerization (it follows a bimolecular mechanism) is rapid over Pt/ZrO₂-SO₄, it is undetectable over Pt/H-Mordenite. The apparent activation energy of *n*-pentane isomerization (which follows a skeletal isomerization route) is significantly higher over the zeolite based catalyst.

These differences were rationalized in terms of different pore geometries: in the one-dimensional pore system of Mordenite the rates are *single-file* diffusion controlled; as a result, bimolecular processes such as isomerization *via* intermediate dimer formation are difficult. Likewise, hydride ion transfer, which is the propagation step in alkane reactions *via* carbenium ions, is sterically inhibited in micro pores and replaced by a process, proposed to involve Pt-proton adducts. The possibility of a bifunctional mechanism was, however, completely ignored for both the Pt containing catalysts.

Asuquo *et al.* [55] show that isomerization of *n*-butane shows appreciable initial activity and selectivity over H-Mordenite. Their results suggest that the reaction follows a bimolecular pathway where first (octyl) dimers are formed which undergo isomerization, cracking and hydride transfer reactions to form isobutane. Deactivation of the H-Mordenite by coking is rapid. Incorporation of Pt to Mordenite can suppress coke formation and improve catalyst stability if hydrogen is cofed [56]. In the presence of Pt a bifunctional isomerization mechanism also contributes to the overall conversion [56 and chapter 5 of this thesis]. Bifunctional nature of Pt/Mordenite is also suggested for C₅/C₆ hydro-isomerisation [62, 63]. A schematic drawing of the bifunctional mechanism as proposed by Weisz is depicted in Figure 4. In this mechanism the

metal performs dehydrogenation of the feed alkane and a hydrogenation of isomer alkenes. The acid sites catalyze the actual isomerization following the outline given above.

Studies by Chao *et al.* [64] of the isomerization of *n*-butane catalyzed by sulfated zirconia and H-form zeolites with the promotion of platinum show results that were also confirmed by Liu *et al.* [60]. These authors have studied the reaction also at higher pressures (up to 20 atm). They suggest isomerization to proceed mainly via the bimolecular mechanism at 1 atm but *via* the monomolecular on Pt/ZrO₂-SO₄ at 20 atm pressure. Interesting to note that Tran *et al.* [65] report a role for the monomolecular mechanism over MOR already at 1 bar and when hydrogen was cofed.

Alkane isomerization over other zeolites such as BEA [66], SAPO's [67] and TON [68, 70] are also reported in the last years. Pt/BEA [66] is an efficient bifunctional catalyst for the isomerization of C₅-C₆ but the material is sensitive to pretreatments such as calcination and (auto-catalytic) steaming. The formation of Extra Framework Aluminum (EFAL) is the direct consequence. However, even though the EFAL blocks some of the Brønsted acid sites, it was suggested to improve the strength of the neighboring hydroxyls and thereby provide improved isomerization activity. Over Pd/SAPO-11, *n*-heptane isomerization follows a bifunctional mechanism [67]. In this work the significance of the steric influences caused by the pore size and the location of the Brønsted sites in different SAPO's is discussed. These factors are attributed for the enhanced selectivity to mono than di- and tri- branched isomers over SAPO-11.

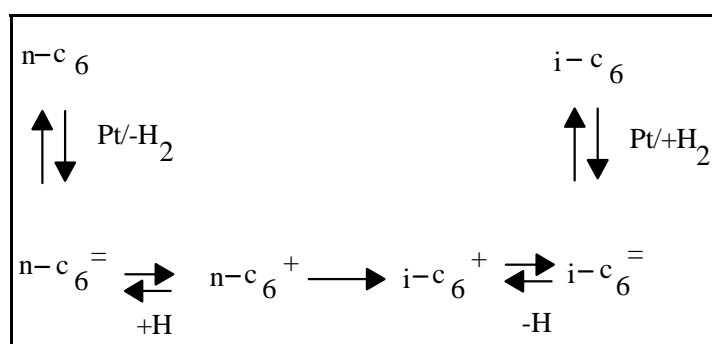


Figure 4. The classical Weisz mechanism.

An interesting communication by Ernst [68] addresses the concept of ‘pore mouth catalysis’ (Martens *et al.* [69]). The reaction is suggested to occur indeed in the pores of the zeolite but near its mouth. This is inferred from the predominance of branching at the second carbon position during isomerization of *n*-heptadecane over TON. This is in sharp contrast to a

larger pore Y zeolite where branching occurs at the more central position of the carbon chain as can be expected from a mechanism involving protonated cyclopropanes. There is sort of epitaxial (1:1) relation is found between the distance between the pores (for a typical 001 crystal face) and the distance between the branching methyl groups during the isomerization of n-heptadecane on the on the 001 crystal face of TON. Questions such as, effect of crystal size, role of the acid sites at the external surface, application of the concept to other zeolites and reactions etc. are factors that need to be still addressed [68]. Attempts to answer (part) of these questions are compiled in chapters 7 and 8.

Acknowledgment

Dr. G.D. Pirngruber is acknowledged for the making of figures 1 and 2.

References

1. Energy Security Analysis, Inc., “*Supply and cost of alternatives to MTBE in gasoline, Report on the Oxygenate Market: Current Production Capacity, Future Supply Prospects and Costs Estimates*”, Wakefield, MA, October 1998 (prepared for the Californian Energy Commission).
2. Matar, S., and Hatch, L.F., *Chemistry of petrochemical processes*, Gulf. Publishing Co., Houston 1994.
3. Venuto, P.B., and Habib, E.T., *Fluid Catalytic Cracking with zeolite catalysts*, Marcel Dekker New York, Basel (1979).
4. De Jong, K.P., Mooiweer, H.H., Buglass, J.G., and Maarsen, P.K., *Stud. Surf. Sci. Catal.* **111**, 127 (1997).
5. Pirngruber, G.P., Seshan, K., and Lercher, J.A., *J. Catal.* **186**, 188 (1999).
6. Nelson, W.L. in ‘Petroleum Refining Engineering’, McGraw-Hill, inc., 1969.
7. Vaughan, D.E.W., ‘Natural Zeolites: Occurrence, Properties and Use’, Sand, L.B., and Mumpton, F.A., Eds., London Pergamon, 1978.
8. Meier, W.M., and Olson, D.H., *Atlas of Zeolite Structure Types*, 3rd ed., Butterworth-Heinemann, London (1992).
9. Sie, S.T. in “Advanced Zeolite Science and Applications”, *Stud. Surf. Sci. Catal.* **85**, 621 (1994).
10. Barthomeuf, D., *Mat. Chem. Phys.* **17**, 49 (1987).
11. van Santen, R.A., Kramer, G.J., and Jacobs, W.P.J.H., *Theory of Brønsted acidity in zeolites*. In: Joyner, R.W., and van Santen, R.A. (eds) Elementary reaction steps in heterogeneous catalysis. Kluwer Academic Publishers, 113 (1993).

12. Redondo, A., and Hay, P.J., *J. Phys. Chem.* **97**, 11754 (1993).
13. Rabo, J.A., and Gajda, G.J., *Catal. Rev.-Sci. Eng.* **31**, 385 (1990).
14. Kramer, G.J., and van Santen, R.A., *J. Am. Chem. Soc.* **115**, 2887 (1993).
15. Karge, H.G., *Stud. Surf. Sci. Catal.* **65**, 133 (1991).
16. Scherzer, J., *ACS Symp. Ser.* **48**, 157 (1984).
17. Lonyi, F., and Lunsford, J.H., *J. Catal.* **136**, 566 (1992).
18. Carvajal, R., Chu, P.-J., and Lunsford, J.H., *J. Catal.* **125**, 123 (1990).
19. Huang, M., and Kaliaguine, S., *Catal. Lett.* **18**, 373 (1993).
20. Huang, M., and Kaliaguine, S., in: *Heterogeneous Catalysis and Fine Chemicals III* (ed.:Guisnet, M. et al.), Elsevier, Amsterdam, 559 (1993).
21. Janssens, G.O.A., Toufar, H., Baekelandt, B.G., Mortier, W.J., and Schoonheydt, R.A., *J. Phys. Chem.* **100**, 14443 (1996).
22. Smit, B., *J. Phys. Chem.* **99**, 5597 (1995).
23. Eder, F., Stockenhuber M, and Lercher J.A., *Stud. Surf. Sci. Catal.* **97**, 495 (1995).
24. Eder, F., Thermodynamics and siting of alkane adsorption in molecular sieves. Ph.D Thesis, University of Twente, The Netherlands: 1996 ISBN No 90-3650861-4.
25. Wei, J., *Chem. Eng. Sci.* **51**, 2995 (1996).
26. Lercher, J.A., and Seshan, K., *Current Opinion in Solid State & Materials Science* **2**, 57 (1997).
27. Bates S. P., van Well W.J.M., van Santen R.A., and Smit, B., *J. Am. Chem. Soc.* **118**, 28 (1996).
28. Xu, Q., Eguchi, T., Nakayama, H., and Nakamura, N., *J. Chem. Soc. Faraday. Trans.* **92**, 1039 (1996).
29. Eder, F., and Lercher, J.A., *J. Phys. Chem.B.* **101**, 1273 (1997).
30. Cavalcante, C. L. Jr., and Ruthven D.M., *Ind. Eng. Chem. Res.* **34**, 177 (1995).
31. June R.L, Bell, A.T., and Theodorou, D.N., *J. Phys. Chem.*, **94**, 1508 (1990).
32. Eder, F., and Lercher J.A., *J. Phys. Chem.* **100**, 41 (1996).
33. Smit, B., and Maesen T.L.M., *Nature* **374**, 42 (1995).
34. van Well W.J,M, Wolthuizen, J.P, Smit, B., van Hooff, J.H.C., and van Santen, R.A., *Angew. Chem. Int. Ed. Engl.* **34**, 2543 (1995).
35. van Well, W.J.M., Cottin, X., de Haan, J.W., Smit, B., Nivarthi, G.S., Lercher, J.A., van Hooff, J. H. C., and van Santen, R.A., *J. Phys. Chem.B* **102**, 3945 (1998).
36. Corma, A., *Chem. Rev.*, **95**, 559 (1995).
37. Temkin, M., *Acta Physiocochem. URSS* **3**, 312 (1935).
38. Narbeshuber, T.F., Vinek, H., and Lercher, J.A., *J. Catal.* **157**, 388 (1995).
39. Kramer, G.J., Van Santen, R.A., Emeis, C.A., and Nowak, A.K., *Nature* **363**, 529 (1993).
40. Blaszkowski, S.R., Jansen, A.P.J., Nascimento, M.A.C., and van Santen R.A., *J. Phys. Chem.* **98**, 12938 (1994).
41. Kramer, G.J., and van Santen, R.A., *J. Am. Chem. Soc.* **117**, 1766 (1995).
42. Kazansky, V.B., Senchenya, I.N., Frash, M., and van Santen, R.A., *Catal. Lett* **27**, 345 (1994).

43. Kazansky, V.B., Frash, M., and van Santen, R.A., *Catal. Lett.* **28**, 211 (1994).
44. Schoofs, B., Martens, J.A., Jacobs, P.A., and Schoonheydt, R.A., *J. Catal.* **183**, 355 (1999).
45. Lee, B., Kondo, J.N., Wakabayashi, F., and Domen, K., *Cat. Letters* **59**, 51 (1999).
46. Blaszkowski, S.R., Nascimento, M.A.C., van Santen, R.A., *J. Phys. Chem.* **100**, 3463 (1996).
47. Narbeshuber, T.F., Stockenhuber, M., Brait, A., Seshan, K., Lercher, J.A., *J. Catal.* **160**, 183 (1996).
48. Farneth, W.E., and Gorte, R.J., *Chem. Rev.* **95**, 615 (1995).
49. Stepanov, A.G., Luzgin, M.V., Romannikov, V.N., and Zamaraev, K.I., *Catal. Lett.* **24**, 271 (1994).
50. Stepanov, A.G., Sidelnikov, V.N., and Zamaraev, K.I., *Chem. Eur. J.* **2**, 157 (1996).
51. Mota, C.J.A., and Martins, R.L., *J.Am.Chem.Soc., Chem. Commun.* 171 (1991).
52. Sommer, J., Hachoumy, M., Garin, F., Barthomeuf, D., and Vedrine, J., *J.Am.Chem.Soc.* **117**, 1135 (1995).
53. Martens, J.A., Parton, R., Uytterhoeven, L., and Jacobs, P.A., *Appl. Catal. A* **76**, 117 (1991).
54. Brouwer, D.M., and Hogeveen, H., *Prog. Phys. Org. Chem.* **9** 192 (1972).
55. Asuquo, R. A., Eder-Mirth, G and Lercher, J. A., *J. Catal.* **155**, 376 (1995).
56. Asuquo, R.A., Eder-mirth, G., Pieterse, J.A.Z., Seshan, K., and Lercher, J.A., *J. Catal.* **168**, 292 (1997).
57. Bearez, C., Chevalier, F and Guisnet, M., *React. Kinet. Catal. Lett.* **22**, 3 (1983).
58. Kwak, B.S., and Sachtler, W.M.H., *J. Catal.* **145**, 456 (1994).
59. Martens, J.A., Jacobs, P.A., and Weitkamp, J., *Appl. Catal. A* **20**, 239 (1986).
60. Liu, H., Lei, G. D., and Sachtler, W. M. H., *Appl. Catal. A* **137**, 167 (1996).
61. Corma, A., Frontela, J., Lazaro, J., and Perez, M., *Prepr.-Am. Chem. Soc., Div. Pet. Chem.* **36**, 833 (1991).
62. Dai, P., *Catal. Today* **26**, 3 (1995).
63. Van de Runstraat, A, Kamp, J.A., Stobbelaar, P.J., van Grondelle, J., Krijnen, S., and van Santen , R.A., *J. Catal.* **171**, 77 (1997).
64. Chao, K., Wu, H., and Leu, L., *J. Catal.* **157**, 289 (1995).
65. Tran, M.-Trung, Gnep, N.S., Szabo, G., and Guisnet, M., *J. Catal.* **174**, 185 (1998).
66. Corma, A., Martinez, A., Fernandes, L.D., Monteiro, J.L.F., and Sousa-Aguiar, E.F., *Stud. Surf. Sci. Catal.* **94** 456, (1995).
67. Parltitz, B., Shreier, E., Zubowa, H.L., Eckelt, R., Lieske, E., Lischke, G., and Fricke, R., *J. Catal.* **155**, 1 (1995).
68. Ernst, S., *Angew. Chem. Int. Ed. Engl.* **35**, 63 (1996).
69. Martens, J.A., Souverijns, W., Verrelst, W., Parton, R., Froment, G.F., and Jacobs, P.A., *Angew. Chem. Int. Ed. Engl.* **107**, 2726 (1995).

Experimental

As the most important experimental systems used for the studies reported in Chapters 3-8 were the same, the setups of the combined calorimetric/gravimetric, the infrared spectroscopic experiments, the kinetic experiments as well as the information to be deduced from them are described here in a separate chapter. The experimental sections of following chapters will therefore only contain information that are either specific for the experiments or deviate from the general procedure.

2.1 Sorption experiments

2.1.1 Microcalorimetry and gravimetry

The gravimetric and calorimetric measurements were performed using a modified SETARAM TG-DSC 111 instrument. As shown in Figure 2.1, the system consists of four main parts, i.e. the balance, the calorimeter, the vacuum system and the mass spectrometer. The calorimeter consists of two heat flow meters. One is used as reference element to eliminate any impact of thermal fluctuations and changes in the thermoconductivity of the gas phase on the heat signal. The sample holders (i.e. quartz crucibles) hang on quartz glass suspension wires from the arms of the balance into the sensitive part of the calorimeter. The calorimeter is equipped with

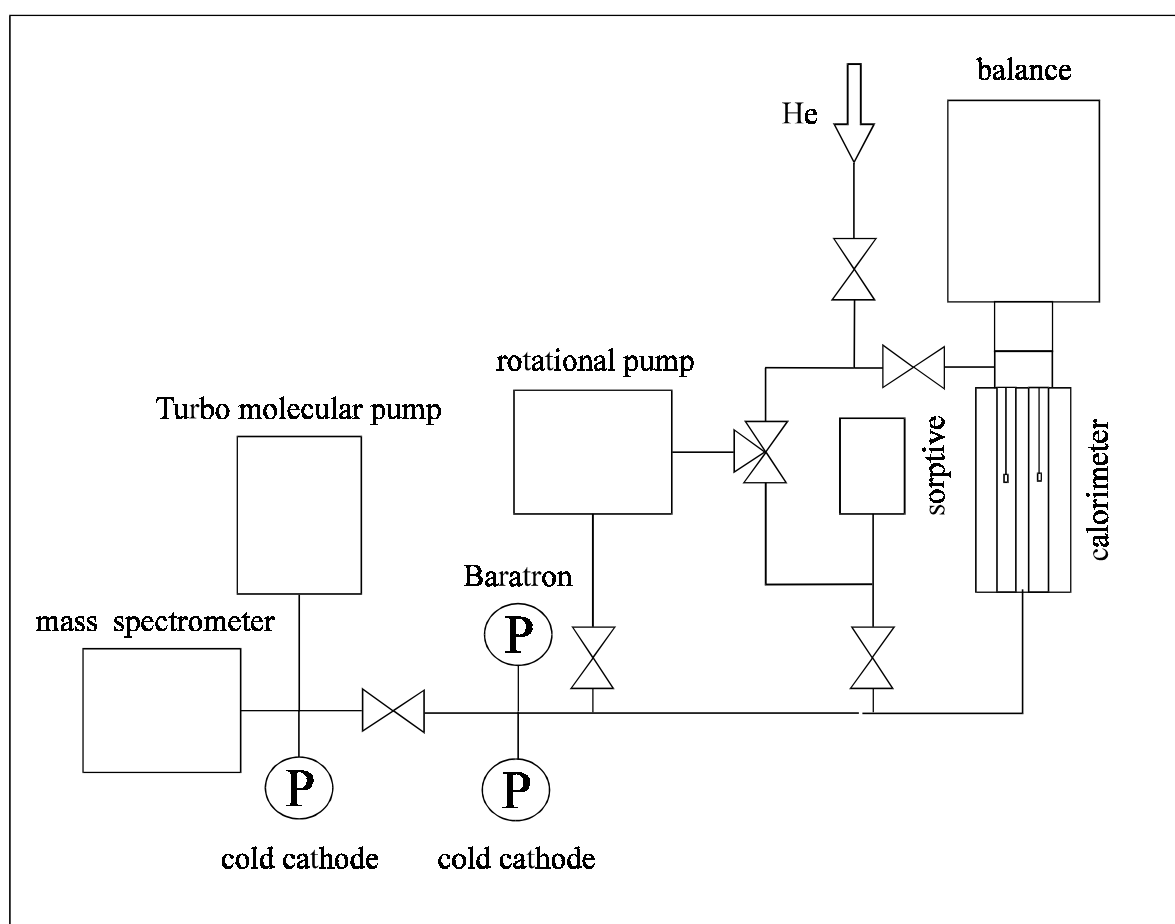


Figure 1. Schematic presentation of the TGA/DSC vacuum system.

quartz glass tubes to prevent adsorption of gases inside the calorimeter. The quartz crucibles are aligned in the centre of these quartz tubes with no physical contact to the walls of the tubes. The calorimeter and the balance can be evacuated by a rotation pump (Edwards High Vacuum Pump E-2M-1.5) and a turbo molecular pump (BALZERS TPU 060) to pressures below 10^{-6} mbar. The pressure is recorded by a BARATRON pressure transducer (type 122A) and two BALZERS IKR-020 cold cathode gauges. To analyze desorbing gases the system is equipped with a BALZERS QMG 420 mass spectrometer. The analog voltage signal of the calorimeter (μV) has to be calibrated to obtain the proper value for the heat flux (mW) inside the calorimeter. As the calibration factor ($\mu\text{V}/\text{mW}$) changes with temperature, it has to be determined at different temperatures. Therefore, known thermal effects at known temperatures have to be generated inside the calorimeter under the same conditions as in the sorption experiments. Two different methods were used for this calibration, i.e. (i) the observation of phase transitions of inorganic compounds and (ii) for lower temperatures ($T < 400\text{K}$) a Joule effect calibration. For the first method a known mass of substance is introduced into the calorimeter and heated in vacuum with a linear and small heating rate (typically 2K or 5K per min.) to a temperature higher than the transition temperature of the inorganic sample. The output signal can then be correlated to the known heat effect inside the calorimeter. A Joule effect calibration is performed by introducing an electrical heater into the inner part of the calorimeter cell. The electrical heater generates pulses of known electrical power and duration. The output signal generated by these pulses was compared at temperatures where the calibration factor was known from the measurement of phase transitions and at lower temperatures. In this way the dependence of the calibration factor on the temperature could be extrapolated to temperatures where phase transitions with a distinct thermal effect were not known.

The samples were pressed to thin wafers and consequently broken into small platelets. 15 to 30 mg of these platelets were charged into the quartz sample holder of the balance. The activation procedures varied upon sample choice and are described in the following chapters.

After activation the system was cooled to the adsorption temperature (323 to 343K). Subsequently, the alkanes were discontinuously dosed into the closed system and equilibrated with the surface. The equilibration was confirmed when no further changes in the heat flow and weight was observed. Reversibility was checked through desorption of the alkanes induced by

evacuation of the system at several points in one experiment. The adsorption isotherms of all the hydrocarbons were determined gravimetrically, simultaneously with the differential enthalpies of adsorption, which is defined as the heat evolved due to adsorption of a gas admitted in small quantities into a closed system at constant temperature and volume [1]. If these doses of sorptive are admitted to the system at different equilibrium loadings (i.e. at different partial pressures) the heat of adsorption can be determined as function of the coverage. The initial heat of adsorption is used to compare the strength of the interactions between sorbed molecules and different molecular sieves as the contribution of sorbate-sorbate interactions can be neglected at zero coverage. The dependence of the sorption enthalpy on the coverage provides more detailed information on the interactions occurring in the zeolite pores. (i) High initial heats of adsorption indicate energetically favored sorption sites, e.g. defect sites or stronger acidic sites. (ii) As the heat of sorption differs depending upon, whether the molecules interact with an acid site or solely

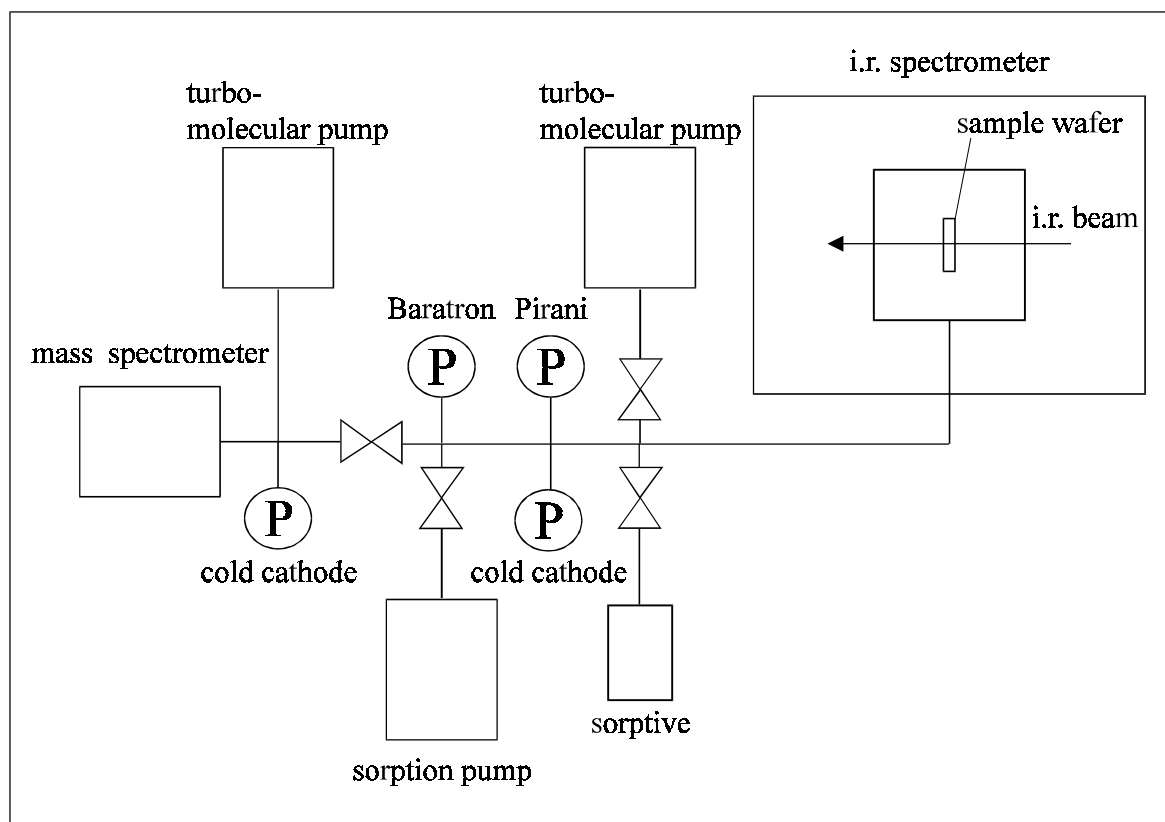


Figure 2. Schematic presentation of the high vacuum IR system.

with each other, conclusions can be drawn about the accessibility of the acid sites and the sorption stoichiometry. (iii) Increasing sorption enthalpies with increasing coverage indicate sorbate-sorbate interactions.

The shape of the gravimetrically determined sorption isotherms can indicate the occurrence of different sorption states. The equilibrium constants of sorption and the initial heats of adsorption can be utilized to determine the Gibbs Free energies and the entropies of sorption, respectively. The entropy loss due to sorption indicates how rigidly the molecules are bound to the sorbent.

2.1.2 IR Spectroscopy

The infrared spectroscopic measurements were performed with a BRUKER IFS-88 spectrometer equipped with a high vacuum cell. A schematic presentation of the setup is given in Figure 2.2. The high vacuum cell consists of a stainless steel chamber equipped with CaF_2 windows and a resistance heated furnace, in which the golden sample holder is placed. The cell can be evacuated by a sorption pump and a turbo molecular pump (BALZERS TPU 050) to pressures $< 10^{-6}$ mbar. The pressure is recorded with a BARATRON pressure transducer, an BALZERS IKR-020 cold cathode gauge and a BALZERS TPR-125 Pirani, depending upon the pressure range. To analyze desorbing gases the system is equipped with a BALZERS QMG 420 mass spectrometer.

Spectra were recorded in the transmission absorption mode. The molecular sieves were pressed to self supporting wafers and placed in a golden sample holder in the furnace of the high vacuum cell. The activation procedures varied upon sample choice and are described in the following chapters. After activation the system was cooled to adsorption temperature (323 to 343 K). The sorptive was introduced into the system *via* a dosing valve. The alkane partial pressure was increased stepwise and after every step equilibration was followed by time resolved infrared spectroscopy. The spectra were recorded with a spectral resolution of 4 cm^{-1} and a time resolution of 10 sec.

Analysis of infrared spectra of alkanes sorbed on acidic molecular sieves provides various information. (i) In general, the band of the OH stretching vibrations of the Brønsted acid sites of zeolites is found between 3650 cm^{-1} and 3550 cm^{-1} . From the change in the integral

intensity of this band upon sorption of alkanes the coverage of the acid sites at a defined hydrocarbon partial pressure can be determined. (ii) If the integral intensity of this band does not decrease to zero at pore filling, this indicates that a fraction of the acid sites is not accessible to the sorbate. The size of this fraction can be determined by comparing the integral intensity of the OH band at zero coverage and at pore filling. (iii) Due to hydrogen bonding of alkane molecules to the acid sites the O-H bond of the hydroxyl groups is perturbed giving rise to a broad band shifted to lower wavenumbers. The stronger the bonding the larger the difference in wavenumber between the bands of the perturbed and the unperturbed hydroxyl groups [2]. Thus, this bandshift can be used to estimate the strength of interaction between the alkane molecules and the acid sites. Moreover, changes in the perturbation and, thus, in the bandshift indicate changes in the sorption stoichiometry. (iv) The bands of the CH-stretching vibrations of the adsorbed alkanes are found between 2800 cm^{-1} and 3000 cm^{-1} . The integral absorption coefficients of these bands can be derived by relating the integral intensity to the uptake (as determined by gravimetry). The integral intensities normalized by the absorption coefficient are used to derive the coverage/pressure dependancies of the individual adsorbate species. By comparison with the integral intensities of the OH band of the acid sites the sorption stoichiometry can be determined.

By combining the information available from the above techniques, a comprehensive description of the hydrocarbon zeolite interactions, taking into account the localized interactions with the acid site, dispersive forces and sorbate-sorbate interactions, can be made.

2.2 Steady state and transient kinetic experiments

A tubular flow reactor (quartz) was used for the catalytic test reactions. The reaction conditions chosen are described in the experimental sections of corresponding chapters. Figure 2.3 shows the corresponding experimental setup. Two equivalent gas lines lead to a two-way, four-port transient valve (TV). One of the gas streams is connected to the reactor system, the other to the vent. By switching this valve, the connections were reversed, i.e. the second gas stream was connected to the reactor and the first to the vent. In this way pressure transient response experiments could be carried out. A step function in the partial pressure of the reactant (pressure transient) is superimposed using He on one gas stream and the desired reaction gas on

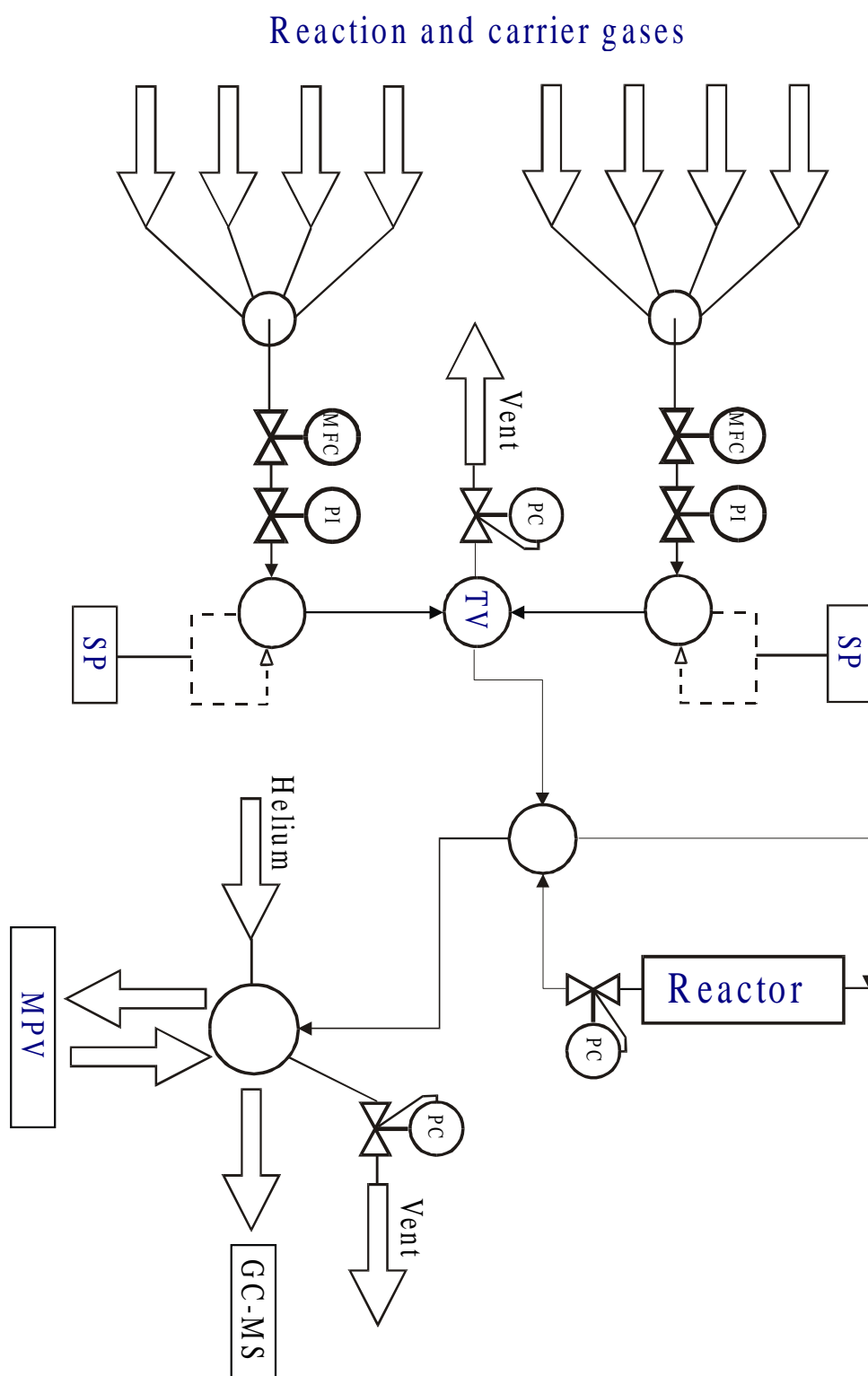


Figure 3. Experimental setup. TV=transient valve, MFC=mass flow controller, SP=syringe pump, PI=pressure indicator, PC=pressure controller, MPV=multiposition gas valve for gas sampling.

the other line. Because the response times of the reaction approaching steady state are far smaller than the time required for GC analysis, two multiposition valves were used to acquire and store samples. The product stream was analyzed by a gas chromatograph (HP 5890) equipped with a flame ionization detector (FID) and coupled to a mass spectrometer (Mass Selective Detector HP 5971 A). The products were separated in a 50 m Chrompack fused silica capillary column (PLOT) with 0.32 mm internal diameter and coated with $\text{Al}_2\text{O}_3/\text{KCl}$ (film thickness= 5 μm). All gas lines were kept as short as possible and dead volumes in the system were minimized. Glass rods were inserted in the reactor tubing up- and downstream of the catalyst bed. These conditions provided fast system response times. Undesired pressure jumps, which are likely to be caused by switching the transient valve, were avoided by providing identical flow rates and pressures in both gas lines.

The product mixture consisted of C_1 to C_8 hydrocarbons. The individual products were identified by the evaluation of the gas chromatographic data of available calibration gas mixtures and confirmation by a mass spectrometer.

A calibration mixture of the products to be detected having different and known concentrations was analyzed. The relative responses of the individual products were normalized to the relative response of the reactant. In this way, relative molar correction factors (RMCF) were determined, which enabled the calculation of mole fractions of each product from the gas chromatographic peak areas (Eq. 2.1). Note, explanations of the symbols used in the equations can be found at the end of the section. The conversions and selectivities were then calculated using Eq. 2.2 and 2.3, respectively.

$$Y_j = A_j \times \text{RMCF}_j / (\sum(A_i \times \text{RMCF}_i)) \quad 2.1$$

$$X = \sum Y_i \times 100 \quad 2.2$$

$$S_j = Y_j / \sum Y_i \times 100 \quad 2.3$$

In most cases, kinetic data are obtained in flow reactors. The mass balance equation for a given reactant (A) in an ideal tubular flow reactor may be represented by equation 2.4

$$F_{A0} \times dX_A = R_A \times dm_{\text{catalyst}} \quad 2.4$$

At high fractional conversions, the reactor is said to be operated in an integral mode, consequently, the rate and kinetic parameters are extracted by the derivation of the conversion against space time data and fitting the experimental result to equation 2.5 [3]

$$R_A = \partial X / \partial (m_{\text{catalyst}} / F_{A0}) = k \times (1-X) / (1+\epsilon X) \times C_{A0} \times a \quad 2.5$$

When fractional conversions are low (< 10 %), there are negligible concentration and temperature gradients along the length of the catalyst bed, hence the reactor is said to be operated in a differential mode. Equation 2.5 then becomes an ordinary algebraic equation and the reaction rates can, thus, be calculated straight from the conversion data as is represented in equation 2.6.

$$R_A = X \times F_{A0} / m_{\text{catalyst}} \quad 2.6$$

The rates of formation of each individual product are thus calculated from equation 2.7

$$R_j = Y_j \times F_{A0} / m_{\text{catalyst}} \quad 2.7$$

The rate of carbon balance is given by equation 2.8. By comparison of the rate of carbon balance to the total rate of conversion, it is possible to estimate the loss due to coke formation on the catalyst. A good mass balance was assumed if the rate of conversion does not differ from the rate of carbon balance by more than 5 %.

$$R_{\text{c-balance}} = 1/n \times [R_{C_1} + 2 \times \Sigma R_{C_2} + 3 \times \Sigma R_{C_3} + \dots + \{n \times \Sigma R_{C_n} - R_{C_{n(\text{feed})}}\}] \quad 2.8$$

Where

- A_j is area of the gas chromatographic peaks of product j
 y_j mole fraction of product
 S_j selectivity to product j (mol %)

X	conversion (%)
k	kinetic rate constant
m_{catalyst}	catalyst weight (g)
a	activity defined as $X/(1-X)$
C_{A0}	initial feed concentration (vol %)
F_{A0}	molar flow rate of A in mol/s
ϵ	volumetric expansion coefficient
R_A	rate of conversion of A (mol/g _{cat} *s)
n	hydrocarbon chain length of feed
$RMCF_i$	relative molar response factor of a product

References

1. Cardone-Martinez, N., and Dumesic, J.A., *Adv. Catal.* **38**, 149 (1992).
2. Hair, L., and Hertl, W., *J. Phys. Chem.* **74**, 91 (1970).
3. Corma, A., Gonzalez-Alfaro, V., and Orchilles, A.V., *Appl. Catal. A* **129**, 206 (1995).

*An IR spectroscopic and isotope
tracer study of site-controlled H/D
exchange over zeolites MFI and BEA*

Abstract

Two reaction pathways for the hydrogen/deuterium exchange of iso- and *n*-butane over zeolites MFI and BEA are proposed both having as key step the dehydrogenation of the alkane. The difference in the apparent activation energies over the two zeolites suggests marked differences in the nature of this step. For H-MFI the absolute rate of H/D exchange increased in parallel with the concentration of Brønsted acid sites. The H/D exchange is suggested to occur *via* the protonation of alkene intermediately formed by protolytic dehydrogenation. For zeolite BEA the Lewis acid sites accelerate the rate of H/D exchange. Lewis acid sites are concluded to facilitate the primary alkane activation by hydride abstraction leading to sorbed hydrogen (atoms) and alkoxy species on the surface. Traces of olefins accelerate the H/D exchange dramatically emphasizing their important role for the H/D exchange of alkanes.

3.1 Introduction

Markedly improved experimental and theoretical methods have led to significant deepening of the understanding of alkane activation over zeolites. This is clearly evidenced in a growing number of papers that provide a detailed insight in two mechanistic routes for activating alkanes over solid acids, i.e. (i) the hydride abstraction from the reacting alkane by Lewis acid sites and surface bound alkoxy groups and (ii) the addition of a proton to the alkane generating a penta-coordinated carbonium ion in the transition state. The first route requires at least two reacting molecules to be involved (bimolecular process [1]), while the latter proceeds monomolecularly [2,3]. Hydrogen-deuterium exchange between alkanes and super acids has been concluded to occur already at low temperatures *via* the direct protonation of σ -bonds in alkanes [4] and the formation of carbonium ions. In contrast to liquid super acids, generation of carbonium ions on zeolites is correlated to high temperatures and low partial pressures of the reactants, conditions under which monomolecular reactions are favored [5,6].

Three different activation energies were found for H/D exchange, monomolecular cracking and dehydrogenation, of *n*-butane on MFI [5,6]. This induced proposing three transition states, for which *ab initio* calculations suggest that all involve pentacoordinated carbon atoms [9]. It is interesting to note that the lowest energy pathway, i.e. the reversible non-reactive protonation (which should lead to H/D exchange provided one of the reaction partners contains deuterium) has been recently suggested to occur *via* the formation of alkenes as reaction intermediates (see papers by Mota *et al.* [7] and Sommer *et al.* [8]). Materials studied were, e.g. sulfated zirconia, H-FAU, H-MFI and H-BEA zeolites. While the product distribution observed (deuterium incorporation did not occur at the tertiary carbon atom) only allows for postulating a carbenium ion intermediate, the mechanistic route to these carbenium ions has not been specified and the implications for tailoring more active catalysts are still unclear. In this context Mota *et al.* showed a remarkably faster H/D exchange on FAU upon dealumination of the parent zeolite indicating a possible role for non-framework aluminum.

Building on these proposals, the aim of the present communication is to quantitatively compare the rates of H/D exchange of two groups of zeolites, i.e. MFI and BEA having markedly different concentration of Lewis acid sites. *In situ* IR spectroscopy, calorimetry and gravimetry

are used as the primary means to characterize the rates of H/D exchange and the nature of interaction between the reacting alkane and the zeolite.

3.2 Experimental

3.2.1 Materials

MFI samples with Si/Al ratios of 35 and 16 were obtained from MOBIL (MFI-1) and Prof. J. Sommer, University of Strassbourg (MFI-2). Sample BEA-1 was obtained from PQ Corporation (806 B-25 LOT #B-12) in the *as-synthesized* form. In order to remove the template and to convert the zeolite to its acidic form, the sample was first heated in dry N₂ (50 ml/min) with 1K/min to 373 K, with 0.4 K/min to 413 K and with 2 K/min to 793 K maintaining it at that temperature for 2 h. Subsequently the temperature was lowered to 573 K. At this temperature, a stream of dry air was passed over the catalyst and the catalyst was again heated with 2 K/min to 793 K at which temperature it was kept for 5 hours. Ion exchange was performed with 1 M NH₄NO₃ at pH = 7 at 323 K using approximately 7 ml liquid per gram solid. The procedure was repeated three times to ensure complete ion exchange. Finally, the sample was washed with distilled water. To eliminate NH₃, the sample was heated in flowing N₂ with 2 K/min to 773 K and kept at that temperature for 2 h.

BEA-2 sample containing slightly larger crystals (synthesized following ref. [19]) was obtained from P. Kunkeler, University of Delft. In order to prepare a sample with a lower concentration of Lewis acid sites, the BEA sample was carefully washed with water until the solution had a pH = 7. Subsequently, the sample was washed once with a 0.025 molar Na₂H₂EDTA solution at room temperature (BEA-2W). This material was evacuated ($p = 10^{-7}$ mbar) and exposed to 10^{-1} mbar H₂O at 823 K for 2 hours (BEA-2M). This treatment was repeated for 12 hours (BEA-2S).

3.2.2 Characterization

NH₃ sorption/desorption in a modified SETARAM TG-DSC 111 apparatus was used to determine the acid site concentration. Approximately 15 mg of sample platelets were charged into the quartz sample holder of the balance. The samples were heated in a vacuum with a temperature increment of 10K/min to 673K and held at that temperature for one hour to desorb water,

subsequently cooled to 373K and exposed to 3 mbar of ammonia. After equilibration, physisorbed ammonia was desorbed at 373K and pressures smaller than 10^{-6} mbar for at least 12 hours. Assuming a stoichiometry of one ammonium ion per acid site, the mass of remaining ammonia normalized to the sample mass was used to calculate the concentration of the acid sites. For extended details of the measurements see chapter 2 and ref. [20]. Temperature programmed desorption (TPD) of ammonia into vacuum was monitored by a BALZERS QMS420 mass spectrometer.

The Si/Al ratios were determined by means of EDAX using a S800 Scanning Electron Microscope from Hitachi Co. equipped with a Kevex Quantum detector Energy Dispersive X-ray system allowing elemental compositions to be determined within an accuracy of 5 % (relative). The instrument had a resolution of 109 eV at 5.9 keV. In order to ensure that the data collected were representative for the whole sample, scans were made at least at five different locations and the average is reported.

^{27}Al -MAS NMR was performed on a multinuclear NMR spectrometer (Varian, Unity WB 400) equipped with a RT CP/MAS probe. The chemical shift was calibrated by using a sample of $\text{Al}(\text{NO}_3)_3 \cdot 9\text{H}_2\text{O}$. The sample was spun with a speed of 10.4 kHz at the magic angle (54.7°) with a pulse width of 0.6 μs for quantification.

FTIR measurements were performed with a BRUKER IFS-88 spectrometer with a spectral resolution of 4 cm^{-1} equipped with a BALZERS QMS420 mass spectrometer and a vacuum cell. The cell consists of a stainless steel chamber equipped with CaF_2 windows and a resistance heated furnace, in which the gold sample holder is placed. The samples were pressed into self-supporting wafers and activated with 5 K/min to 773 K (723 K for BEA-1 and 673 K BEA-2) at 10^{-7} mbar and kept there for an hour, subsequently cooled down with 10 K/min to 373 K. A spectrum of the empty IR cell was used as reference (I_0) to convert the single beam spectra (I) into absorbance spectra $\log(I_0/I)$. The latter were baseline corrected in the region from 3800 to 1300 cm^{-1} . D_2O was dosed in the system (10^{-2} mbar) at 373 K until complete deuteration of the bridging hydroxy groups was observed. The sample was then evacuated at $1 \cdot 10^{-7}$ mbar for at least 2 hours after which olefin-free isobutane was dosed at desired loading. The removal of olefins in isobutane was achieved by passing the as received isobutane 3.5 (99.95 % purity) through a mixture of molsieve 4A and mordenite (1:1 vol%) and checked with GC.

3.2.3 Kinetic experiments

Pressure step transients were performed in a fixed bed tubular quartz reactor with an inner diameter of 5 mm operated in continuous flow mode. 150 mg of catalyst were used for each test. The catalyst was activated in flowing air at high flow rate (40 ml/min, to efficiently remove heat and moisture), at 10 K/min to 773 K. It was held at this temperature for one hour. The reactant gas contained olefin-free isobutane and helium. The reactor effluent was collected by means of an automatic sampling valve system, stored in multi-loop valves and subsequently analyzed by a HP5890 gas chromatograph using a 50 m Al₂O₃/KCl capillary column, equipped with a flame ionization detector and coupled to a mass selective detector HP 5971A.

3.3 Results

3.3.1 Characterization of MFI and BEA samples

The physico-chemical properties of the investigated zeolites are compiled in Table 1. The activated zeolite was equilibrated with pyridine at 10⁻² mbar and 323 K. Complete coverage of

Table 1. Physico-chemical properties of the materials studied.

Catalyst	Si/Al _{total}	C _{total} ^{*1} (mmol/g)	C _{BA} ^{*2} (mmol/g)	C _{LA} ^{*2} (mmol/g)
MFI-1	35	0.42	0.40	0.02
MFI-2	16	0.98	0.95	0.03
BEA-1	15	1	0.66	0.34
BEA-2W	11.6	1.18	1.01	0.17
BEA-2M	11.6	0.92	0.61	0.31
BEA-2S	11.6	0.45	0.12	0.33

*1- determined by ammonia sorption *2-determined by combining data of ammonia and pyridine sorption

all acidic hydroxy groups at about 3610 cm⁻¹ was ensured. Then, the sample was out gassed (p = 10⁻⁶ mbar) to eliminate physisorbed pyridine. The concentration of Lewis and Brønsted acid sites was evaluated using the characteristic bands at 1455 and 1542 cm⁻¹. The molar extinction coefficients for these bands, $\gamma(1455) = 1.5 \mu\text{mol}^{-1}.\text{cm}$ and $\gamma(1542) = 1.8 \mu\text{mol}^{-1}.\text{cm}$, respectively, were taken from ref. [21].

The ²⁷Al- MAS NMR spectrum of the BEA-1 sample indicates the presence of substantial

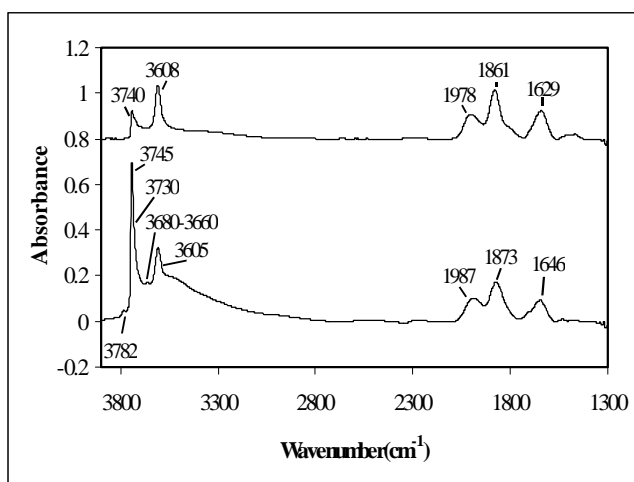


Figure 1a. IR spectra of activated MFI-1 (top) and BEA-1 at 373 K.

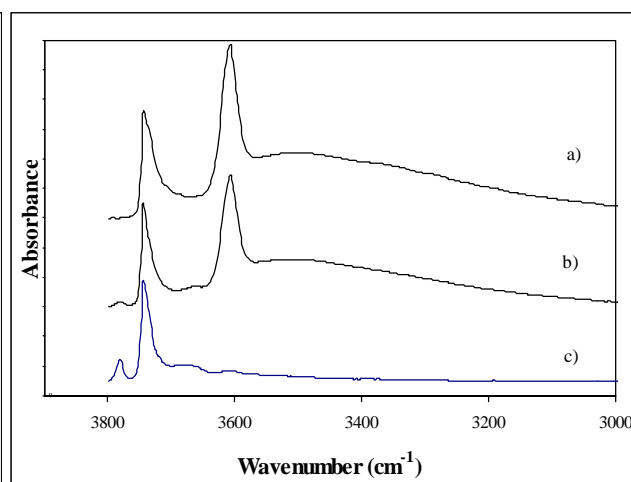


Figure 1b. IR spectra of activated BEA-2W (a), BEA-2M (b) and BEA-2S (c) at 373 K.

concentrations of extra lattice aluminum. In contrast, both MFI samples hardly contained extra framework material as deduced from the MAS-NMR, IR spectroscopy and temperature programmed desorption.

Figure 1a shows the IR spectra of MFI-1 and BEA-1. The IR spectrum of MFI-1 exhibited bands at 3740 cm^{-1} and 3608 cm^{-1} assigned to OH stretching vibrations of terminal (SiOH) and bridging (Si-OH-Al) groups, respectively. Bands at 1978 cm^{-1} , 1861 cm^{-1} and 1629 cm^{-1} are attributed to overtones of the zeolite lattice vibrations. The IR spectrum of activated BEA-1 showed bridging hydroxy groups (3605 cm^{-1}), silanol groups resulting from lattice defects (3730 cm^{-1}), terminal silanol groups (3745 cm^{-1}), hydroxy groups attached to extra frame work alumina species ($3660 - 3680\text{ cm}^{-1}$ and 3782 cm^{-1}) [22]. Note that the latter were also observed for activated γ -alumina [24,25]. Figure 1b shows the IR spectra of BEA-2W, BEA-2M and BEA-2S. Note that the spectrum of activated BEA-2W did not show the band at 3782 cm^{-1} attributed to hydroxy groups of extra lattice alumina. Upon exposure to 10^{-1} mbar H_2O at 823 K for 2 hours, the OH bands at $3660-3680\text{ cm}^{-1}$ increased in intensity, while the band of the Si-OH-Al groups decreased. In parallel, the band of the external silanol group at 3745 cm^{-1} gained intensity at the expense of the band of the internal silanol groups at 3730 cm^{-1} . After repeating the exposure of BEA-2M to 10^{-1} mbar H_2O at 873 K for 12 hours caused the bands $3680-3660\text{ cm}^{-1}$, 3782 cm^{-1} and at 3745 cm^{-1} to increase further at the expense of the bridging OH band. After this treatment only 10 % of the original intensity of bridging OH was preserved.

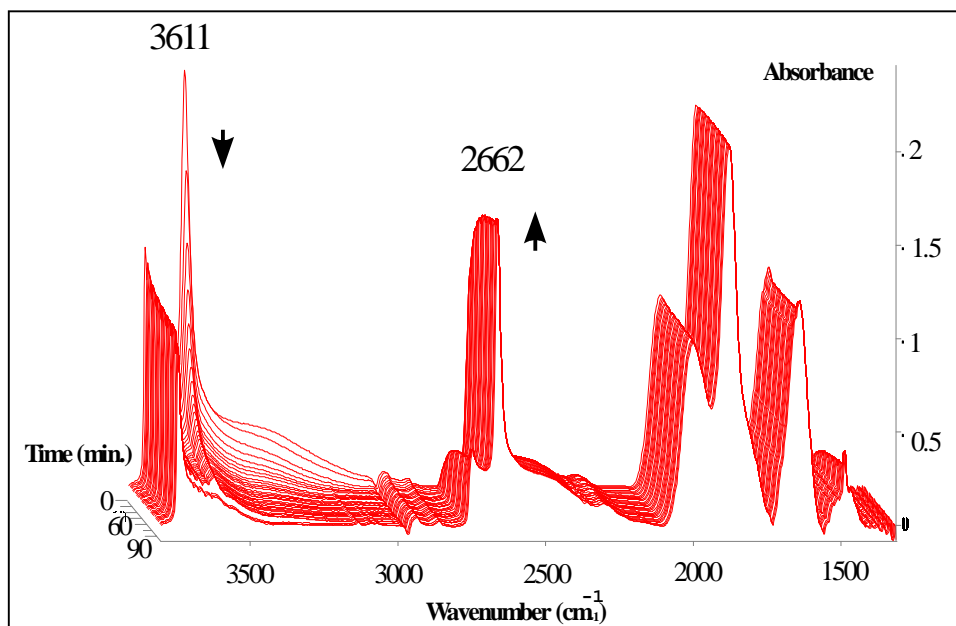


Figure 2. Exchange of bridging Si-OH-Al of MFI-1 with D₂O at 373 K.

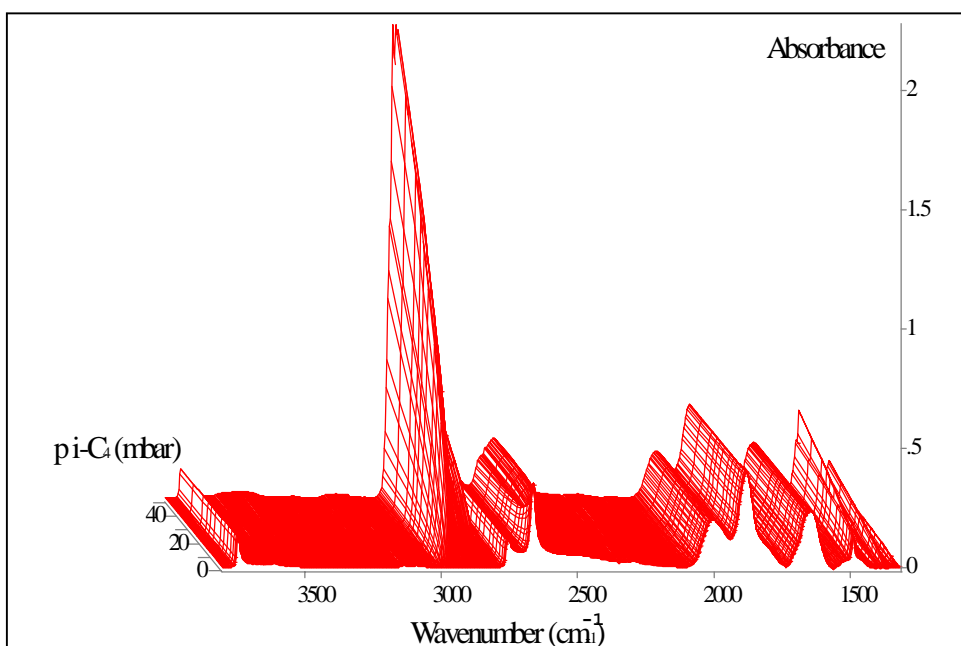


Figure 3. Sorption of purified iC₄ on DMFI-1 at 373 K.

3.3.2 IR spectroscopic study of H/D exchange

3.3.2.1 Results with MFI

Upon admitting D₂O to the activated MFI-1, the OH stretching bands decreased in intensity, while new bands appeared at 2746 cm⁻¹ and 2662 cm⁻¹ (Fig.2) attributed to terminal and bridging OD groups, respectively. Within 70 minutes the bridging hydroxy groups were fully exchanged together with a small fraction of the terminal SiOH groups. Upon admission of gradually increasing

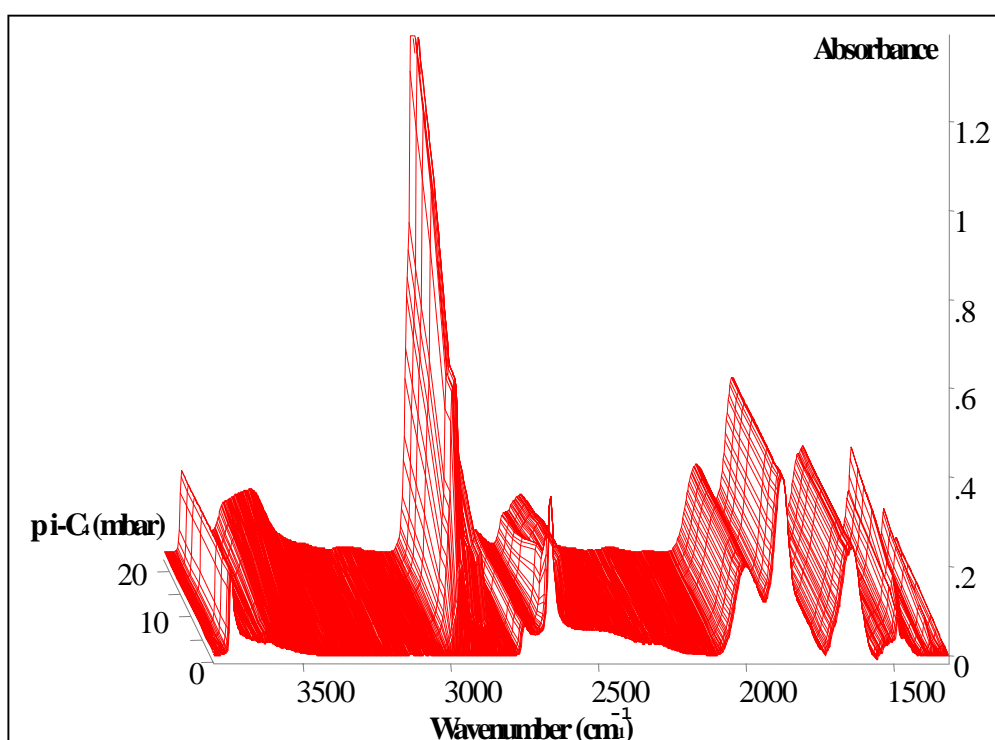


Figure 4. Sorption of non-purified iC_4 on DMFI-1 at 373 K.

amounts of isobutane at 373 K (0.01 - 1000 mbar) the band at 2662 cm^{-1} decreased and a new band at 2589 cm^{-1} appeared suggesting hydrogen bonding of isobutane to the Si-OD-Al groups (see Fig.3).

At 1000 mbar isobutane this resulted in the nearly complete disappearance of the band of free deuterioxy groups. From the intensity of the CH stretching vibrations of isobutane (the bands between 2800 and 3000 cm^{-1}) it was concluded that one molecule of isobutane was adsorbed per deuterioxy group. During this experiment, exchange between the hydrogen of the sorbed isobutane and the deuterium of the bridging deuterioxy group did not take place.

However, when the temperature was raised to 573 K, rapid H/D exchange between isobutane and the deuterioxy groups occurred already at 10^{-1} mbar isobutane. It should be mentioned that rapid exchange took place even at 100 K and 0.1 mbar when non-purified isobutane containing 200 ppm alkenes was used (see Fig 4).

The kinetics of the H/D exchange was determined at 10 mbar isobutane between 423-673 K. The gradual increase of the bridging hydroxy bands (resulting from the exchange of deuterioxy groups by isobutane) was normalized to the concentration of Brønsted acid sites. The intensities of all bands were corrected for the temperature induced change in the extinction coefficients. The rate of increase of the OH intensity and the rate of decrease of the OD intensity corresponded

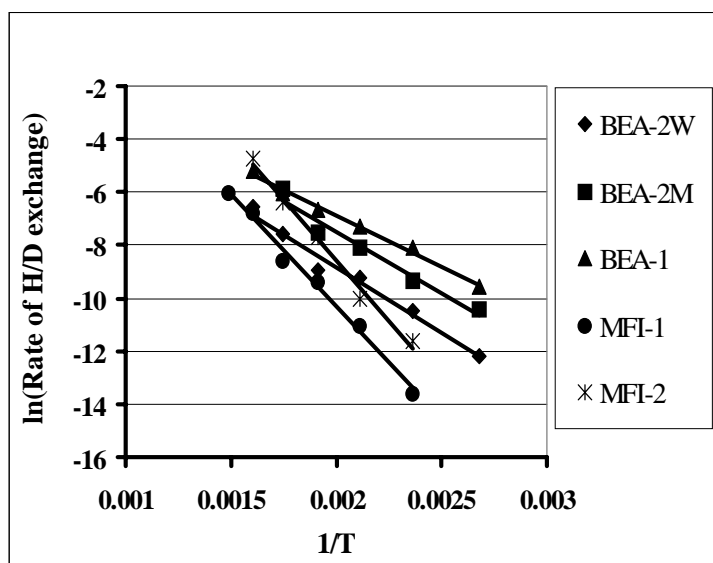


Figure 5. Arrhenius correlations of MFI and BEA samples.

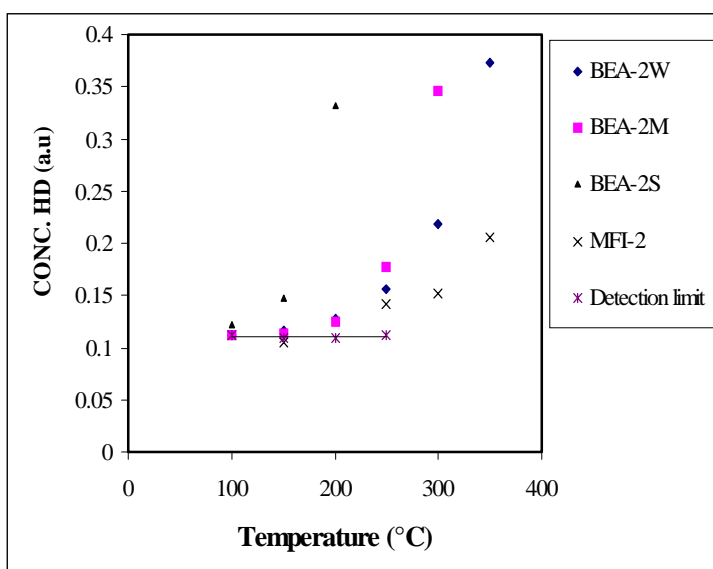


Figure 6. Evolution of HD in the gas phase during H/D exchange.

perfectly. The rates of H/D exchange were calculated from the initial increase in the OH concentration with time. An apparent activation energy of 71 kJ/mol was observed while with MFI-2 (having higher Brønsted acid site concentration than MFI-1) a value of 73 kJ/mol was determined (see Fig. 5). It is important to note that the rates of H/D exchange were strictly proportional to the concentration of Brønsted acid sites. Using the data of these kinetic experiments

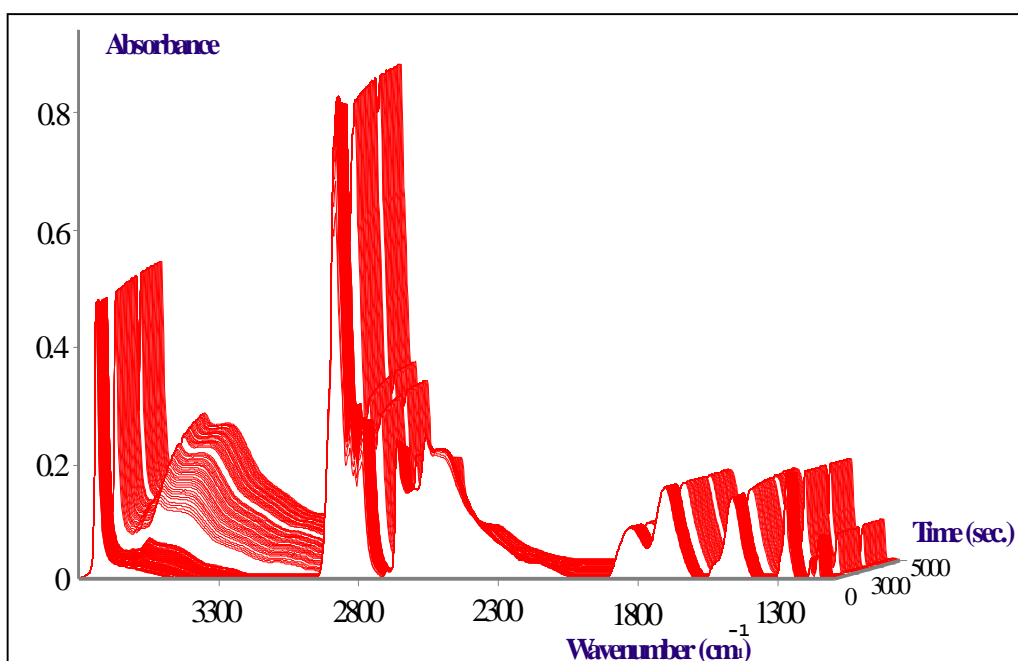


Figure 7. Sorption of purified iC4 on DBEA-1 at 373 K.

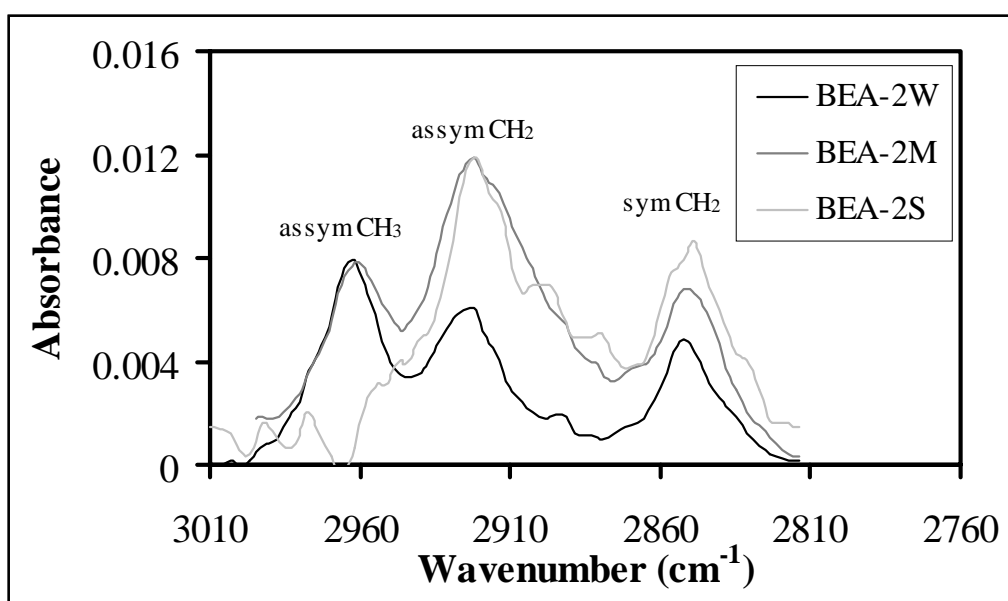


Figure 8. Hydrocarbon left on BEA-2 samples after H/D exchange at 473 K.

one would expect to find approximately 0.3 % exchange at 373 K during the duration of the experiment, which is below the detection limit. Using the spectroscopically calculated coverage of isobutane, the isosteric heat of sorption was determined to be 60 kJ/mol. On line MS gas phase analysis after 2 hours of H/D exchange over MFI-2 (m/e 3 was normalized to m/e 58) showed

significant lower concentrations of HD than observed during reaction over BEA samples (Fig.6).

3.3.2.2 Results with BEA

When the surface functional groups of BEA were exposed to D₂O, the bands attributed to the OH stretching vibrations of BEA-1 decreased in intensity and, in parallel, new bands appeared at 2792, 2753, 2702 and 2661 cm⁻¹. These bands are attributed to stretching vibrations of terminal OD (internal and external SiOD) groups, AlOD and Si-OD-Al groups. After 60 minutes all OH bands disappeared except the band at 3720 cm⁻¹ (attributed to SiOH at lattice defect sites), which exchanged only to an insignificant extent.

The kinetics of the H/D exchange was studied between of 373 - 673 K using 10 mbar isobutane. In contrast to MFI, H/D exchange with isobutane occurred already at 373 K (Fig. 7) at an appreciable rate. An apparent activation energy of 34 kJ/mol was determined (Fig. 5), the isosteric heat of sorption of isobutane was 55 kJ/mol. On line gas phase analysis indicated a nearly exponential increase of HD in the gas phase, which exceeded by far the concentrations observed with MFI-1 (see Fig. 6).

As the two zeolites showed drastically different rates and activation energies of H/D exchange which were not related to the heat of sorption of isobutane, the role of the most differing feature, i.e. the concentration of Lewis acid sites was explored. For that purpose BEA-1 was compared to BEA-2W having a lower Lewis acid site concentration. The rates of H/D exchange were significantly lower than with BEA-1, however, the apparent energies of activation of the two zeolites were identical. When BEA-2W was steamed (BEA-2M) and, after deuteration, subsequently exposed to isobutane the H/D exchange rates were higher than with the parent BEA-2W, similar to those observed with BEA-1. The rates and concentration of HD in the gas phase were similar to the values observed for BEA-1. BEA-2S exchanged hydrogen for deuterium approximately 1.5 times faster than the shorter steamed sample BEA-2M and also the concentration of HD in the gasphase was highest with BEA-2S. It should be noted that a small amount of D₂ was also detected indicating the occurrence of multiple exchange with BEA-2S. It is interesting to note that for steamed BEA, the hydrocarbon species sorbed after H/D exchange and subsequent evacuation at 473 K have the character of larger linear oligomers as concluded from the intensity of the asymmetric and symmetric vibrations of the C-H bands (see Fig. 8).

3.3.3 Pressure step transient experiments

In order to investigate the potential formation of butenes during the experiments outlined and the role of the catalytic and surface chemical routes, the transient response after a step wise increase of isobutane was investigated. For this, a pressure step up of 100 mbar isobutane was realized over the fresh and activated catalysts over a period of 10 minutes after which the feed was switched to He for 5 minutes. Subsequently, the pressure step up and down procedure was repeated. Figure 9 shows the transient response function (normalized to steady state value) of isobutene at 523 K for BEA-1 at a total conversion level of 0.7 mol%. It should be noted that at such low temperatures the reaction pathways will be dominated by secondary reactions as hydride transfer which complicate the analysis of isobutene formed in a primary reaction. For BEA-1 a

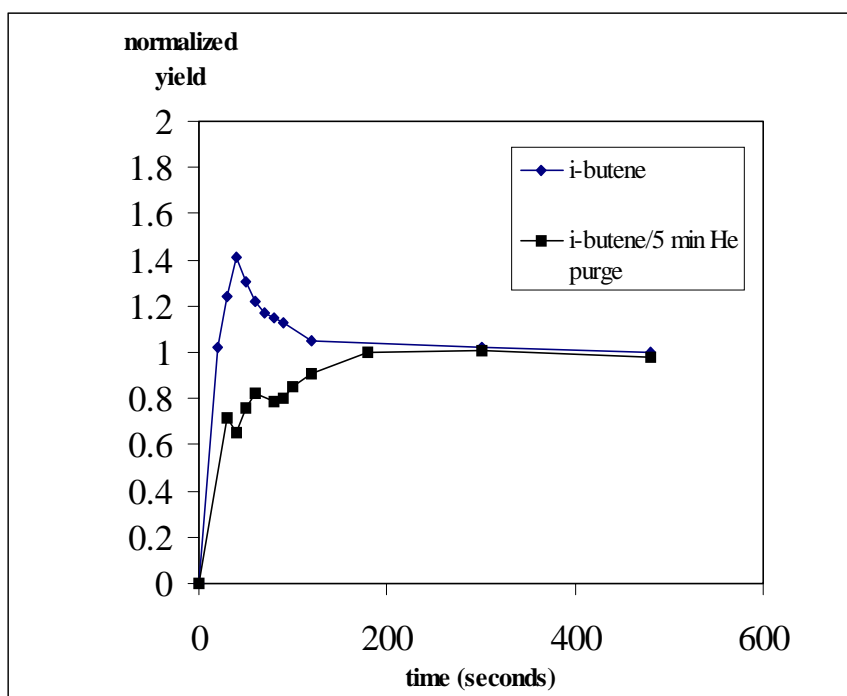


Figure 9. Pressure step transient iC_4 (0 \rightarrow 100 \rightarrow 0 \rightarrow 100 mbar), 523 K, response function dehydrogenation on BEA-1.

1.5 times higher initial amount of isobutene is still observed than at steady state. After a regeneration period of 5 minutes in He this transient dehydrogenation was not observed indicating that hydrogen and/or isobutene initially formed during the first pressure step up resides on the surface. Under the experimental conditions used such transitory behavior was not observed with MFI-1.

3.4 Discussion

Previous work [5,6] in our group addressing the nature and stability of carbonium ions involved in the acid catalyzed monomolecular reactions of *n*-butane suggested that (1) the H/D exchange is the process with the lowest energy of activation, followed by dehydrogenation and cracking; (2) the protonation of the alkane (deprotonation of the zeolite) is close to the transition state of protolytic cracking while it is rather the product desorption for dehydrogenation; (3) hydrogen exchange proceeds stepwise, i.e. only one hydrogen (deuterium) of the substrate is exchanged with one deuterium (hydrogen) in a single catalytic turnover. For elevated temperatures (around 773 K) all three pathways can be rationalized by assuming zeolite stabilized pentacoordinated transition states [5]. The energetics observed and the proposed transition state for H/D exchange with *C_s* symmetry is in accordance with theoretical calculations by Kramer *et al.* [9]. According to these calculations the exchange path where two different oxygen atoms are involved is energetically favored over the one that involves just a single oxygen. Likewise, the substituents in the substrate molecule point favorably outwards. The activation barriers are determined by the energy of the charge separation. This charge separation is provided by compensating interactions between the evolving positive charge on the substrate atom involved in the reaction and a negatively charged oxygen atom of the zeolite around the site of sorption. The energy difference between the hydrogen bound ground state and the hydrogen bound carbonium ion would be substantially positive resulting in a very small equilibrium concentration of the carbocations.

The markedly different activation energies of H/D exchange over MFI and BEA zeolites suggest, however, a different mechanism or rate determining step in H/D exchange over the latter materials. The activation energy found with MFI is substantially higher than with BEA. Summarizing the experimental evidence collected, the H/D exchange over purely Brønsted acidic MFI can be rationalized with the symmetric transition state as proposed by Kramer *et al.* as (1) a higher concentration of Brønsted acid sites leads to higher absolute rates of H/D exchange; (2) the $E_{\text{act,app}}$ for exchange with isobutane is 10-15 kJ/mol lower than the value found for *n*-butane with the same material which is explained with the slightly lower barrier for exchange in the tertiary position; (3) significant lower concentration of HD in the gas phase was found than with BEA; (4) a second transient dehydrogenation pathway was not observed (under the reaction conditions employed).

This reaction pathway is shown in Figure 10.1.

It should be noted that the dominating presence of a symmetric transition state, however, is in contrast with results of Sommer *et al.* on H/D exchange showing that the tertiary methine deuteron did not exchange. Note that our mass spectrometric analysis of the gas phase during the H/D exchange is in line with these results. Taking m/e 16 as a measure for the presence of CH_2D^+ and m/e 15 as a measure of non-deuterated CH_3^+ , it appears that the ratio m/e 16/15 increases already between 423 and 523 K, at temperatures at which methane (also m/e 16) is not produced. As both fragments correlated perfectly with the relative fraction of m/e 44 and 43 for deuterated and non-deuterated propoxy species, the results suggest primarily exchange in the methyl positions. This makes it unlikely that a symmetric transition state is involved in the dominating reaction pathway. More likely, thus, that the transition state resembles the one for protolytic dehydrogenation as presented first by Lercher *et al.* [5] and adopted by Mota *et al.* [10] to explain protolytic dehydrogenation prior to H/D exchange. The observations discussed which are compatible with the symmetric transition state for H/D exchange are not in contradiction with a dehydrogenation model and also allow to rationalize the regiospecific exchange [8] and the presence of HD in the gas phase.

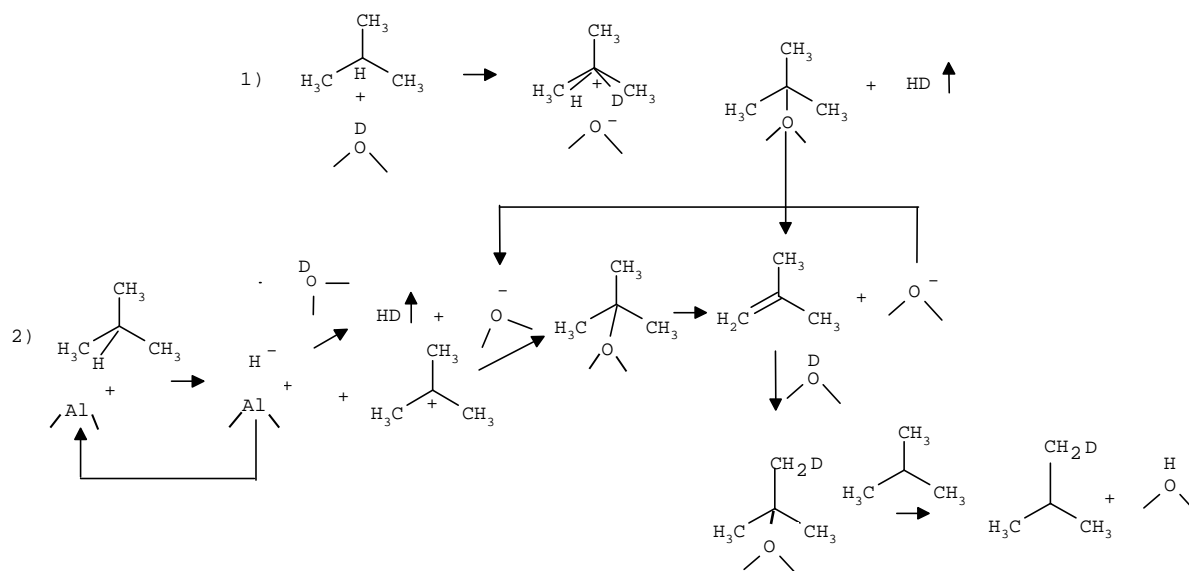


Figure 10. Mechanisms of dehydrogenation and H/D exchange of isobutane.

With BEA, higher concentrations of Lewis acid sites were found to be beneficial for the rate of H/D exchange in accordance with a previous finding [7]. Originally, this was explained

as an increase of the zeolite acid strength. Translated to the present interpretation it suggests that a similar transition state and rate determining step is assumed and the presence of Lewis acidity decreases the activation barrier for forming this transition state. However, ammonia TPD indicates similar Brønsted acid strength for all samples studied. The peak maxima for MFI-1 and BEA-1 differed only by 30 K. As BEA-1 has higher acid site concentration than MFI-1 the slightly higher temperature of the desorption maximum is attributed to readsorption effects leading to a delay in the release of ammonia. Thus, it is concluded that the presence of extra lattice alumina does not lead to a higher acid strength for samples presently studied, but that the Lewis acid-base sites directly take part in the alkane activation.

We propose that the higher rate of H/D exchange is caused by hydrogen abstraction by a Lewis acid site and the simultaneous formation of a butoxy group. Upon desorption as butene another hydrogen atom is left behind and hydrogen adatoms remain initially at the surface (see Figure 10, Scheme 2). The very slow release of these two hydrogens would suggest low mobility of the species or a complex transition state (low transition entropy). Once desorbed the olefin initiates carbenium ion chemistry. As described in abundance previously, this route is much faster (see also the beneficial nature of alkene impurities in the present study) than the activation *via* protolysis on strong Brønsted acid sites.

Alternative (de)hydrogenation mechanisms have been reported before in the literature. It was suggested that at low temperatures sodium cations were the active sites for hydrogen activation during the ethylene hydrogenation in metal-free zeolites while at higher temperatures (723 K) Brønsted acid sites were held responsible for the activity [13]. Moreover, on converting light alkanes on Brønsted acidic H-MFI-1 and H-Y containing Lewis acid sites, the presence of Lewis acidity caused an extended production of dehydrogenation products in the absence of secondary hydride transfer reactions [14,15]. A fraction of the hydrogen produced during the dehydrogenation was seen to remain on the surface and to desorb only slowly. Based on Temkins model of virtual pressure [16] (and adopted by Iglesia [18] and Boudart [17]), the dehydrogenation over EFAL species was thought to occur *via* stepwise removal of hydrogen (in contrast to the protolytic dehydrogenation) with the Lewis acid site acting as a porthole for the recombined hydrogen to desorb. Moreover, pressure step transient kinetic experiments with nC_4 over HY zeolites showed the transient production of butenes (without the release of hydrogen) when monomolecular cracking reached steady state

values. This transient effect was found to be more pronounced with higher concentration of EFAL. These transient response experiments were repeated here with isobutane at lower temperatures which made it difficult to detect the (transient) dehydrogenation route due to secondary reactions of isobutene. Nevertheless, at very low conversions the transient formation of isobutene was clearly observed with H-BEA-1. The sites responsible for the initial dehydrogenation activity could not be regenerated by short purging at reaction temperatures. Gas phase HD produced during H/D exchange which increased with the degree of steaming of H-BEA-2 indicates that the hydrogen formed eventually desorbs. The presence of olefins is also seen directly by *in situ* IR spectroscopy. The olefins oligomerize, however, to larger hydrocarbon fragments.

In agreement with other researchers, we conclude that BEA comprises aluminium in different coordinations, the extent of which can be controlled by temperature and steaming pretreatment. As determined by Kunkeler *et al.* [12] the total Si/Al ratio did not vary among the dry activated and steamed samples. This strongly suggests that part of the loss in Brønsted acid sites is due to aluminium oxide migration toward the ion-exchange positions. It is interesting to note that BEA-1 and mildly steamed BEA-2M had similar behavior in the H/D exchange reactions and similar concentration and nature of acid sites as concluded from IR analysis. This indicates that the calcination procedure of BEA-1 resembles the so-called deep-bed calcination [11]. The water normally liberated during the process apparently led to steaming and caused the formation of aluminium species with a coordination different from that of non-distorted tetrahedral framework Al ions. The 3782 cm^{-1} and 3680 cm^{-1} bands in the IR spectra of the activated samples are associated aluminumoxide species showing Lewis acidity. While the band at 3680 cm^{-1} is attributed to relatively large clusters of aluminum oxide in the pores, the band at 3782 cm^{-1} has controversial assignments. This band is attributed to a transient species by Kiricsi *et al.* [22], as an unusual aluminium site associated with the framework by Beck *et al.* [23], as an aluminium species still connected to the framework by Jia *et al.* [11] and to a distorted tetrahedrally coordinated FAI by Kunkeler *et al.* [12]. It is intriguing, however, to note that this band was reported earlier by Peri *et al.* [24,25] on γ -alumina. However, in the absence of this band (BEA-2W) the $E_{\text{act,app.}}$ resembled the values found for any of the other BEA samples studied. Thus, whatever the nature of this species is, its intensity did not correlate with the relevant Lewis acid sites responsible for hydride abstraction.

3.5 Conclusions

Based on data for isobutane and *n*-butane H/D exchange over zeolites MFI and BEA, two different dehydrogenation pathways preceding hydrogen/deuterium exchange are suggested. The difference in the apparent activation energies for the two zeolites indicates marked variations in the activation of the alkanes. For Brønsted acidic MFI an decrease of the bulk Si/Al ratio and, thus, increase of Brønsted acid sites, results in an increase of the absolute rate of H/D exchange. In agreement with the literature, mass spectrometric analysis indicates the exchange in the primary carbons only. Therefore, the H/D exchange is believed to occur *via* the protonation of alkene intermediates formed by protolytic dehydrogenation. Traces of olefin in the feed were seen to accelerate the H/D exchange stressing the need of rigorously purified feed alkane to study activation of saturated hydrocarbons. In the case of BEA, the presence of Lewis acidity is seen to accelerate the rate of H/D exchange, to increase the amount of HD in the gas phase and to oligomerized butenes. This clearly indicates a reaction pathway with a significant role for the Lewis acid site. The presence of Lewis acidity is concluded to initiate the reaction by activating the alkane *via* hydrogen abstraction and formation of alkoxy species. This is suggested to be a transient effect. The alkoxy group decomposes into hydrogen and an olefin which is readsorbed and protonated on Brønsted acid sites initiating well-established carbenium ion chemistry.

Acknowledgment

Dr. Paul Kunkeler is gratefully acknowledged for synthesis of the BEA-2W sample, Prof. Jean Sommer and Drs. Jeroen van Bokhoven for fruitful discussions.

References

1. Kwak, B.S., and Sachtler, W.M.H., *J. Catal.* **145**, 456 (1994).
2. Gates, B.C., Katzer, J.R., and Schuit, G.C.A., in "*Chemistry of Catalytic processes*", McGraw-Hill, New York, 1979.
3. Haag, W.O., and Dessau, R.M., *Proc. 8th Int. Congr. On Catalysis*, Vol. 2, Berlin 1984, Dechema Frankfurt, 1984.
4. Olah, G.A., Prakash, S.K., and Sommer, J., in "*Superacids*", Wiley, New York, 1985.

5. Lercher, J.A., Van Santen, R.A., and Vinek, H., *Cat. Letters* **27**, 91 (1994).
6. Narbeshuber, T., Stockenhuber, M., Brait, A., Seshan, K., and Lercher, J.A., *J. Catal.* **160**, 183 (1996).
7. Mota, C.J.A., and Martins, R.L., *J. Am. Chem. Soc.* 171 (1991).
8. Sommer, J., Hachoumy, M., Garin, F., Barthomeuf, D., and Vedrine, J., *J. Am. Chem. Soc.* **117**, 1135 (1995) and references therein.
9. Kramer, G.J., and Van Santen, R.A., *J. Am. Chem. Soc.* **117**, 1766 (1995).
10. Mota, C.J., Menezes, S.C., Nogueira, L., and Kover, W.B., *Appl. Catal. A* **146**, 181 (1996).
11. Jia, C., Massiani, P., and Barthomeuf, D., *J. Chem. Soc. Faraday Transactions* **89**, 3659 (1993).
12. Kunkeler, P.J., Zuurdeeg, B.J., Van der Waal, J.C., Van Bokhoven, J.A., Koningsberger, D.C., and van Bakkum, H., *J. Catal.* **180**, 234 (1998).
13. Kanai, J., Martens, J.A., Jacobs, P.A., *J. Catal.* **133**, 527 (1992).
14. Narbeshuber, T., Brait, A., Seshan, K., and Lercher, J.A., *J. Catal.* **172**, 127 (1997).
15. Narbeshuber, T., Brait, A., Seshan, K., and Lercher, J.A., *Appl. Catal. A* **146**, 119 (1996).
16. Temkin, M.I., and Pyzhev, V., *Acta Physicochim.* **12**, 237 (1940).
17. Boudart, M., *J. Phys. Chem.* **87**, 2786 (1983); Boudart, M., *Ind. Eng. Chem. Fund.* **25**, 70 (1986).
18. Iglesia, E., Baumgartner, J.E., and Price, G.L., *J. Catal.* **134**, 549 (1992).
19. Wadlinger, R.L., Kerr, G.T., and Rosinsky, E.J., *U.S. Patent* 3,308,069, 1967.
20. Eder, F., Stockenhuber, M., and Lercher, J.A., *Stud. Surf. Sci. Catal.* **97**, 495 (1995).
21. Khabtoui, S., Chevreau, T., and Lavalley J.C., *Microp. Mater.* **3**, 133 (1994).
22. Kiricsi, I., Flego, C., Pazzuconi, G., Parker, W.O. Jr., Millini, R., Perego, C., and Bellusso, G., *J. Phys. Chem.* **98**, 4627 (1994).
23. Beck, L., Haw, J.F., *J. Phys. Chem.* **99**, 1076 (1995).
24. Peri, J.B., *J. Phys. Chem.* **69**, 211 (1965).
25. Peri, J.B., *J. Phys. Chem.* **69**, 220 (1965).
26. Weitkamp, J., Traa, Y. in “*Handbook of heterogeneous catalysis*”, Vol. 4, Ertl, G., Knozinger, H., Weitkamp, J., eds., VCH Verlagsgesellschaft mbH, Weinheim, 2039 (1997).
27. Nivarthi, G.S., He, Y.J., Seshan, K., and Lercher, J.A., *J. Catal.* **176**, 192 (1998).

On the Role of Adsorption Effects for the Enhanced Activity of Dealuminated Mordenite Catalysts in the Conversion of Light Alkanes

Abstract

A series of mordenites (with Si/Al_f ranging between 6 and 52) was prepared by acid leaching and steam dealumination and characterized by using different physico-chemical methods and adsorption of light alkanes. The main incentive here was to understand how structural changes brought about by dealumination affect sorption behavior and catalytic activity. Dealumination was found to increase the accessibility of acid sites, as a consequence, resulting in higher activity in both *n*-butane cracking and *n*-hexane hydroisomerization. Adsorption data of light alkanes show that the enhanced activity upon dealumination of mordenite is favorably explained by the increase of the pore size of the side pockets to an intermediate size between 8MR and 12MR making them accessible to *n*-alkanes. The sorption environment in the side pockets constitute higher energy of adsorption compared to the larger 12MR (main) channels and their acid sites appear to be of higher acid strength. This results in lower reaction barriers for the formation of carbocations explaining the higher activity. No experimental evidence on the theoretical concept of the acidity of mordenite was found.

4.1 Introduction

At present, dealuminated mordenite zeolites are extensively used as catalytically active components in hydroisomerization catalysts [1]. Generally, it is well accepted that acidity of zeolites govern their activity, explaining why many studies have been devoted to the determination of the nature, the number, and the strength of acid sites [2,3].

Brønsted acidity is concluded to be very complex and depends on many factors such as the local environment (chemical composition and structure): the T-O-T angle and the density of acid sites are among the most important factors. Additional complexity in the acidic nature of zeolites is caused by their metastability transforming zeolites at higher temperatures into dense silica phases. This will proceed by breaking the most labile bonds first (which are Si-O-Al) leading to a partial dealumination of the zeolite structure. Steam greatly enhances the rate of this T-O-T bond cleavage and removes tetrahedrally coordinated aluminum from the lattice, which reduces the concentration of Brønsted acid sites [4] creating extra-framework Al (EFAL). The leached alumina species can remain in the micropores and may affect the catalytic activity. The possible influence ranges from action as a Lewis acid that activates alkanes [5,6,7], interactions with Brønsted acid sites enhancing their catalytic activity [8,9], replacement of the proton of Brønsted acid sites and neutralizing the acid site [10] to the formation of large clusters of amorphous alumina species (or alumina/silica species) that block the access to certain micropores [11].

While all these issues should be taken into account upon dealing with mordenite (MOR) zeolite, additional complexity respective to the accessibility of acid sites results from the unique morphology of MOR. MOR has a pore structure consisting of main straight channels in the *c* direction having a slightly elliptical cross-section 0.67×0.70 nm (12-membered rings) and secondary channels (side pockets) in the *b* direction with a 0.26×0.57 nm aperture (8-membered ring channels) [12]. The diameter of these side pockets prevents most molecules to interconnect the main channels. It has been shown [13] that even small linear alkanes do not enter the side pockets and only sorb in the main channels. More basic molecules, like ammonia, amines, or alcohols sorb on all acid sites, provided their size allows it.

Most authors address the nature of the acidity of mordenite and the accessibility to acid sites in order to explain catalytic activity. Springuel-Huet *et al.* [14], using ^{129}Xe -NMR, report a selective modification of the side-pockets by steam dealumination increasing its internal volume. This modification of the side-pockets enhances the accessibility to larger molecules as well. Also, a larger accessibility after dealumination due to the generation of mesopores is reported [15].

Adsorption of basic probe molecules and observation with spectroscopic and thermoanalytic methods is generally applied to determine acid strength. Ammonia TPD, for example, is often applied. Generally, the temperature of desorption maxima are related to the acid strength [16, 17]. An important argument against this method is that a decrease in acid site concentration also leads to less retention of ammonia in the micropores resulting in a lower temperature of desorption. The desorption maxima therefore reflect the adsorption – desorption equilibrium of ammonia instead of acid strength [18]. Calorimetry of sorption of strong bases should provide more accurate information on the acid strength [19]. Usually the heat of sorption of ammonia versus coverage shows initially stronger acid sites after dealumination. However, the possible sorption on Lewis acid sites, which shows a higher heat of sorption, is easily ignored. Also, dealumination may affect the inherent structure of zeolites, e.g. generating mesopores, resulting in differences in confinement and thus stabilization energy of the basic probe molecules in the pores, which eventually renders different strength of interaction.

Notwithstanding the usual good analogy between theoretical and experimental definitions of acidity and their correlation with catalytic activity [19], another elegant approach would be to explore possible differences in the sorption characteristics (e.g. strength of interaction) of hydrocarbons in mordenite upon dealumination and compare the same hydrocarbons in their catalytic reactions on the same materials. The weak basicity of the alkane (the heat of sorption comprises only about 10 kJ/mol from the dipole-induced acid-base interaction) may not be sufficient to render small and subtle differences in the strength of the acid sites. However, this also means that such subtle site strength heterogeneity may not be important for explaining catalytic activity of the weak base (alkane).

Conceptually, tighter bound surface complexes results in higher coverage and could eventually lead to a higher concentration of carbenium ions and a change in the micro kinetics

of acid catalyzed reactions (note e.g. Temkin's relation on coverage and activation energy [21]). Experimental work demonstrate that cracking of alkanes obeys Temkin's equation and is primarily governed by adsorption of the alkane [29, 34].

Building on these proposals, the present contribution presents a gravimetric and calorimetric study of light alkane sorption on (dealuminated) mordenites together with thorough physico-chemical characterization of the materials. Differences in activity in (hydro-) isomerization of *n*-hexane and monomolecular cracking of *n*-butane are discussed in view of structural changes caused by chemical leaching and steaming. The choice of the probe reactions allows studying the formal interaction between an alkene, and an alkane with the zeolite framework, respectively.

4.2 Experimental

4.2.1 Catalysts

Mordenite samples in the hydrogen form were obtained from BP-Amoco and are commercially available. These samples are listed in table 1 together with the coding we will refer to in the sequential sections. CBV30a was subsequently steamed at different conditions as is listed in table 1.

Table 1. Sample coding

Sample	Pretreatment	Pp H ₂ O (Torr)	time (hours)	Coding
LZM-5	none	-	-	PMOR
CBV30a	Chem. Leached	-	-	LMOR
-	Steamed	50	1	LS501
-	Steamed	100	1	LS1001
-	Steamed	200	1	LS2001
-	Steamed	300	1	LS3001
-	Steamed	400	1	LS4001
-	Steamed	700	1	LS7001
-	Steamed	400	24	LS40024

Dealuminated H-mordenite (HMOR) with a $\text{SiO}_2/\text{Al}_2\text{O}_3$ ratio of 20 (provided by the Japanese Catalytic Society; JRC-HM20) was also used in this study as a reference material. This sample was previously studied [20, 23]. A very detailed characterization of the material is also given in ref. [24].

4.2.2 Microcalorimetry and gravimetry

The gravimetric and calorimetric measurements were performed in a modified SETARAM TG-DSC 111 instrument (see Chapter 2).

Hydrogen form MOR was heated in vacuum with a temperature increment of 10K/min to 673K and held at that temperature for one hour to desorb water and traces of other sorbed substances. After activation the system was cooled to 323 K. Subsequently, the alkanes ($\text{C}_3 - \text{C}_6$) were discontinuously dosed into the closed system and equilibrated with the surface. The equilibration was assumed when no changes in the heat flow and the uptake could be observed. The adsorption isotherms of all the hydrocarbons were determined gravimetrically together with the differential enthalpies of adsorption. The isotherms were fitted with a sum of Langmuir type adsorption isotherms, describing local adsorption at the acid sites and intermolecular interactions. The equilibrium constants and the directly measured enthalpies were used to calculate the Gibbs free energies and the entropies of sorption, respectively.

To allow for a correlation of the uptake with the total amount of acid sites in the acidic samples, the concentration of the acid sites was determined by adsorption/desorption of ammonia. For this, the samples were activated as outlined above, cooled to 373 K and exposed to 3 mbar of ammonia. After equilibration, ammonia was desorbed for at least 12 hours at 373 K and at pressures smaller than 10^{-6} mbar. Assuming a stoichiometry of one ammonium ion per acid site, the mass of remaining ammonia normalized to the sample mass was used to calculate the concentration of the acid sites, the estimated error being $\pm 5\%$.

4.2.3 IR Spectroscopy

FTIR measurements were performed on a BRUKER IFS-88 spectrometer equipped with a flow cell and a vacuum cell. Approximately 3 mg of the *ex situ* pre-calcined samples were

pressed into self-supporting wafers (see chapter 2 for details). The samples were activated in a stream of helium at 673 K in order to remove moisture and measured under helium flow. A spectrum of the empty IR cell was used as reference (I_0) to convert the single beam spectra (I) into absorbance spectra ($\log I_0/I$). The latter were baseline corrected in the region from 3800 to 1300 cm^{-1} . To correct for the varying sample thickness of the different wafers, the spectra were normalized by the integral intensity of the overtones of the lattice vibrational bands at 1972 and 1865 cm^{-1} .

The activated zeolite was equilibrated with pyridine at 6 mbar and 473 K. Then, the sample was outgassed ($p = 10^{-6}$ mbar) to eliminate physisorbed pyridine. The concentration of Lewis and Brønsted acid sites was evaluated using the characteristic bands at 1455 and 1542 cm^{-1} , respectively. The molar extinction coefficients for these bands, $\gamma(1455) = 1.5 \mu\text{mol}^{-1}\text{cm}$ and $\gamma(1542) = 1.8 \mu\text{mol}^{-1}\text{cm}$ were taken from ref. [25]. The integrated intensities of a band characteristic for pyridinium ions and the decrease in the intensity of the hydroxyl bands were used to determine the fraction of Brønsted acid sites accessible.

Alkane sorption was studied at 323 K between 0.02 and 25 mbar. The self-supporting sample wafers were activated in the same way as in the TGA/DSC experiments.

4.2.4 Kinetic experiments

n-Butane cracking experiments were performed in a tubular quartz reactor operated in continuous flow mode. All catalysts were activated in flowing air by heating at 10 K/min to 823 K and holding this temperature for 1 hour. *n*-Butane cracking was carried out using 1 % *n*C₄ in helium, at 1 bar and 773 K. The samples were diluted with quartz to minimize the pressure drop across the catalyst bed. The reactant mixture was passed over the catalyst at 4 different WHSV values and a least square fit was used to calculate first order reaction constants. The activity of the catalysts was monitored as a function of time on stream between 10 and 60 min. The reactor effluent was collected on-line and analyzed by gas chromatography with a flame ionization detector.

n-Hexane hydroisomerization was performed in a tubular quartz reactor operated in continuous flow mode at 3 bar total pressure and an H_2/nC_6 of 9. Pt (2 wt%) was incorporated by ion exchange from a solution of $\text{Pt}(\text{NH}_3)_4(\text{OH})_2$ (according to the standard procedure). The

catalysts were calcined at 823 K *ex situ* and reduced *in situ* at 823 K for 1 hr in hydrogen flow (35 ml/min) before being used. The samples were diluted with quartz. WHSV was varied in order to study the catalysts at a similar conversion level of 1 %. The reactor effluent was collected on-line and analyzed by gas chromatography (HP 5890 with a 50 m Al₂O₃/KCl column, flame ionization detector). External mass transfer limitation was checked for by changing the flow rate at constant space time and found to be absent under the present conditions.

The dispersion of the Pt for the Pt-loaded samples was determined by volumetric hydrogen chemisorption (see ref. 20 for details) to be between 30 - 40 %. EXAFS analysis showed coordination numbers between 6.5 and 7, characteristic for particle sizes around 1.2 nm.

4.3 Results

The physico-chemical characteristics of the materials studied are shown in Table 2. Figure 1 shows the accessibility of the MOR structure to ammonia (obtained using the Insight II program from Biosym/MSI) revealing main channels and side pockets.

4.3.1 IR Spectroscopic study of mordenite samples

Figure 2 represents spectra of activated samples in the absorbance mode at 373 K.

The IR spectrum of PMOR (2a) exhibited bands at 3744 cm⁻¹ and 3607 cm⁻¹ assigned to OH stretching vibrations of terminal (SiOH) and bridging (Si-OH-Al) groups, respectively. Also, a significant asymmetry at about 3660 cm⁻¹ suggests the presence of some aluminum clusters in an extra frame work position. The bridging OH at 3607 cm⁻¹ has been frequently reported to exist of two contributions, 3612 cm⁻¹ and 3585 cm⁻¹ (at room temperature), assigned to OH groups in the main channels and side pockets, respectively. It is interesting to note that during dealumination the maxima of the Si-OH-Al centered around 3607 cm⁻¹ did not shift to any significant extent indicating the synchronous extraction of aluminum out of the main channels and the side pockets. Upon leaching the sample (2b), which reduced the total amount of aluminum, the band at 3607 cm⁻¹ significantly decreased in intensity and other bands at slightly higher wavenumbers, i.e. 3660 - 3695 cm⁻¹ appeared, indicating the presence of large alumina clusters (hydroxy groups attached to extra frame work alumina species). Also the band attributed

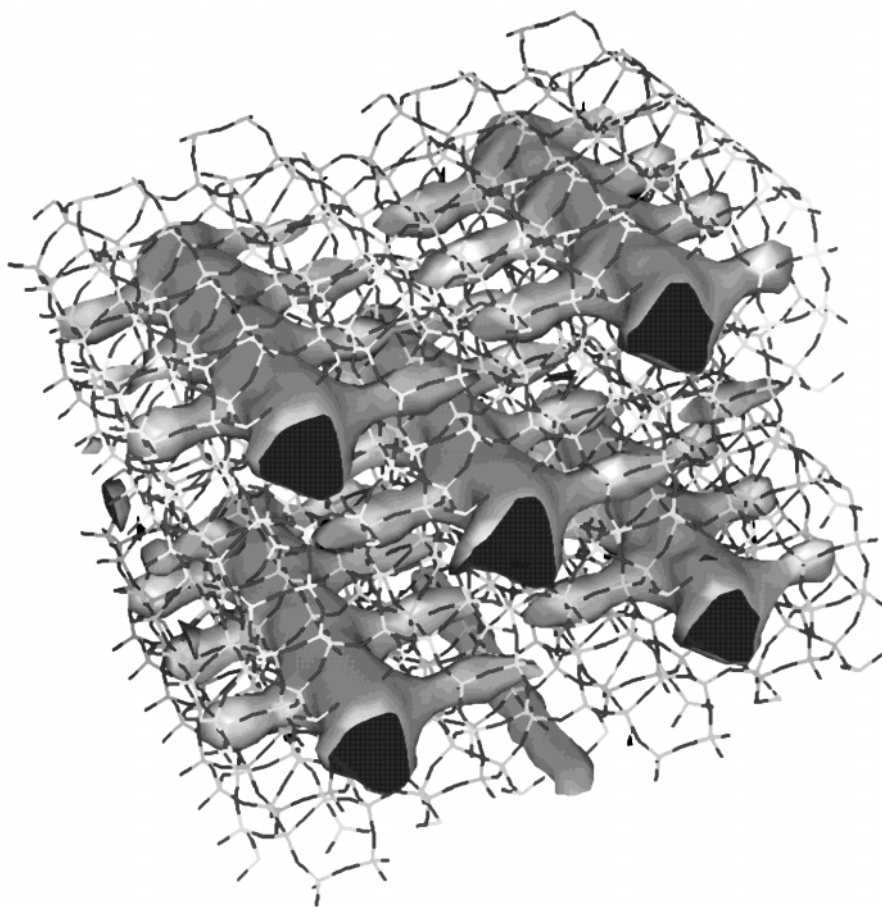


Figure 1. MOR structure and accessibility for ammonia (dark region).

to terminal SiOH tremendously increased in intensity and was broadened revealing the maximum at slightly lower wavenumber 3730 cm^{-1} . Hence, this suggests the presence of silanol groups resulting from lattice defects [26]. A broad background absorption is also observed in the whole $3700\text{--}3400\text{ cm}^{-1}$ region. Several authors [26, 27] have pointed out that during partial dealumination (which generates extraframework species) small hydroxylated cavities (nests) are created. Hydrogen-bonded silanol nests are probably responsible for the broad structureless absorption in this region. Steaming the sample at 100 torr for 1 hour decreased the extend of the hydrogen bonded species due to apparent healing of defect sites (maximum of the SiOH blueshifts). Also, the bridging OH groups still decreased. Enhanced severity of the steaming conditions simply pronounced these effects, resulting in a reduction of silanol groups affiliated with lattice defects and the presence of only a marginal concentration of bridging OH groups for the severest steamed sample (2c-e).

Figure 3 shows the difference IR spectra obtained for pyridine sorption in time at 473 K. Upon admittance of pyridine to PMOR, the band at 3740 cm^{-1} disappeared (all SiOH are fully accessible) while the band of bridging OH groups at 3603 cm^{-1} disappeared only in part. Approximately 40 % of the Brønsted acid sites were concluded to interact. The strong and broad absorption band between 3300 and 2000 cm^{-1} indicates moderately strong hydrogen bonding of pyridine. The skeletal combination modes (overtones of the lattice vibrations) shifted to slightly lower wavenumber upon exposure to pyridine. Ring vibration bands were observed at $1640, 1623, 1600, 1547, 1494, 1456, 1446$ and 1384 cm^{-1} . Comparing these bands with the wavenumbers reported by Glazunov *et al.* [28] they were assigned to ring stretching modes ($1640, 1623, 1547$, (PyH^+), $1600, 1491$ (PyL)). The band at 1547 cm^{-1} serves as a characteristic band for quantifying pyridinium ions (PyH^+).

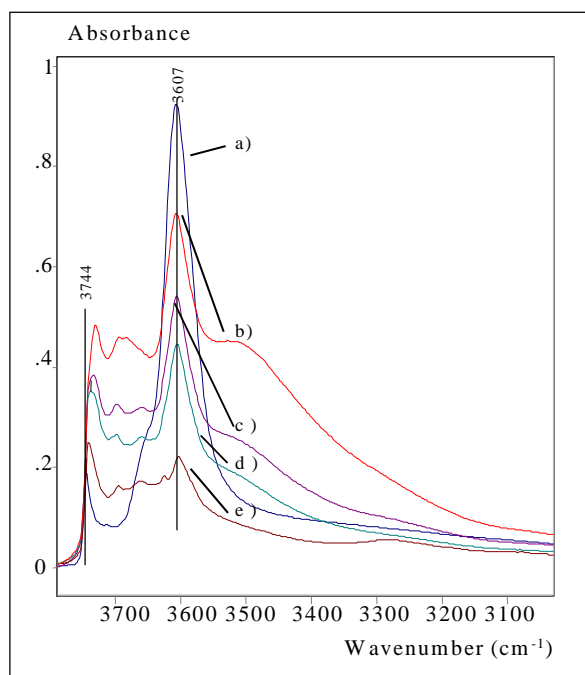


Figure 2. IR spectra of activated samples in the absorbance mode at 373 K; a) PMOR b) LMOR, c) LS1001 d) LS4001 and e) LS40024.

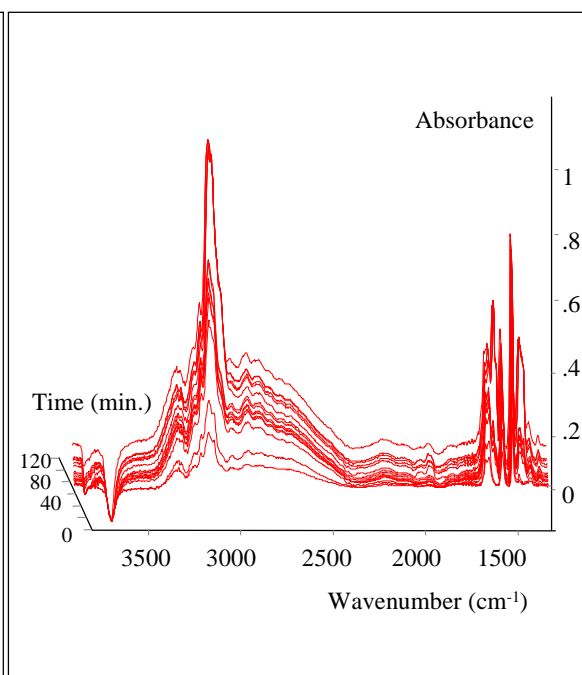


Figure 3. Difference IR spectra of pyridine sorption on PMOR at 473 K.

To quantify pyridine adsorbed coordinatively to accessible Al^{3+} cations (PyL) the band at 1456 cm^{-1} , and for physisorbed pyridine the band at 1446 cm^{-1} were used. The latter disappeared completely after desorption in a stream of helium at 473 K. After correction is made

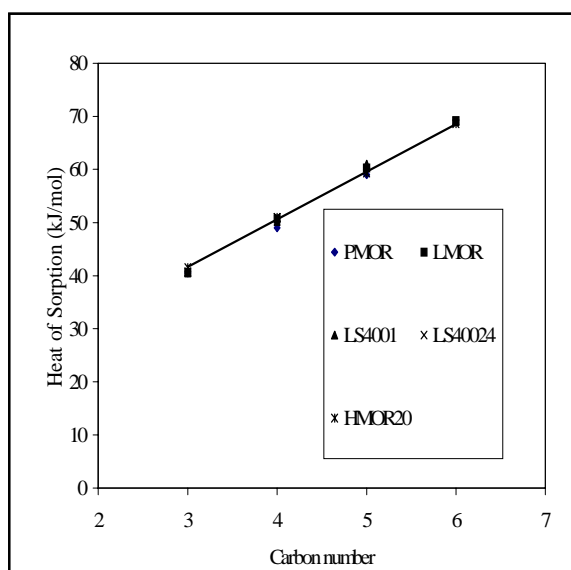


Figure 4. Heat of sorption of as a function of the carbon number for localized sorption at 323 K.

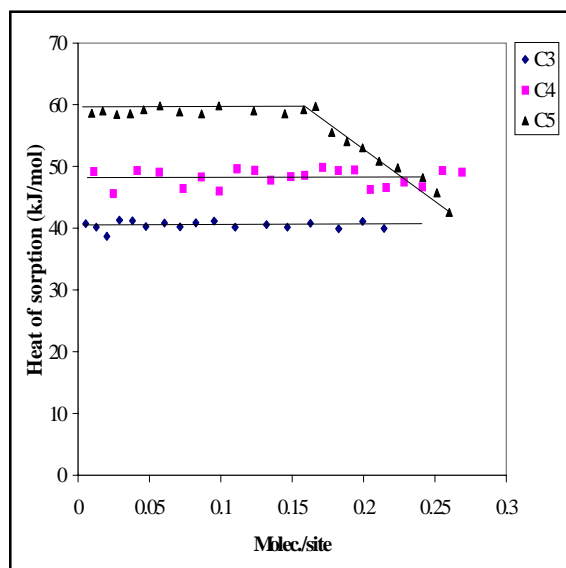


Figure 5. Heat of sorption versus coverage at 323 K on PMOR.

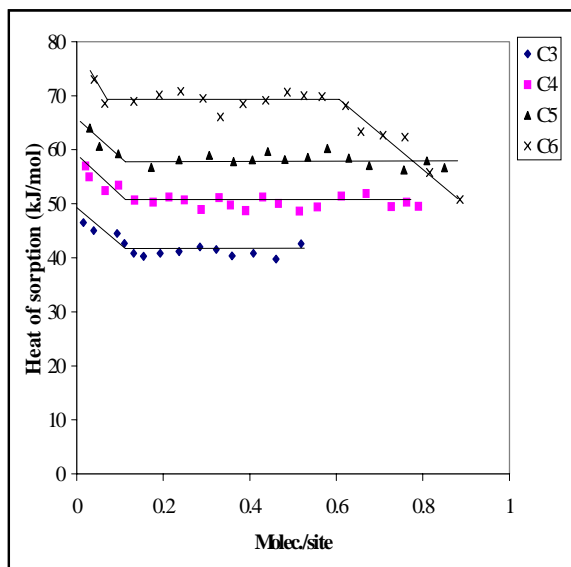


Figure 6. Heat of sorption versus coverage at 323 K on LMOR.

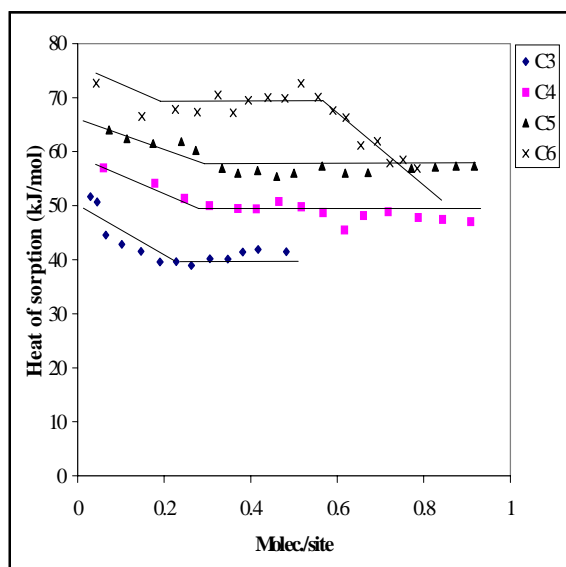


Figure 7. Heat of sorption versus coverage at 323 K on L4001.

for the extinction coefficients only a marginal concentration of Lewis acid sites is detected (see Table 2). The leached sample rendered bridging hydroxy groups readily accessible to pyridine resulting in the complete disappearance of this group after roughly 10 minutes. The percentage of Lewis acid sites as well as their absolute concentration was higher than for the parent sample. Increasing the degree of steaming led to a further increase of the concentration of Lewis acid

On the role of adsorption effects.....

Table 2. Physico-chemical characterization of the mordenite samples

	BET (m ² /g)	Micro pore vol. (cm ³ /g)	Meso poreVol. (cm ³ /g)	Ext. Area (m ² /g)	Si/Al ¹	Si/Al ²	nPA (mmol/g) ⁴	iPA (mmol/g) ⁵	Al/u.c ²	FAL (mmol/g) ²	NH ₃ (mmol/g) ³	BA (mmol/g) ⁶	LA (mmol/g) ⁶
PMOR	525	0.19	0.04	24	6.0	5.74	2.12	1.47	7.12	2.11	2.25	2.21	0.04
LMOR	584	0.20	0.11	90	20.2	15.5	1.12	1.10	2.9	0.96	0.74	0.68	0.06
LS501	573	0.19	0.11	98	20.3	nd.	nd.	1.00	nd.	0.87	0.72	0.64	0.07
LS1001	604	0.21	0.10	93	20.2	13.2	nd.	0.85	3.37	1	0.71	0.62	0.10
LS2001	594	0.21	0.09	73	20.3	13.7	nd.	1.05	3.24	1.04	0.71	0.61	0.11
LS3001	593	0.20	0.12	89	20.2	13.3	nd.	0.78	3.35	0.99	0.64	0.54	0.10
LS4001	602	0.21	0.11	92	20.2	15.6	0.80	0.79	2.9	0.85	0.58	0.48	0.10
LS7001	588	0.20	0.11	99	20.2	35.2	nd.	0.65	1.32	0.33	0.48	0.35	0.13
LS40024	588	0.18	0.15	119	20.3	52.5	0.50	0.51	0.9	0.27	0.34	0.20	0.14

1- XRF, 2-²⁹SiNMR, 3- ammonia adsorption, 4- n-propylamine TPD, 5- i-propylamine TPD, 6- pyridine adsorption/desorption, nd = not determined

sites at the cost of the Brønsted acid sites (see Table 2). The total amount of acid sites also decreased significantly with degree of steaming. The number of strong Brønsted acid sites determined with pyridine sorption were used to determine sorption capacity of light alkanes in terms of molecules per Brønsted acid site.

4.3.2 Sorption of light alkanes

Figure 4 shows the heat evolved during sorption of propane, *n*-butane, *n*-pentane and *n*-hexane on non-dealuminated PMOR, LMOR, LS4001 and LS40024 in dependence on the carbon number. The values are the averaged values for local sorption at the majority of the Brønsted acid sites at low coverage. The heats of sorption increased linearly with the chain length of the

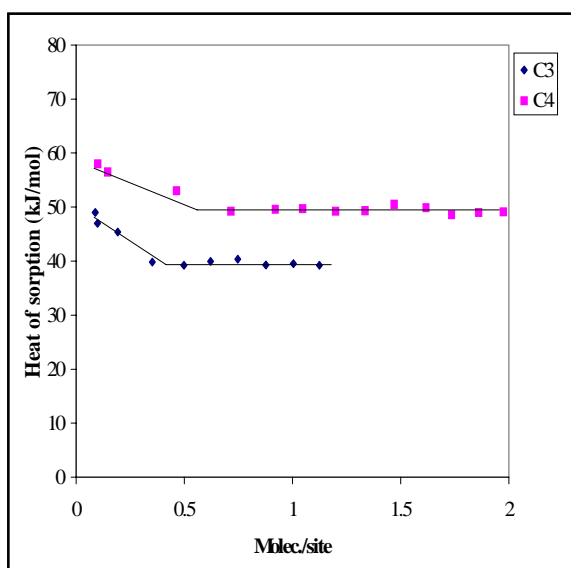


Figure 8. Heat of sorption versus coverage at 323 K on LS40024.

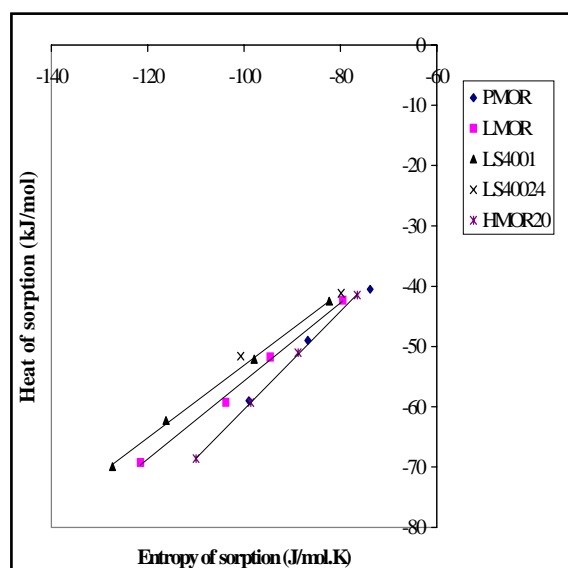


Figure 9. Interdependence of the enthalpies and entropies of *n*-alkane sorption.

molecules adsorbed (increment of 10 kJ/mol per additional CH₂-group) and were similar for all the samples. Although the heat of sorption for local adsorption at the majority of the Brønsted acid sites did not vary among the samples, striking differences could be observed in dependence of the heat of sorption on the coverage. For PMOR the heat of sorption remained constant up to the maximum coverage studied in case of propane (0.2 molecule/site) and butane (0.25 molecule/site) but dropped markedly for *n*-pentane at a coverage of 0.20 molecule/site (Fig. 5). Note, the loadings were normalized on the number of Brønsted acid sites determined with

ammonia and pyridine sorption. Due to the fact that ammonia accesses the acid sites in the side pockets and alkanes larger than ethane do not, only the Brønsted acid sites located in the main channels were taken into account (40 % of the total concentration of Brønsted acid sites). Figure 6 shows the heat evolved during sorption of propane, *n*-butane, *n*-pentane and *n*-hexane on LMOR as a function of the coverage of the acid sites. The higher enthalpy of sorption at very low coverages indicates that the sample studied contained a small amount of favored sorption sites like lattice defects or stronger acidic sites. When these sites were covered the heat of adsorption remained constant up to the maximum coverage studied (0.5 molecule/site) in case of propane, *n*-butane (0.8 molecule/site) and *n*-pentane (0.85 molecule/site) but dropped markedly for *n*-hexane at a coverage of 0.6 molecule/site. LS4001 showed essentially similar sorption characteristics (Fig. 7). The heat of sorption of *n*-hexane markedly decreased at a coverage of 0.6 molecule/site. Sorption of propane and *n*-butane on the severest steamed sample (LS40024) showed (apart from the slightly higher heat of sorption at the very initial loadings) again constant values (Fig. 8).

Differences could also be observed with regard to the sorption capacities and the Henry

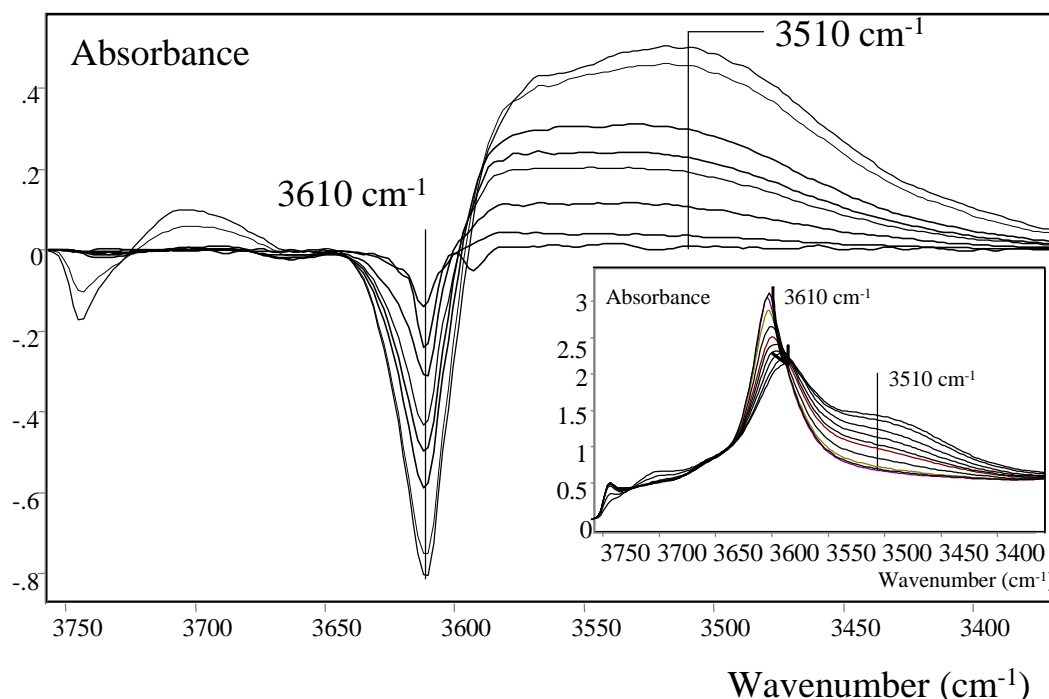


Figure 10. Difference IR spectra of the OH-bands of PMOR during sorption of *n*-butane at 323 K. The lines correspond to increasing equilibrium pressure of *n*-butane. The inset shows the IR spectra and the shift of the free Si-OH-Al groups upon loading.

constants as deduced from the isotherms. The Henry's constants exhibited an exponential dependence on the chain length (in accordance to [13]). The sorption capacity (expressed in mmol/g) decreased in the order PMOR>>LMOR>LS4001>>LS40024 conform their Brønsted acid site density.

A compensation effect between the enthalpy and entropy of sorption of *n*-alkanes on acidic and neutral zeolites was reported previously [13] and also found here. A significant difference in the interdependence of the enthalpy and the entropy of sorption for medium and large pore zeolites was shown by Eder *et al.* [13]. In Figure 9 the enthalpies and entropies of

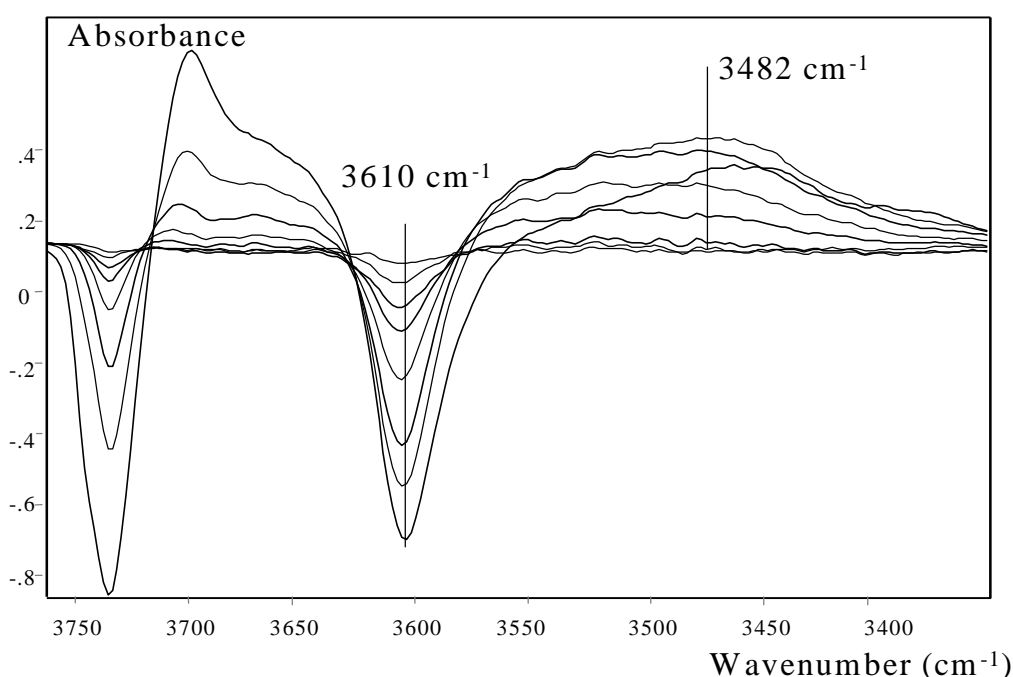


Figure 11. Difference IR spectra of the OH-bands of LMOR during sorption of *n*-butane at 323 K. The lines correspond to increasing equilibrium pressure of *n*-butane.

adsorption on the mordenite samples are compiled. Values for the heat of sorption plotted were chosen as the average of the heat of sorption for local adsorption on the majority of the Brønsted acid sites and, thus, highly similar for all samples for the sorption of an alkane with the same carbon number. It shows that the loss in entropy of sorption, induced by leaching the parent sample (PMOR) is significant and shows that the 12MR sorption behavior change to characteristics intermediate of 12MR and 10MR zeolites (e.g. MFI and TON).

The sorption of *n*-butane was also studied with IR spectroscopy between 0.02 and 25

mbar for PMOR, LMOR and LS4001, and shown in figures 10, 11 and 12, respectively. The IR spectra of PMOR showed a band at 3610 cm^{-1} (at 323 K) attributed to the OH-stretching vibrations of the Brønsted acid Si-OH-Al groups. Upon contact with *n*-butane the intensity of this band decreased progressively with increasing sorbate pressure. In parallel, a broad band appeared at 100 cm^{-1} lower in wavenumber indicating hydrogen bonding interaction. The intensity of the band of the free Si-OH-Al groups decreased to only 75 % of its original value. Even at pressures up to 25 mbar this did not change suggesting that only 25 % of the Brønsted acid sites is able to sorb *n*-butane. The concentration of hydrocarbons molecules adsorbed corresponded well to the fraction of hydroxy groups in interaction. Thus, one alkane is adsorbed per accessible Brønsted acid site. The band of the OH stretching vibrations of free and perturbed Si-OH-Al groups of

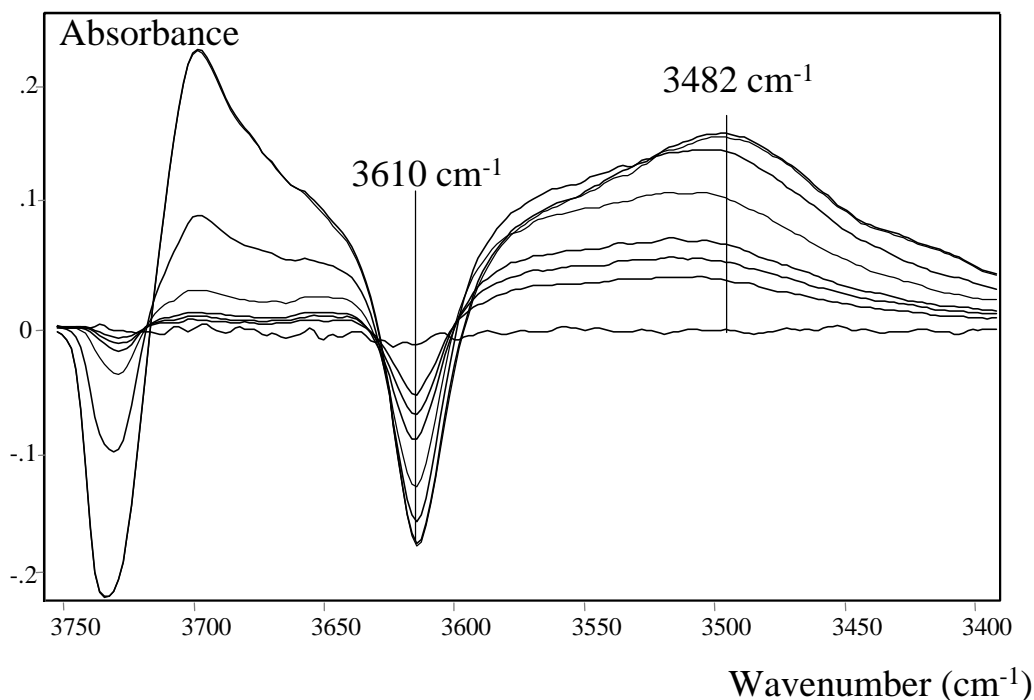


Figure 12. Difference IR spectra of the OH-bands of LS4001 during sorption of *n*-butane at 323 K. The lines correspond to increasing equilibrium pressure of *n*-butane.

PMOR had a markedly asymmetric form. With increasing coverage the maximum of the free Si-OH-Al groups shifted to lower wavenumbers. In perfect agreement with sorption data on HMOR20 as described in ref. 13, this suggests that the band has two contributions with maxima of intensity at 3612 cm^{-1} and 3590 cm^{-1} . The band at 3590 cm^{-1} is attributed to OH groups weakly

perturbed due to interaction with a closer environment in the lattice (located in the side pockets [13 and references therein]).

In case of LMOR (Fig. 11), the consumption of the free Si-OH-Al groups occurred already at the very initial loading and disappeared nearly complete at higher loadings (approximately 0.07 mmol/g of the Brønsted acid sites remained) indicating that almost all the Brønsted acid sites were accessible to *n*-butane. It is interesting to note that the location of the perturbed Si-OH-Al groups maximized at 125 cm⁻¹ lower wavenumber. Similar adsorption data were obtained for LS4001, including the significant larger shift to lower wavenumber than obtained for PMOR upon loading of *n*-butane as can be clearly seen in Fig. 12.

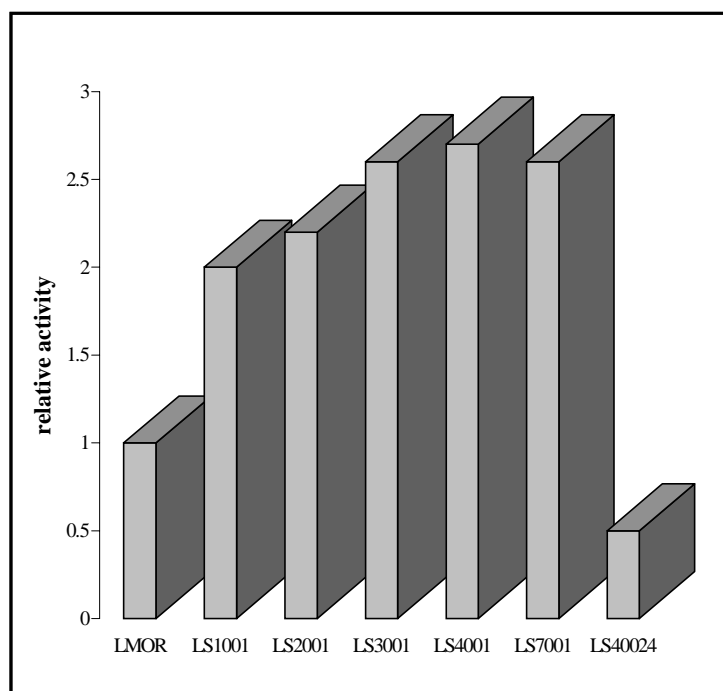


Figure 13. Activity (normalized to LMOR) of mordenite samples in *n*-butane cracking at 723 K.

4.3.3 Alkane conversion with mordenite samples

The rate constants of *n*-butane conversion were determined at 723 K from the slope of the conversion-WHSV plots fitting first order kinetics. The catalysts were stable with time on stream. Selectivities were essentially as reported earlier (Narbeshuber *et al.* [29]) and, in

agreement with literature, did not change with temperature. The catalyst activity (all rate constants normalized on the rate constant of LMOR) as function of degree of dealumination followed an interesting trend as shown in Fig. 13. Steaming the leached sample (LMOR) increased the activity with roughly a factor 2 for LS3001, LS4001 and LS7001 while the severest steamed sample LS40024 is two times less active than LMOR.

Table 3. Space velocity (W/F) necessary to obtain 1 % conversion at 473 K and 1 bar total pressure.

Catalyst	W/F (Kgcatal.s/mol)
PMOR	1.66
LMOR	0.22
LS4001	0.04
LS40024	0.25

The activity of Pt loaded PMOR, LMOR, LS4001 and LS40024 in hydroisomerization of *n*-hexane was studied at 473 K by changing the WHSV and the results are shown in Table 3. It was found that leaching and subsequent steaming decreased the contact time necessary to obtain 1 % conversion dramatically. The LS40024 was again found to be less active than mild steamed MOR, however, was still more active than the parent sample. Selectivity to monobranched products increased with leaching and steaming at cost of dibranched cracking products.

4.4 Discussion

The cracking of *n*-butane at elevated temperatures and isomerization of *n*-hexane at lower temperatures is often shown to occur exclusively on Brønsted acid sites. Three major reasons for enhanced activity upon dealumination can be put forward: 1) adsorption effects, i.e. an increase in the concentration of hydrocarbons around the acid site, 2) the generation of a secondary porous system enhancing accessibility of Brønsted acid sites, and 3) the Brønsted acid site strength dependency on the FAL and EFAL content. These three potential reasons will be discussed in view of the experimental results, after a brief discussion on the fundamentals of sorption.

The sorption of an alkane in a zeolite pore occurs *via* interactions based on London dispersion forces and localized induced dipole acid-base hydrogen bonding [30]. The induced dipole acid-base hydrogen bonding with alkanes has been shown to contribute only 6 kJ/mol for FAU and 10 kJ/mol for H-ZSM5 independent of the size of the *n*-alkane [Chapter 1]. This should be compared with the overall heat of adsorption of *n*-hexane on H- FAU and H-ZSM5, which were 53 kJ/mol and 82 kJ/mol, respectively. This indicates that for non-polar and weakly polarizable molecules the energy of interaction and the heat of sorption are fairly well described with non-localized bonding. From the side of the sorbent, the bonding forces involved are mostly determined by the geometry of the environment. As these forces are additive over the environment of the molecule, the strong interaction of weakly polar molecules in microporous materials has been explained by the optimized interactions through the curved surface (see, e.g. the formulation of the confinement effect by Derouane [31]). This has proven to be in excellent agreement with experiments [13, 32-33]. The heat of sorption was concluded to depend subtly on the fit between the size of the molecule and the size of the zeolite pores.

The relation between adsorption effects and the kinetics of alkane conversion becomes clear when considering a simple Langmuir-Hinschelwood type of mechanism. The kinetic expression shows the dependency of rate constant on the nature of acid sites, number of acid sites and the adsorption capacity. The relation deduced by Temkin upon combining the Clausius-Clapeyron equation and the power rate law

$$E_{app} = E_t + \sum n_i \Delta H_i \quad (1)$$

relates the activation energy, the order n_i and the adsorption enthalpy. Experimental work demonstrate that cracking of alkanes with first-order kinetics obeys equation (1) and is primarily governed by adsorption of the alkane [29, 34]. For *n*-alkanes Haag *et al.* [34], Narbeshuber *et al.* [29] and Wei [35] showed that the decrease in the apparent activation energy of first order protolytic cracking with increasing alkane chain length is compensated for by the increase in heat of adsorption leading to a constant true energy of activation independent of the carbon chain length. Thus, the higher reactivity of larger hydrocarbons is due to their higher abundance in the molecular sieve pores and not to their intrinsically higher reactivity. For the present discussions

it is also important to understand how structural changes brought about by dealumination affect sorption behavior.

In Figures 6 - 8 a higher energy of adsorption is found at the very low coverages for the dealuminated samples, whereas a constant value is found at higher coverages (as long as the sorption capacity allows the local adsorption on the Brønsted acid sites). The heat of local adsorption on the majority of the Brønsted acid sites as a function of carbon number is identical for all samples. This indicates that the local environment around the majority of the Brønsted acid sites is not affected by dealumination. Nevertheless, Barthomeuf [36] and Stach *et al.* [37] describe (subtle) differences in the effective acidity with varying framework Si/Al ratios. Starting with a low Al content (a high Si/Al ratio), the number of the strong acidic sites increases with increasing Al number of the frame work up to 4.6 Al atoms/ u.c. (Si/Al=9.5) and then decreases. The decrease of the strong acidity above 4.6 Al atoms/ u.c. is explained by the appearance of an aluminium atom in the second coordination sphere of the Si-OH-Al group. A higher acidity of the materials would affect the activity in alkane conversion due to the smaller barriers to form carbocations, thus, resulting in a higher surface coverage. Although this theoretical model was shown to closely match activity trends found for xylene disproportionation and isomerization [37, 38], the significance of this model is not obvious in our experiments. It is important to note that the highest activity in the present study was found at Al/u.c. of about 3, a value significant lower than the theoretically predicted optimum value. These values were, however, determined by ²⁹Si-NMR. The Al/u.c. and Si/Al ratios listed in column 10 and 7 of Table 2 were calculated assuming that SiOH groups do not contribute to the spectra.

Since we have shown with IR spectroscopy on the samples under study that acid leaching brings about many defect sites representing large SiOH intensities, and that subsequent steaming heals these defect sites only very slowly, the values in column 7 are quite meaningless. It is however possible to recalculate the contribution of SiOH to the ²⁹Si-NMR spectra [19, 41, 42] using compositional data obtained from chemical analysis and ²⁷Al-NMR. After correction following the procedure given by Bodart *et al.* [41] and Hunger and co-workers [37], the optimum Al/u.c. value is much lower than the predicted one by Barthomeuf [36]. As pointed out by others [39], one could argue whether the nature of the NNN tetrahedra could generate enough perturbation to affect the acid strength. The acid strength of a Brønsted acid site is primarily

governed by the Si-OH-Al angle. Dwyer *et al.* [40] showed that for Mordenite this angle is much less sensitive to changes in the Si/Al of the framework than in the case of, e.g. faujasite zeolites.

Another concept to describe the interaction of molecules in the pore structure of zeolites is based on the hydrophobic and hydrophilic properties of molecular sieves, i.e. their polarity. The HSAB concept was introduced (e.g. Pearson [43]) in order to explain affinities between acid and bases that do not depend on macroscopic properties as electronegativity (direction of electron density) and related acidity. Hardness (resistance to change in electron density) is a property fundamentally different from acid strength and a direct correlation between them should not exist [44]. While acid strength is a local property and therefore very liable to explain chemical reactivity, the chemical hardness is rather a global property and local importance is tempered in zeolites due to delocalization of charge in the bulk structure. When the Si/Al ratio increases (e.g. with dealumination) the zeolite becomes more hydrophobic, the metal-oxygen bonds more covalent, the structure becomes softer and tends to interact more favorably with soft bases, i.e. apolar alkanes. In this respect, Almanza *et al.* [39] proposed that the rate of *n*-hexane conversion over Pt-MOR increases with the affinity of the zeolite framework to paraffines. This explanation is, however, ambiguous on the base of the following facts; 1) hydroisomerization over Pt-MOR is numerously shown to occur via a bifunctional mechanism with a dehydrogenation of the paraffin on the metal site and the thus formed olefin protonation on the Brønsted acid sites [e.g. 23]. The “affinity of the zeolite to paraffines” is therefore solely determined by the metal sites incorporated and not the acid sites since the primary activation of paraffines on metal sites is much faster than over Brønsted acid sites; 2) *ab initio* and semi-empirical calculations show that the hardness of the zeolite increases with decreasing Si/Al ratio [44]. Therefore, if the catalytic activity was solely governed by the polarity of the bulk structure a maximum in activity as shown in Fig. 13 would not be expected. Most importantly, 3) a measure for the hardness, which is experimentally measurable, are the London dispersive forces [45, 46]. Although the dipole-induced acid-base interaction contributes only marginally to the energy of interaction with alkanes rendering them difficult to quantify in the sense of subtle differences in the acid strength, the dispersive forces form the main contribution to the heat of sorption. We would therefore expect higher heat of sorption in a wide range of coverages which is not the case. The importance of the HSAB concept is well recognized in the competitive sorption of apolar and polar

molecules what is, however, not the case in the present study.

Besides, additional complexity to deduce structure-activity correlations for *n*-hexane hydroisomerization lies in the fact that the reaction over PMOR is possibly micro pore diffusion limited [52].

A very important factor to account for upon explaining the enhanced activity of dealuminated mordenite catalysts is the accessibility of the acid sites to *n*-alkanes. The relative largest increase in mesopore volume resulted from leaching the parent sample PMOR, generating LMOR. Also, the adsorption of *n*-and-*i*-propylamine (with similar basicity) shows a strikingly 30 % lower value for *i*-propylamine in PMOR compared to the linear analogue while this was not the case for LMOR. Therefore, an important reason for the increase in activity in *n*-alkane conversion is the generation of a secondary pore system easing the accessibility of the acid sites in the main channels [52]. Note, the enhanced loss of entropy of sorption (see Fig. 9) suggests that the molecules eventually sorb in the micropores and that mesopores may only ease the accessibility of these micropores.

Dealumination probably generate interconnections between the main channels thus firstly increasing the micropore volume. The micropore volume appears to decrease at higher steam severity. A structural decline or partial blockade of the main channels by non-framework aluminium could be responsible for this [24]. Stach *et al.* [37] suggest the responsibility of another factor, the shrinking of the unit cell with dealumination. Indeed, XRD [52] and IR measurements indicate this phenomenon going from PMOR to LMOR in agreement with findings of others [50, 51]. The number of the silanol groups, which represent the defect structure caused after the leaching treatment, becomes smaller upon steaming indicating an increase of the crystallinity (as also indicated by XRD [52]). Parallel to this, the unit cell dimensions start to increase again with steaming. We suggest that initially, i.e. considering PMOR and LMOR, there is a loss of FAL resulting to a decrease of unit cell size. Apparently, with steaming the aluminium oxide clusters in the EFAL position are (partly) present as a cation increasing the unit cell dimensions and this also constitutes part of the increase of the (apparent) crystallinity. Note, NMR and ammonia sorption do not indicate a reinsertion of aluminum into the unperturbed tetrahedral frame work position upon steaming.

The mesopore volume of the steamed samples was only slightly higher than for LMOR,

the number of acid sites counted with *n*- and *i*-propylamine was equal and the bulk properties essentially similar. As the concentration of Brønsted acid sites as well as the total concentration of acid sites decreased with steam severity it means that the TOF values per accessible Brønsted acid site increased to a larger extent until LS40024, which showed reduced micropore volume and only very few Brønsted acid sites left for reaction. Therefore, a further increase of the effective usage of acid sites left after steaming, as the main reason for the steam-induced further enhanced activity is not likely.

In this respect, it is interesting that, in contrast to the constant values found at higher coverage, the heat of sorption at low coverage shows higher values. Three possible arguments for the higher initial strength of interaction can be given: 1) adsorption on strong Lewis acid sites, 2) adsorption on Brønsted acid sites of enhanced acid strength, and 3) adsorption in a pore of intermediate size. The 8MR side pockets are fully accessible after leaching, increasing the pore size to an intermediate size yielding higher energy of adsorption compared to the larger 12MR channels. The significance of these three options for explaining the steam-induced enhanced activity need to be distinguished for.

Only Brønsted acid sites are known to be active for *n*-hexane isomerization and *n*-butane monomolecular cracking. Lewis sites were reported to play a role in the initiation step of carbenium ion chemistry in metal-free zeolites [7, 47] or being a source of hydride affecting the termination of the catalytic cycle [48]. As the metal-free mordenite and the metal loaded mordenites, with the metal performing the (de-)hydrogenation reactions, showed essentially the same trends as a function of steam severity we do not believe that Lewis site catalytic activity on their own is of significant importance on the activity. However, synergistic effects between Lewis acid sites and Brønsted acid sites were reported to increase the effective acidity of the Brønsted acid sites due to polarization effects [8, 49]. Additionally, for both LMOR and LS4001 (see Figs. 11 and 12, respectively) a larger shift to lower wavenumber compared to PMOR was found. The wavenumber of the perturbed OH group is indicative for the strength of the interaction [22] and hence, the increasing shift points to a higher strength. Therefore, the acid sites located in the side pockets represent acid sites of higher acid site strength and these sites are available for reaction after dealumination.

Moreover, as mentioned before, Fig. 9 shows the interdependency of the heat of sorption

and the entropy of sorption. As discussed in abundance, the heat of sorption is higher at the initial coverages. Therefore, the weighed averaged values for the heat of sorption are plotted and used for the calculation of the entropy of sorption plotted in Fig. 9. The amount of preferred adsorption sites with higher heat of sorption is higher after steaming the leached mordenite sample, i.e. is higher for LS4001 compared to LMOR. Therefore, the weighed average for the heat of sorption is higher for LS4001 and also the loss of entropy of sorption is higher after steaming. Accordingly, the higher activity brought about by steam dealumination can be rationalized with the higher strength of interaction resulting from favorable sorption in a more confined environment. This suggest that (part of) the side pockets are modified by steam dealumination, i.e. the size of the 8 MR channels are modified to an intermediate size between 8MR and 12MR. One should however be cautious with the interpretation of figure 9 for explaining the catalytic activity. Part of the higher heat of sorption can originate from sorption on Lewis sites. The IR studies on alkane sorption show an immediate consumption of the bridging Si-OH-Al groups, i.e. at the very initial coverages, indicating that Brønsted acid sites constitute at least part of the higher strength of interaction at low alkane loading.

Although the increase of the activity upon comparing PMOR and LMOR seems now satisfactorily explained by the increase of the accessibility and the more efficient utilization of Brønsted acid sites (of higher acid site strength) in the side pockets, the steam induced increase of activity cannot yet be rationalized conclusively. The most plausible explanation seems that in case of LS4001, at the catalytic working conditions, a relative larger fraction of the Brønsted acid sites in the side pockets are utilized.

4.5 Conclusions

A series of mordenites (with Si/Al_f ranging between 6 and 52) was prepared by acid leaching and steam dealumination and characterized by using different physico-chemical methods and adsorption of light alkanes. In the past, the higher concentration of larger alkanes, i.e. adsorption effects, were the cause of their higher activity in the pores of molecular sieves compared to smaller alkanes. The main incentive here was to understand how structural changes brought about by dealumination affect sorption behavior and catalytic activity. Dealumination was found

to increase the accessibility of acid sites, as a consequence, resulting in higher activity in both *n*-butane cracking and *n*-hexane hydroisomerization. Adsorption data of light alkanes show that the enhanced activity upon steam dealumination is favorably explained by the modification of the side pockets that increased the pore size to an intermediate size between 8MR and 12MR yielding higher energy of adsorption compared to the larger 12MR (main) channels. The sorption environment in the side pockets constitute higher energy of adsorption compared to the larger 12MR (main) channels and their acid sites appear to be of higher acid strength. This results in lower reaction barriers for the formation of carbocations explaining the higher activity. No experimental evidence on the theoretical concept of mordenite acidity was found.

Acknowledgment

Dr. J. Miller (BP-Amoco) for providing the Mordenite samples and part of the activity measurements. Drs. M. Rep (University of Twente) is kindly acknowledged for part of the TGA/DSC work. Drs. J.A. van Bokhoven, M. Tromp and Dr. H. Bitter (University of Utrecht) are acknowledged for the fruitful collaboration. Dr. V.A. Veefkind is kindly acknowledged for the making of Fig. 1.

References

- 1- Moulijn, J.A., in “*Catalysis; An Integrated Approach to Homogeneous, Heterogeneous and Industrial Catalysis*”, Moulijn, J.A., van Leeuwen, P.W.N.M., Van Santen, R.A., (Editors), Elsevier, Amsterdam, 1993.
- 2- Rabo, J.A., and Gajda, G.J., *Catal. Rev.-Sci. Eng.* **31**, 385 (1989).
- 3- Jacobs, P.A., *Catal. Rev.-Sci. Eng.* **24**, 415 (1982).
- 4- Scherzer, J., *ACS Symp. Ser.* **48**, 157 (1984).
- 5- Zholobenko, V.L., Kustov, L.M., Borovkov, V.Y., and Kazanskii, B.V., *Kinet. Catal.* **28**, 847 (1987).
- 6- Chen, F.R., and Fripiat, J.J., *J. Phys. Chem.* **97**, 5796 (1993).
- 7- Pieterse, J.A.Z., Seshan, K., and Lercher, J.A., *Stud. Surf. Sci. Catal.*, in press.
- 8- Lonyi, F., and Lunsford, J.H., *J. Catal.* **136**, 566 (1992).
- 9- Carvajal, R., Chu, P.-J., Lunsford, J.H., *J. Catal.* **125**, 123 (1990).
- 10- Lischke, G., Schreier, E., Parltitz, B., Pitsch, I., Lohse, U., and Woettke, M., *Appl. Catal. A:General* **129**, 57 (1995).

- 11- Zholobenko, V., Garforth, A., Makarova, M., and Dwyer, J., *Stud. Surf. Sci. Catal.* **94**, 560 (1995).
- 12- Meier, W.M., Olson, D.H., "Atlas of Zeolite Structure Type", Int. Zeolite Assoc. (1978).
- 13- Eder, F., Stockenhuber, M., Lercher, J.A. in: *Zeolites: A Refined Tool for Designing Catalytic Sites*, Bonneviot, L.; Kaliaguine S. (editors), Elsevier, Amsterdam, 495 (1995).
- 14- Springuel-Huet, M.A., and Fraissard, J.P. *Zeolites* **12**, 841 (1992).
- 15- Olken, M.M., Garces, J.M., *Poc. 9th Int. Zeolite Conf.* Butterworth-Heinemann, Montreal, 1992; Tran, M-Trung., Gnep, N.S., Szabo, G., and Guisnet, M., *Appl. Catal. A:General* **170** 49 (1998).
- 16- Karge, H.G., and Dondur, V., *J.Phys.Chem.* **94**, 765 (1990).
- 17- Meyers, B.L., Fleish, T.H., Ray, G.Y., Miller, J.T., and Hall, J.B., *J. Catal.* **110**, 82 (1988).
- 18- Gorte, R.J., and White, D., *Topics Catal.* **4**, 57 (1997).
- 19- Stach, H., Janchen, J., Jerschewitz, H.G., Lohse, U., Parltitz, B., Zibrowius, B., and Hunger, M., *J. Phys. Chem.* **96**, 8480 (1992).
- 20- English, M., PhD Thesis, University of Twente, 1996.
- 21- Temkin, M., *Acta Phsiocochim. USSR* **3**, 312 (1935).
- 22- Hair, M.L., and Ertl, W. *J. Phys. Chem.* **74**, 91 (1970).
- 23- Asuquo, R.A., Eder-mirth, G., Pieterse, J.A.Z., Seshan, K., and Lercher, J.A., *J. Catal.* **168**, 292 (1997).
- 24- Sawa, M., Niwa, M., and Murakami, Y., *Zeolites* **10**, 532 (1990)
- 25- Khabtou, S., Chevreau, T., and Lavalley, J.C., *Microp. Mater.* **3**, 133 (1994).
- 26- Sayed, M.B., Kydd, R.A., and Cooney, R.P. *J. Catal.* **88**, 137 (1984).
- 27- Bordiga, S., Platero, E.E., Arean, C.O., Lamberti, C., and Zecchina, A., *J. Catal.* **137**, 179 (1992).
- 28- Glazunov, V.P., and Odionokov, S.E., *Spectrochim. Acta* **38A**, 399 (1982).
- 29- Narbeshuber, T.F., Vinek, H., and Lercher, J.A., *J. Catal.* **157**, 388 (1995).
- 30- Barrer, R.M., *J. Coll. Interf. Sci.* **31**, 415 (1966).
- 31- Derouane, E.G., Andre, J.M., and Lucas, A.A., *J. Catal.* **110**, 58 (1988).
- 32- Eder, F., and Lercher, J.A., *J. Phys.Chem. B* **101**,1273 (1997).
- 33- Van Well, W.J.M., Cottin, X., de Haan, J.W., van Hooff, J.H.C., Nivarthi, G., Lercher, J.A., Smit, B., and van Santen, R.A., *J. Phys. Chem.* **102**, 3945 (1998).
- 34- Haag, W., *Adv. Catal.* **27**, 247 (1977).
- 35- Wei, J., *Chem. Eng. Sci.* **51**, 2995 (1996).
- 36- Barthomeuf, D., *Mat. Chem. Phys.* **17**, 49 (1987).
- 37- Stach, H., Janchen, J., Jerschewitz, H.G., Lohse, U., Parltitz, B., Zibrowius, B., and Hunger, M., *J. Phys. Chem.* **96**, 8473 (1992).
- 38- Wu, P., Komatsu, T., and Yashima, T., *J. Chem. Soc., Faraday Trans.* **92**, 861 (1996).
- 39- Almanza, L.O., Narbeshuber, T., D'Araujo, P., Naccache, C., and Ben Taarit, Y., *Appl. Catal A :General* **178**, 39 (1999).

- 40- Dwyer, J, and O'Malley, P.J., *Stud. Surf. Sci. Catal.* **35**, 5(1988).
- 41- Bodart, P.B., Nagy, J., Debras, G., Gabelica, Z., and Jacobs, P.A., *J. Phys. Chem.* **90**, 5183 (1986).
- 42- Van Geem, P.C., Scholle, K.F.M.G.J., Van der Velden, G.P.M., and Veeman, W.S., *J. Phys. Chem.* **92**, 1585 (1988).
- 43- Pearson, R.G., *J. Am. Chem. Soc.* **85**, 3533 (1963).
- 44- Corma, A., Sastre, G., Viruela, R., and Zicovich-Wilson, C., *J. Catal.* **136**, 521 (1992).
- 45- Haag, W.O., *Stud. Surf. Sci. Catal.* **84A**, 1375 (1994).
- 46- Sauer, J., Ugleingo, P., Carrone, E., and Saunders, V.R., *Chem. Rev.* **94**, 2095 (1994).
- 47- Kwak, B.S., and Sachtler, W.M.H., *J. Catal.* **145**, 456 (1994).
- 48- Lukyanov, D.B., *Zeolites* **14**, 233 (1994).
- 49- Mirodatos, C., and Barthomeuf, D.J., *J. Chem. Soc. Chem. Commun.* 39 (1981).
- 50- Scherzer, J., *ACS Symp. Ser.* **157**, 248 (1984).
- 51- Olsson, R. W., and Rollman, L.D., *Inorg. Chem.* **16**, 651 (1977).
- 52- Tromp, M., Van Bokhoven, J.A., Bitter H., and Koningsberger, D.C., *in preparation*.

*Improving the Stability of H-Mordenite for *n*-Butane Isomerization*

Abstract

The conversion of *n*-butane over mordenite based catalysts in the presence of hydrogen was investigated for reaction temperatures between 523 K and 623 K. Special attention was given to the influence of Pt upon catalytic activity, selectivity and stability. With parent mordenite the catalytic activity for *n*-butane conversion decreased markedly after short time on stream. Deactivation can be minimized by hydrogen in the presence of Pt. This is thought to be due to a reduction of the concentration of intermediate olefins in the zeolite pores. The best results with respect to selective conversion of *n*-butane to isobutane were obtained for Pt loadings between 0.1 and 0.25 wt % on mordenite in the presence of hydrogen. Higher concentrations of Pt in the catalyst are shown to be detrimental for *n*-butane isomerization because of increasing selectivity to hydrogenolysis. A detailed mechanistic scheme for *n*-butane conversion over Pt containing mordenites is presented. *n*-Butane conversion is concluded to occur *via* a bimolecular mechanism involving a complex network of hydrogen transfer, oligomerization/cracking, isomerization, dehydrogenation, and hydrogenolysis.

5.1 Introduction

The use of Brønsted acidic zeolites (e.g. H-mordenite) as a component of commercial *n*-butane isomerization catalysts has received much attention in both academic and industrial research [1-6]. This is mainly due to the specific pore geometry combined with the strong acidic properties of these molecular sieves. *n*-Butane conversion over H-mordenite occurs mainly *via* a bimolecular mechanism [3]. For this bimolecular mechanism, two main reaction routes, isomerization (formation of isobutane) and disproportionation (i.e. formation of propane and pentane isomers), have been identified. The contribution to the two reaction routes depends upon the reaction temperature, the concentration of the acid sites and the concentration of reactants in the pores of the catalyst [3].

The main problem associated with the use of strongly acidic zeolites as isomerization catalysts is the fast rate of deactivation. For the protonic form of mordenite, for example, the initial yields of isobutane are high. An optimal catalytic activity in the isomerization of *n*-butane [3] and *n*-pentane [4] was found for mordenite samples with a Si/Al ratio of 10. Blocking of the catalytic active sites by adsorbed (polymeric) hydrocarbons and partial pore blockage, however, cause loss of catalyst activity with time on stream.

Enhancement of the stability might be achieved by introducing additives into the feed stream which prevent the formation of polymeric hydrocarbons or help to decompose and desorb them [7]. In this context, improved stability is expected by the addition of hydrogen to the feed stream, especially for catalysts containing low concentrations of Pt [8]. The role of Pt has been reported to be in the activation of the hydrogen. The activated hydrogen is reported to react with the carbocationic intermediates, thus, reducing their concentration in the zeolite pores [7,11]. This reduction in the concentration of the carbocations, however, might also cause a decrease in the rate of *n*-butane transformation as the carbocations are part of the catalytic cycle. Pt when present in a zeolite (MOR) or sulfated zirconia has also been suggested to contribute to the isomerization of butane *via* a parallel bifunctional route involving dehydrogenation of the alkane on the metal site [5,6]. As a side effect, the presence of Pt can also be expected to cause a new hydrogenolysis route in the presence of hydrogen thus affecting isobutane selectivity.

The present contribution addresses the effect of the modification of H-mordenite with Pt and

the addition of hydrogen to the feedstream on the activity, selectivity and stability with the goal to understand and to be able to control the influence of these additives on the *n*-butane conversion over H-mordenite.

Table 1. Physico-chemical characteristics of the samples.

Catalyst	BET surface area (m ² /g)	Pt content (wt %)	Pt dispersion (%)	IR OH/lattice vibration
HMOR	388	0	-	1.3
PtMOR1	226	0.02	^a	1.2
PtMOR2	241	0.25	100	1.3
PtMOR3	259	1.3	80	1.1

^a Not measured

5.2 Experimental

5.2.1 Catalyst preparation and characterization

H-mordenite (HMOR) with a SiO₂/Al₂O₃ ratio of 20 (provided by the Japanese Catalytic Society) was used in this study. A detailed characterization of the material is given in ref. [12]. Three different Pt/H-mordenite samples were prepared by contacting HMOR with a 1 M solution of Pt(NH₃)₄Cl₂ to obtain Pt loadings between 0.02 and 1.3 wt %. After contacting HMOR with the appropriate amounts of the Pt-salt solution for 1 hour at ambient temperature under constant stirring, the solution was filtered and the catalyst washed with deionized water. This precipitate was dried overnight at ambient temperature and then at 383 K for 2 hours. The dry powder was ground and calcined in air at 823 K. The samples are denoted PtMOR1, PtMOR2 and PtMOR3 corresponding to the Pt loadings of 0.02, 0.25 and 1.30 wt %, respectively. Dispersion of Pt in the samples was measured by volumetric hydrogen chemisorption (see Chapter 3, ref.20). The IR spectra of the catalysts, to determine the concentration of OH groups, were recorded using a Bruker IFS88 FTIR spectrometer. The physicochemical characteristics of these catalysts are

shown in Table 1.

5.2.2 Activity measurements

The catalytic tests were performed in a tubular quartz reactor operated in continuous flow mode (see chapter 2 of this thesis). A catalyst loading of about 300 mg was used. The catalyst was diluted with inert quartz beads in the ratio of 1:1. A gas mixture of 20 % *n*-butane in helium was used. The experiments were conducted between 523 K and 623 K and with *n*-butane partial

Table 2. Product selectivity over HMOR and PMOR3 at 523 K, Conversion = 5 %

Catalyst	HMOR		PtMOR3	
H ₂ / <i>n</i> -butane ratio	0	11	0	11
Products	Selectivity (mol %)			
methane+ethane	1	1	0.5	61
propane	34	31	33	31
isobutane	53	55	52	7.5
pentanes	11	12	13	0.4
C ₆₊	1	1	1.5	0

pressures between 74 and 150 mbar and at total pressures between 1.5- 2.5 bar. The partial pressure of hydrogen was varied between 0 and 1500 mbar.

All catalysts were activated in flowing air by heating at 10 K/min to 823 K and holding this temperature for 1 hour. For the Pt containing catalysts an additional prereduction step was carried out at 823 K for 1 h in H₂. The activity of the catalysts was monitored as a function of time on stream between 10 and 60 min. The reactor effluent was collected in the sample loops of a multi-loop valve and subsequently analyzed by gas chromatography (HP 5890 with a 50 m Al₂O₃/KCl column, flame ionization detector).

5.2 Results

5.2.1 Effect of hydrogen on the activity and stability of H-mordenite

The rate of conversion of *n*-butane at 523 K over H-mordenite as a function of time on stream at various H_2/n -butane ratios is depicted in Fig. 1. The main products in the conversion of *n*-butane over H-mordenite were isobutane (“isomerization route”), propane and pentane isomers (“disproportionation route”) as reported earlier [3]. The addition of hydrogen to the *n*-butane feed led primarily to a decrease in the rate of *n*-butane conversion. The lower activity in the presence of hydrogen was also accompanied by a slower relative deactivation.

The selectivity to the main products was not significantly influenced by the increase in the H_2/n -butane ratio. The influence of hydrogen on the product distribution over H-mordenite is shown in Table 2. Only a slight increase in the selectivity to isobutane and pentane was noticed, while the selectivity to propane and to the cracking products methane and ethane slightly decreased. This can also be seen in Fig. 2, in which the iC_4/C_3+C_5 ratio is plotted against the H_2/n -butane ratio.

5.2.2 Effect of platinum loading on *n*-butane conversion

The effect of the Pt loading on the rate of conversion of *n*-butane (at 523 K) is shown in Fig. 3. It can be seen from Fig. 3 that the Pt containing catalysts show higher catalytic activity than the parent H-mordenite. However, the presence of Pt did not lead to any improvement in the stability of the catalysts in the absence of hydrogen. The selectivity to various products for the different catalysts is shown in Fig.4. With regard to the product distribution, only minor changes were observed upon Pt incorporation. A small increase in the selectivity to isobutane and a corresponding decrease in the selectivity to propane and pentane were the most significant changes over the Pt containing catalysts in comparison to HMOR (Fig.4, see also Fig. 2). In all cases, low concentrations (<3 %) of methane, ethane and hexanes were also observed.

In the presence of hydrogen, however, a substantial decrease in the initial activity was observed with all the Pt containing catalysts (see Fig.5). It should be recalled that this was also

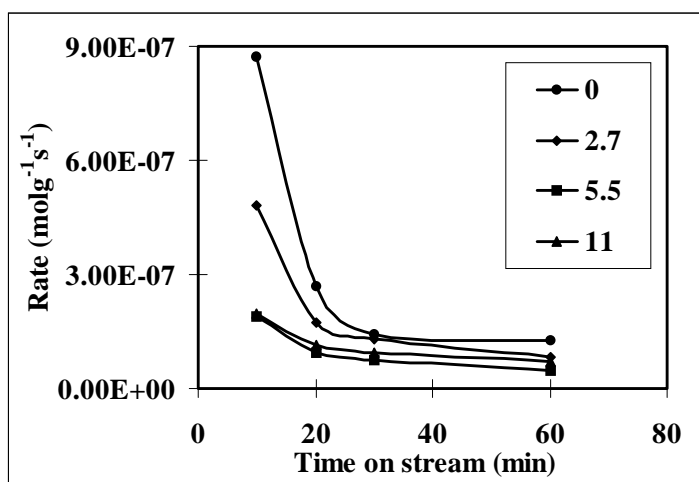


Figure 1. Effect of hydrogen on the activity and stability of HMOR at 523 K, $P_{\text{tot}}=2.5\text{bar}$, $P_{n\text{-butane}}=150\text{ mbar}$, flow rate = 15 ml/min, WHSV=1.87 hr⁻¹; the values 0, 2.7, etc., indicate the H₂/n-butane ratios.

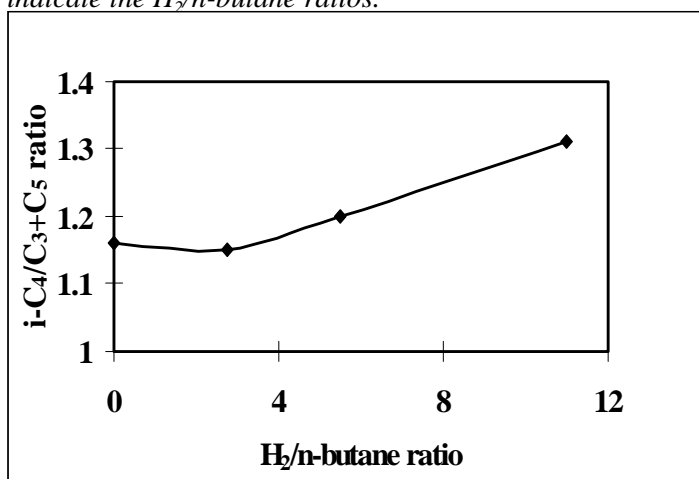


Figure 2. Effect of hydrogen on iC₄/C₃+C₅ ratio over HMOR at 523 K, $P_{\text{tot}}=2.5\text{bar}$, $P_{n\text{-butane}}=150\text{ mbar}$, flow rate = 15 ml/min, WHSV=1.87 hr⁻¹; conversion = 5 %.

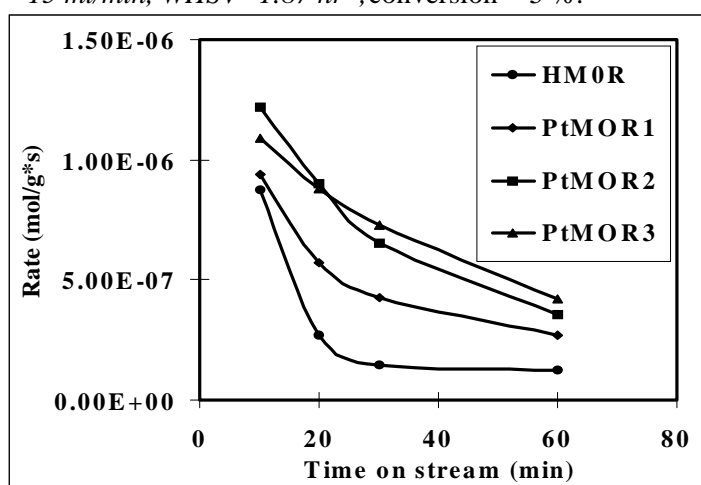


Figure 3. Effect of Pt on rate of conversion and stability at 523 K, $P_{\text{tot}}=2.5\text{bar}$, $P_{n\text{-butane}}=150\text{ mbar}$, flow rate = 15 ml/min, WHSV=1.87 hr⁻¹.

observed over H-mordenite (compare Figs. 3 and 5). However, the loss of activity in the presence of hydrogen was much more significant with Pt containing catalysts than for HMOR at 523 K. The presence of hydrogen affected also the activity during time on stream. It can be seen from Fig. 5 that, in the presence of hydrogen, all catalysts reached steady state after 30 minutes on stream. In the absence of hydrogen, these catalysts continued to deactivate even after 60 min on stream (see Fig. 3). PtMOR3 which was the least active catalyst did not deactivate at all in the presence of hydrogen (Fig. 5). For this reason, the effect of hydrogen pressure was further tested with that catalyst. The influence of hydrogen on the product selectivity for HMOR and PtMOR3 is compiled in Table 2. For PtMOR3, the rates for isomerization (isobutane) and disproportionation (propane+pentanes) decreased, while the rates of hydrogenolysis (methane+ethane) increased in the presence of hydrogen. In contrast, in the case of H-mordenite, the presence of hydrogen did not cause any appreciable changes in selectivity. For Pt containing catalysts, also similar product distribution to H-mordenite were observed in the absence of hydrogen (Fig. 4 and table 2).

The relative contribution of the three main reactions (isomerization, disproportionation and hydrogenolysis) to the total rate of conversion at 523 K is depicted as a function of H_2/n -butane ratio in Fig. 6 for PtMOR3. It can be seen that the presence of hydrogen induced a large negative effect on isomerization and disproportionation and a positive effect on hydrogenolysis at 523 K.

As already mentioned, the addition of hydrogen to enhance the stability of the catalyst led to lower rates of *n*-butane conversion over Pt containing catalysts. In order to improve the yields of isobutane, under practical reaction conditions it was necessary to work at temperatures higher than 573 K. The conversions and product distributions obtained over H-mordenite and two Pt-MOR samples at 623 K are summarized in Table 3. It can be seen from Table 3 that over Pt containing catalysts an appreciable improvement in isobutane selectivity is observed. Even though Pt caused hydrogenolysis at higher temperatures, this was much less than at the lower temperature of 523 K (see Table 2). The stability of H-mordenite and Pt-mordenites in presence of hydrogen (H_2/n -butane =15) at 623 K is presented as a function of time on stream in Fig.7. In contrast to the lower activity (PMOR1, PtMOR2, PtMOR3) and the fast initial deactivation (PtMOR1, PtMOR2) observed even in the presence of hydrogen at 523 K, a higher and stable

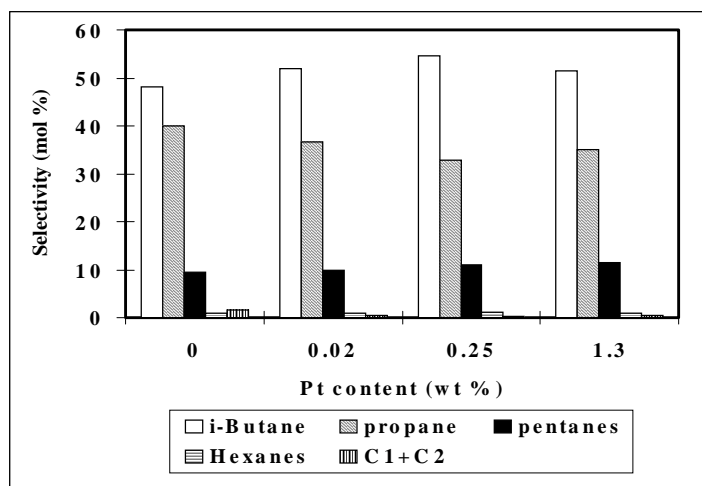


Figure 4. Selectivity as a function of Pt loading at 20 % conversion in the absence of hydrogen. $P_{tot}=2.5\text{bar}$, $P_{n\text{-butane}}=150\text{ mbar}$, flow rate =15 ml/min, WHSV=1.87 hr⁻¹.

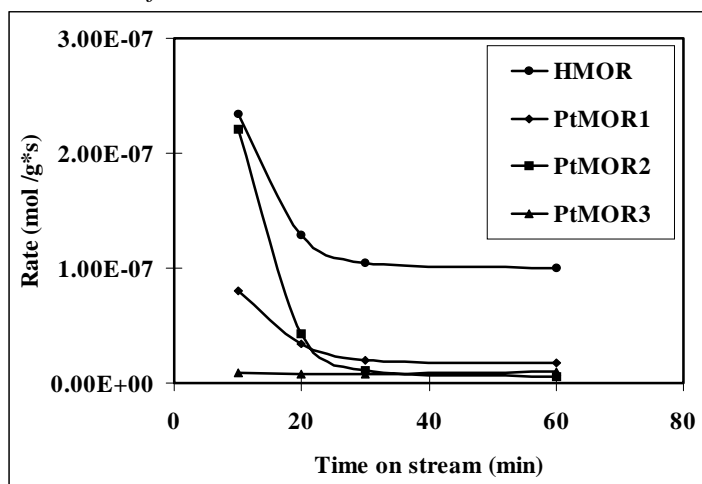


Figure 5. Effect of Pt on activity and stability at 523 K in the presence of hydrogen $P_{tot}=1.5\text{bar}$, $P_{n\text{-butane}}=72\text{ mbar}$, flow rate =20 ml/min, WHSV= 3.72 hr⁻¹, $H_2/n\text{-butane}=11$.

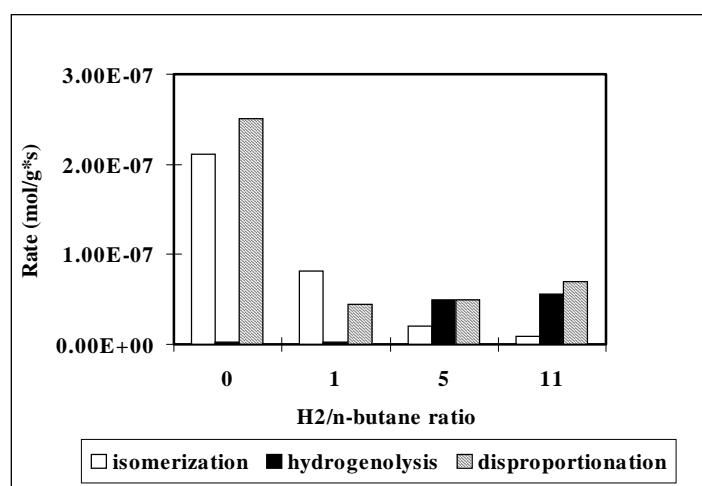


Figure 6. Rate of reactions as a function of $H_2/n\text{-butane}$ ration over PtMOR3 at 523 K, $P_{tot}=2.5\text{ bar}$, $P_{n\text{-butane}}=150\text{ mbar}$, flow rate=15 ml/min, WHSV=1.87 hr⁻¹.

activity was obtained for the Pt-mordenite samples at 623K. However, even though H-mordenite deactivated under these conditions, it still had a better activity after 60 min on stream than the Pt containing catalysts.

Fig. 8 shows the activity as a function of time on stream for PtMOR2 at varying H_2/n -butane ratios all lower than H_2/n -butane ratio of 15 shown in Fig. 7. It is evident from Fig. 8 that the

Table 3. Product distribution for *n*-Butane conversion over various catalysts at 623 K, H_2/nC_4 ratio 15, Selectivities at 50 % conversion.

Catalyst	HMOR	PtMOR1	PtMOR2
metane +ethane	4	8.7	17
propane	53.7	34	23
isobutane	33	48	52
pentane	7	9	6.8
others	2.3	0.3	1.2

stability of the catalysts is improved by an increasing H_2/n -butane ratio at the expense of catalytic activity. The results agree with those of Maness and Dooley for *n*-butane isomerization over fluorided Pd-mordenite [13]. However, at the optimal H_2/n -butane ratio of 10 stable behavior combined with good activity is achieved.

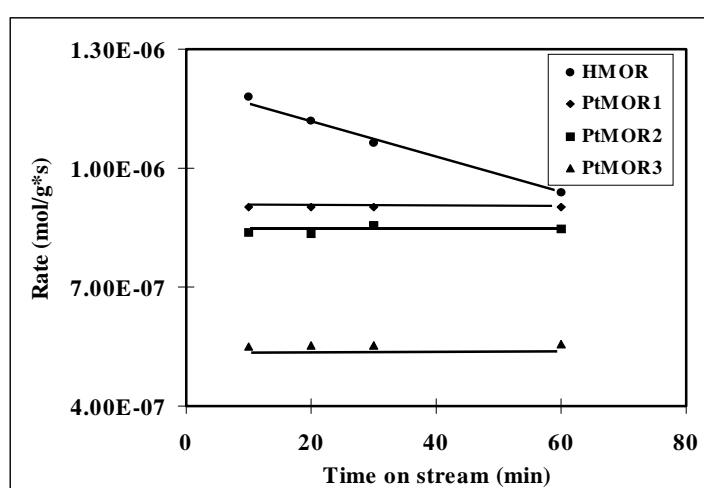


Figure 7. Rate as a function of time on stream at 623 K for various catalysts, H_2/n -butane ratio =15, $P_{tot}=1.5bar$, $P_{n-butane}=74 mbar$, flow rate =15 ml/min, $WHSV=3.72hr^{-1}$.

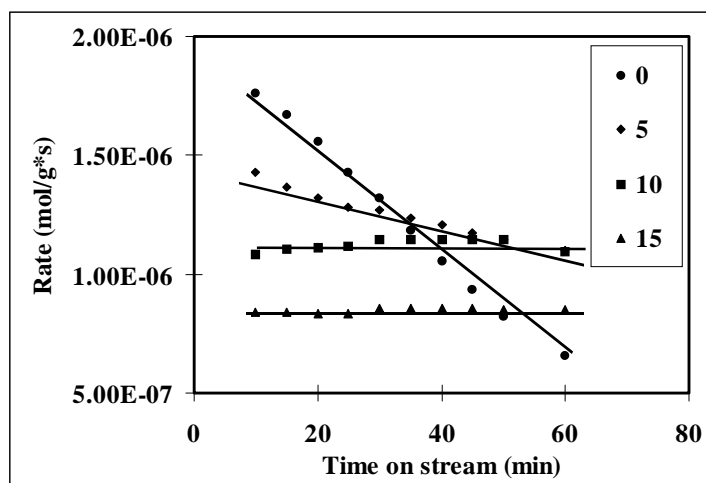


Figure 8. Rate as a function of time on stream for various H_2/n -butane ratio over PtMOR2, $T=623$ K, $P_{tot}=1.5$ bar, $P_{n-butane}=74$ mbar, flow rate =20 ml/min, WHSV=3.72 hr^{-1} .

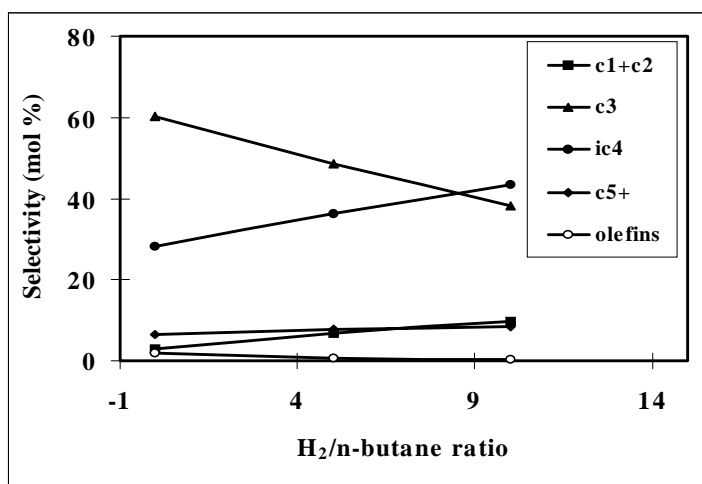


Figure 9. Selectivity as a function of H_2/n -butane ratio at 50% conversion over PtMOR2. $T=623$ K, $P_{tot}=1.5$ bar, $P_{n-butane}=74$ mbar, flow rate =20 ml/min, WHSV=3.72 hr^{-1} .

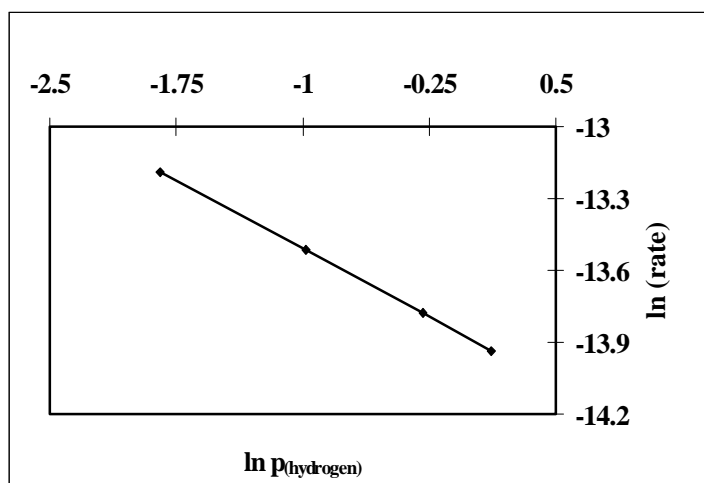


Figure 10. Effect of hydrogen on the rate of n -butane conversion over PtMOR2 at 623 K.

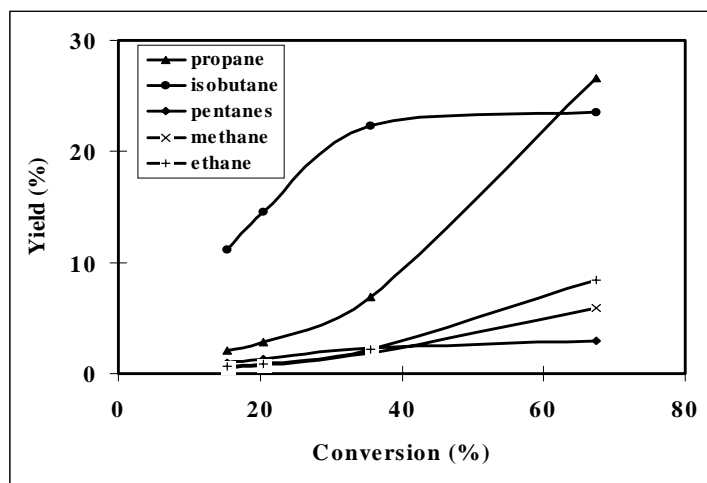


Figure 11. Product yield as a function of conversion over PtMOR2 at 623 K, $P_{n\text{-butane}} = 75$ mbar.

The influence of $H_2/n\text{-butane}$ ratio on the product distribution at about 50 % $n\text{-butane}$ conversion is shown in Fig. 9 for PtMOR2. The selectivity to isobutane increased with increasing $H_2/n\text{-butane}$ ratio, while the selectivity to propane showed the opposite trend. The extent of hydrogenolysis also increased with increasing $H_2/n\text{-butane}$ ratio. The negative effect of hydrogen on the overall rate of $n\text{-butane}$

conversion over PtMOR2 is depicted on Fig. 10. From the data displayed a negative order of 0.4 with respect to H_2 was calculated. In Fig. 11 the yield of products as a function of conversion is represented for PtMOR2. The conversion was changed by changing the WHSV. Under these conditions ($H_2/n\text{-butane} = 20$), catalyst deactivation was not observed during time on stream. Propane is a primary (below 15% conversion) and a secondary product. Isobutane and pentane which are also primary products at low conversion are further converted to methane, ethane and propane at higher conversion.

5.4 Discussion

It was shown earlier that over H-mordenites $n\text{-butane}$ is mainly converted *via* a bimolecular mechanism at 523 K [3]. This mechanism avoids the formation of the energetically unfavorable primary carbenium ions which are unavoidable, if isomerization occurs *via* a monomolecular skeletal isomerization route. We will show here that the results obtained over Pt modified mordenites also point to a bimolecular reaction route. The proposed reaction network is shown in Fig. 12.

Two main reaction routes, isomerization (isobutane) and disproportionation (propane and pentane isomers), contribute to the product selectivity in the overall reaction. It was shown earlier that the relative importance of the two reaction routes depends subtly upon the reaction

temperature and the concentration of acid sites [3]. In the bimolecular reaction sequence proposed in [3], *n*-butane is first protonated at the strong Brønsted acid sites to form a butyl carbonium ion. Subsequent dehydrogenation of this leads to a surface bound carbenium ion (alkoxy group) and hydrogen (initiation step). As pointed out in chapter 3 of this thesis, especially for HMOR *n*-butane could also be first dehydrogenated at the strong Brønsted acid sites (or Lewis acid sites) to initiate the catalytic cycle. Also, traces of olefins in the feed are protonated. Note that it is now generally accepted that chemisorbed alkenes exist as alkoxy groups which on excitation form the carbenium ions in the transition state.

It is significant to recall at this point the negative half order (-0.4) in hydrogen observed for the rate of *n*-butane conversion. This suggests dissociation of hydrogen as playing a part in the mechanism. Negative order in hydrogen has been observed recently and attributed as indication for a bifunctional mechanism [5] involving dehydrogenation of butane at the Pt site and subsequent formation of butyl carbenium ion from the butene formed. It is, therefore, possible that in our experiments an additional route for the formation of butyl carbenium ions as in a bifunctional route exist (see Fig.12).

The butylcarbenium ion may desorb as butene or react with another butene molecule to form an octyl carbenium ion which subsequently isomerizes and cleaves by forming *tert*-butyl carbenium ion and *n*-butene (isomerization route). The *tert*-butyl carbenium ions leave the catalyst surface as isobutane after abstracting a hydride from another *n*-butane feed molecule. In a second pathway the octyl carbenium ion undergoes cracking and hydride transfer reactions to give propane and pentyl carbenium ion (disproportionation route). The pentylcarbenium ions crack to form propyl carbenium ions and some ethene or undergo hydride transfer reactions with reactant molecules before leaving the catalyst as alkanes [3].

It has been found that the high hydride transfer ability of the H-mordenite causes the formation of almost exclusively saturated products (methane and ethane, propane, isobutane, *n*-butane and pentanes) and coke upon conversion of *cis*-2-butene [14]. The catalyst deactivates very rapidly during this experiment indicating that the extensive hydride transfer leaves increasingly hydrogen- deficient carbonaceous material on the catalyst surface. Similarly under the reaction conditions during *n*-butane isomerization, the formation of oligomeric, olefinic species is favored. These molecules will transform by hydrogen redistribution to form paraffins

and increasingly carbon-rich and unreactive carbonaceous material. Their accumulation leads to the reduction of the catalytic activity with time on stream.

From the reaction network shown in Fig.12, the lower activity of HMOR in the presence of hydrogen can be explained by a reduced rate of butenes formation and, thus, also in butyl carbenium ions. This can be expected to reduce the overall rate of the reaction. A remarkable change in selectivity to various routes (disproportionation and isomerization) in the product distribution upon addition of hydrogen is neither expected nor seen. Thus, the selectivity to coke formation will also not change, although a slower coking rate will be expected as a result of reduced formation of olefins. The increased stability of H-mordenite in the presence of hydrogen is proposed to be due to the lower concentration of the olefins.

In the case of Pt-containing catalysts, paraffin isomerization is known to occur via a bifunctional mechanism involving the dehydrogenation of the paraffin on the metal, transport of the olefin to the acid site, isomerization of the alkenes at the acid site, followed by a hydrogenation of the iso-alkenes on the metal site to form iso-alkanes [15,16]. A mechanism involving protonated cyclopropane as intermediates in the monomolecular route for the isomerization of light paraffins has also been proposed. But this is limited to hydrocarbons with 5 or more carbon atoms that do not require the formation of primary carbenium ions for isomerization [16,17].

The presence of hydrogen led to a reduction in the rate of *n*-butane conversion over Pt-mordenites just as in the case of H-mordenite. This negative effect of hydrogen upon the rate of the reaction was more drastic for Pt containing catalysts than for H-mordenite at lower temperatures. This indicates that the formation of butenes is reduced. The addition of Pt is, thus, proposed to help in reducing the concentrations of butenes by controlling directly or indirectly their dehydrogenation.

The presence of hydrogen did not cause any change in the selectivity to different routes over H-mordenite. From the proposed mechanism, changes are not to be expected as the major reforming reactions will take place at the unmodified acid sites of mordenite. However, for the Pt-containing catalysts drastic changes are observed in the presence of hydrogen (Table 2 and Fig. 9). In the absence of hydrogen, the products obtained over the Pt containing catalyst are similar to those over H-mordenite. Apart from the low concentration of cracking products

observed, only a slight increase in the selectivity to isobutane and a decrease in the selectivity to propane is observed with increasing Pt loading. This suggests that Pt alone does not induce any major changes in the mechanistic pathway as seen over mordenite. We should recall at this point (see Table 1) that addition of Pt did not cause any appreciable changes to the acidity of mordenite.

In Pt/H-mordenites, the main role of Pt is to activate hydrogen and establish the butane/butene equilibrium. The hydrogen can react with the olefinic species in the mordenite pores and help in the formation of alkanes and this can be expected to cause a decrease in coke formation. The retardation of coking by hydrogen *via* reaction with benzylic carbocations has also been reported during toluene disproportionation over H-mordenites by Gnep and Guisnet [11]. The reduction in the rate of conversion over Pt/mordenite is, thus, largely attributed to lower concentration of carbocations.

From the product distribution in Table 2, we conclude that the presence of H_2 caused hydrogenolysis, i.e. a high extent of $C_1 + C_2$ formation. Hydrogenolysis increases in importance with increasing Pt loading and H_2/n -butane ratio (Fig. 9), and at lower temperatures. In order to minimize the negative effects of hydrogenolysis, the reaction conditions need to be subtly adjusted. An optimal H_2/n -butane ratio of 10, a Pt loading between 0.1 and 0.25 %, and at 598K gives the best results for *n*-butane isomerization.

Regarding the sequence of reactions over Pt containing catalysts, positive slopes for the yields (Fig. 11) at low conversion levels show that propane + pentane and isobutane are primary products formed in parallel reactions. Methane and ethane can be formed as primary products by hydrogenolysis of *n*-butane or as secondary products resulting from cracking of C_5 hydrocarbons. Propane has also a very strong contribution from some secondary route.

The increase in the formation of propane with increasing conversion cannot be accounted for by the cracking of pentane to ethane and propane. This means that an additional route for the formation of propane exists. Because of the increase of methane and propane and the limiting value of isobutane yield at higher conversion we propose that oligomerization of isobutyl carbenium ion with a pentene occurs to form a C_9 species and subsequent cracking and hydride transfer will generate propane. Initially this hydride transfer should occur from *n*-butane. As the *n*-butane concentration decreases (i.e. at higher conversions) hydride transfer will occur

preferably from isobutane. This explains the upper limit of 25 mol% isobutane yield. Note that this does not affect the other reactions occurring and as a consequence selectivity to isobutane will decrease at the expense of oligomerisation/cracking products. Dumesic *et al.* [18], proposed a microkinetic model to account for all the major products of isobutane conversion over acidic HY catalysts. The formation of excess propane during this reaction was accounted for by taking

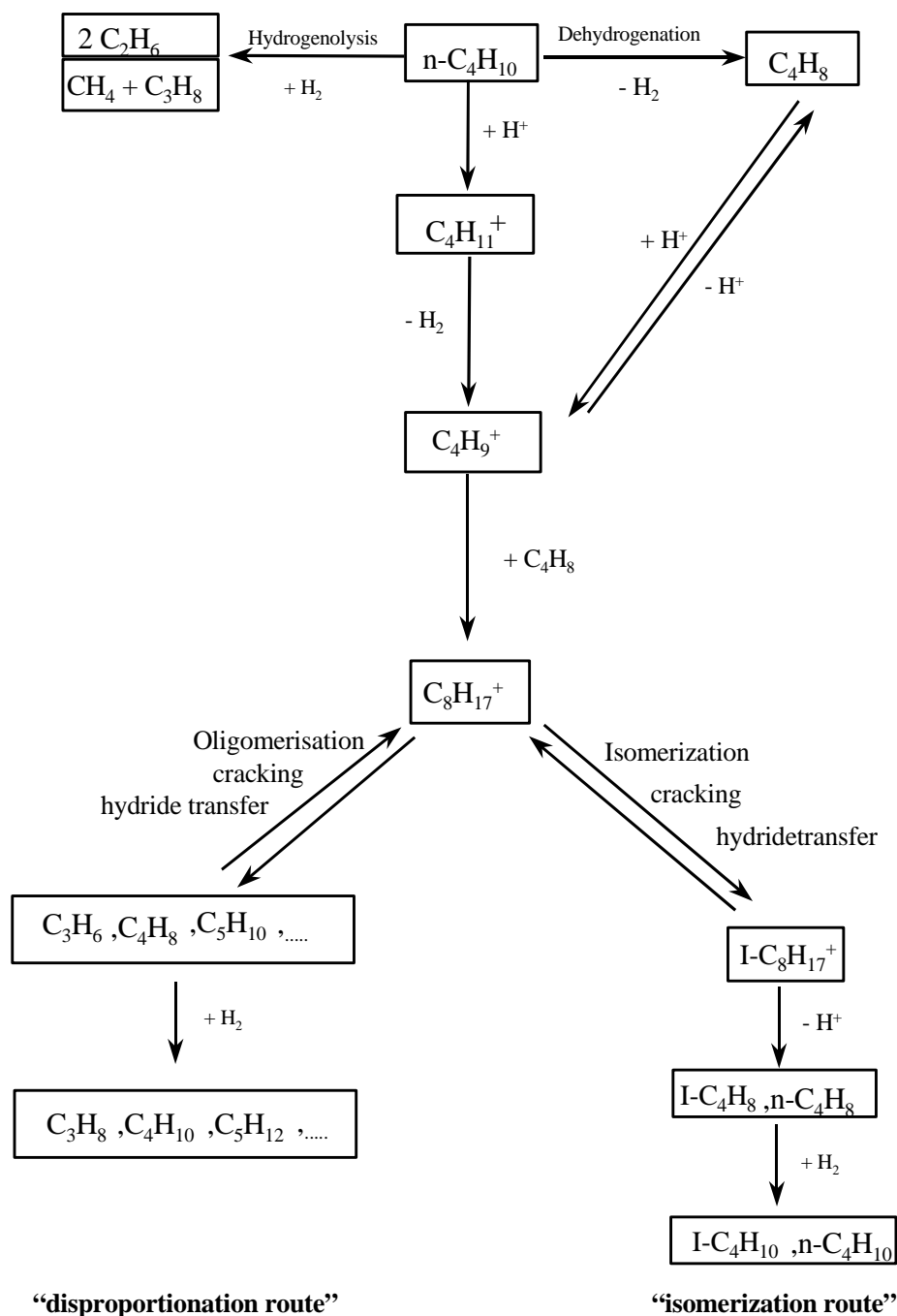


Figure 12. Reaction pathways for *n*-butane isomerisation over (Pt-)mordenites

into account a secondary route involving C₄-C₄ and C₄-C₅ oligomerization and cracking steps. In this way propane was identified as both a primary and secondary product of isobutane conversion. The present experiments suggest that the additional secondary route propane is at the expense of isobutane formation. To summarize, with the present Pt mordenites, two routes, namely, hydrogenolysis of *n*-butane and oligomerization/cracking of tertiary butylcarbenium ion (precursor for isobutane) can cause losses in isobutane yield with increasing conversions.

5.5 Conclusions

The mechanism of isomerization of *n*-butane over Pt mordenites follows a bimolecular pathway as in the case of H-mordenite. In the presence of Pt an additional pathway for the conversion of *n*-butane *via* a bifunctional mechanism is also identified. Pt also induces high stability to the mordenite catalysts, which otherwise deactivate rapidly. The stability of Pt mordenites, especially in the presence of hydrogen is achieved by suppressing coking, regulating the concentration of butene and offering a pathway alkene hydrogenation in addition to hydride transfer reactions. Under these conditions Pt catalysts hydrogenate the coke precursors. The presence of Pt, however, also causes hydrogenolysis of *n*-butane to methane, ethane and propane. It has been shown that by the proper choice of reaction conditions, the route to hydrogenolysis could be minimized. Oligomerization/cracking of isobutane has been identified as a possible secondary route for the formation of propane.

Acknowledgment

Dr. R.A. Asuquo is gratefully acknowledged for the fruitful collaboration.

References

1. Tonks, G. V., and Verstappen, A.E.L.M.M., US Patent No. 5073667 (1991).
2. Mitsce, R. T., and Pollitzer, E. L., U.S Patent No. 3544,451 (1970).
3. Asuquo, R. A., Eder-Mirth, G and Lercher, J. A., *J Catal.* **155**, 376 (1995).
4. Sie, S.T., *Stud. Surf. Sci. Catal.* **85**, 587 (1994).
5. Liu, H., Lei, G.D., and Sachtler, W.M.H., *Appl. Catal. A:General* , **137**, 167 (1996).
6. Chao, K., Hung-chung, W., and Leu, L., *J. Catal.* **157**, 289, (1995).

7. Polta, J. A., Flynn, D. K. and Thiel, P. A., *J. Catal.* **99**,88 (1986).
8. Guisnet, M. and Fouche,V., *Appl. Catal.* **71**, 283 (1991).
9. Kouwenhoven, H.W., *Adv.Chem. Ser.* **121**, 529 (1973).
10. Benesi, H. A., and Winquist, B. H. C., in “Advances in Catalysis”, **27** (1978).
11. Gnep, N. S., and Guisnet, M. *Appl. Catal.* **1**, 329 (1981).
12. Sawa, M., Niwa, M., and Murakami, Y., *Zeolites* **10**,532 (1990).
13. Maness, J. A. and Dooley, K. M., *J. Catal.* **117**, 322 (1989).
14. Asuquo, R.A. Seshan, K and Lercher, J. A., unpublished results.
15. Kuchar, P. J., Bricker, J. C., Reno, M. E., and Haizmann, R. S., *Fuel Processing Technology*, **35**,183 (1993).
16. Chevalier, F., Guisnet, M., and Maurel, R. *Proc. 6th Int. Conf. on Catal.* London 1977.
17. Bearez, C., Chevalier, F and Guisnet, M., *React. Kinet. Catal. Lett.*, **22**, 405 (1983).
18. Dumesic, J. A., Rudd, D. F., Apericio, L. M., Rekoske, J. E. and Trevino, A, A., in “*The Microkinetics of Heterogeneous Catalysis*”, ACS, Washington DC, 1993.p.272

*Sulfur Tolerant Catalysts based on Mordenite for the Hydro- isomerization of *n*-Butane*

Abstract

PtMOR and PtZrMOR catalysts for hydroisomerization of *n*-butane reveal an outstanding sulfur tolerance up to 1000 ppm. In both cases, the only impact upon sulfur in the feed was a lower steady state activity: catalytic stability and selectivity were retained. Although a Pt sintering process due to irreversible bound sulfur species is evident the prevailing reason for reduced steady state activity has found to be binding of reversible sulfur species. Oxidative regeneration at high temperature is sufficient to remove these species and to restore the initial conversion. Although the total metal area became significantly less after sulfur exposure also the stability could be entirely preserved. Sequential experiments show that the restorative properties of the sulfur poisoned catalysts can be entirely extended to *n*-pentane hydroisomerization and also to other molecular sieves. The combination of zirconia, H₂S and regeneration brought about an additional mechanistic complexity under sulfur cofeed. This has shown to be due to the formation of sulfated zirconia. The presence of sulfated zirconia increased the overall acidity of the catalysts resulting to higher cracking activity at the expense of isomerization and lowered the catalyst stability.

6.1 Introduction

The increasing demand for high quality motor fuel and the legislative restrictions on the composition of gasoline has stimulated academic and industrial research to develop alternative processing technology. Great attention is paid in this respect to the catalytic conversion of low value hydrocarbons to more valuable fuels, fuel components or intermediate feedstocks [1]. Important processes for the production of high octane gasoline are the alkylation of isobutane with olefins and the etherification of isobutene with methanol to methyl tertiary butyl ether (MTBE). In these cases, the starting material is obtained from *n*-butane by isomerization and dehydroisomerisation [2].

Conventional processes for *n*-butane isomerization use $\text{AlCl}_3 + \text{HCl}$, or chlorinated Pt/alumina [1,3,4] as catalysts. Due to rapid catalyst deactivation and the environmental and corrosion problems affiliated with these catalysts, acidic molecular sieves have been studied as alternatives [1,5-9].

H-MOR has been reported to be an active catalyst for *n*-butane isomerisation that, however, deactivates rapidly due to coking [5,6]. Previous work in our own group [5] and other groups [7] revealed that the conversion of *n*-butane over mordenite is mainly a bimolecular process with isomerization and disproportionation as the predominating reaction routes. Incorporation of Pt and carrying out the reaction in presence of hydrogen suppresses coking and improves the catalysts stability during *n*-butane isomerization.

The presence of Pt induces two major problems; 1) Pt is very sensitive toward sulfur poisoning. Sulfur containing compounds like thiophenes and hydrogen sulfide, usually present in crude oil, react irreversibly with Pt reducing available metal area for (de)hydrogenation reactions[1]; 2) the presence of Pt cause hydrogenolysis reactions that may limit selectivity toward isomerization. Hydrogenolysis, being a structure sensitive reaction, is reported to be dependent on Pt particle size. It was reported by Nazimek *et al.* [10] that 2 to 4 nm Pt particle size shows maximum activity for *n*-butane hydrogenolysis. The addition of zirconia to Pd-ZSM-5 has been reported to improve the dispersion of Pd [8] that, thus, may affect hydrogenolysis activity. Additionally, careful pre-sulfiding of bifunctional catalysts has been reported to suppress hydrogenolysis in bifunctional reforming catalysts [1,28] while leaving (de)hydrogenation

activity unaffected.

The present contribution is the second in a series aiming at the design of an active, selective, stable and sulfur tolerant catalyst for *n*-butane isomerization. For this, the addition of Zr to Pt/MOR as well as pre-sulfidation were tried to reduce metal hydrogenolysis activity. The sulfur tolerance, the restorative nature of sulfur induced catalyst deactivation and the mechanism in which sulfur poisons these catalysts will be dealt with in this contribution.

6.2 Experimental

6.2.1 Catalysts

The Na⁺ form of MOR (Si/Al = 10) was obtained from the Japanese Catalysis Society. The ammonium form was prepared by ion exchange with 1M solution of NH₄NO₃. Zr⁴⁺ was ion exchanged into NH₄MOR using a solution of ZrOCl₂·8H₂O in the presence of excess 0.01 M HCl. The resulting Zr-MOR catalysts were thoroughly washed in order to remove chlorine and subsequently dried in air at 390 K for two hours. They were then calcined for 2 hours at 823 K (heating rate 5 K/min). Pt was incorporated by ion exchange from a solution of Pt(NH₃)₄(OH)₂. The catalysts were reduced *in situ* at 823 K for 1 hour before being used.

6.2.2 Characterization

ZrO₂ contents of the catalysts were determined by X-ray Fluorescence analysis (XRF), platinum contents were determined by AAS.

Structure determination was performed using X-ray diffraction analysis using CuK α radiation on a Philips PW1710 X-ray diffractometer. The Pt particle size was determined using high resolution transmission electron microscopy (HREM). A Philips CM30T electron microscope with a LaB₆ filament as the source of electrons was used, operated at 300 kV. Samples were mounted on a carbon polymer microgrid supported on a copper grid by placing a few droplets of a suspension of a ground sample in ethanol on the grid, followed by drying at ambient conditions. Elemental analysis was performed using a LINK EDX system.

²⁷Al-NMR was performed on a multinuclear NMR spectrometer (Varian, Unity WB 400) equipped with a RT CP/MAS probe. The chemical shift was calibrated by using a sample of

$\text{Al}(\text{NO}_3)_3 \cdot 9\text{H}_2\text{O}$.

The surface area and micropore volumes were determined with N_2 using the BET method on a Micromeritics instrument (ASAP 2400). The samples were degassed at 573 K for 2 hrs before the measurement.

Gravimetric and calorimetric measurements were performed in a modified SETARAM TG-DSC 111 instrument comprising the balance, the calorimeter, a UHV system and a mass spectrometer [11]. Details can be found in chapter 2 of this thesis. The samples were heated in a vacuum with a temperature increment of 10K/min. to 673K and held at that temperature for one hour to desorb water, subsequently cooled to 373K and exposed to 3 mbar of ammonia in order to determine the concentration of acid sites. Additionally, the sample was cooled to 323 K to sorb *n*-butane and to determine sorption capacity for *n*-butane together with the heat of sorption

FTIR measurements were performed with a BRUKER IFS-88 spectrometer equipped with a flow cell and vacuum cell as described in chapter 2.

6.2.3 Activity measurements

The kinetic experiments were performed in a fixed bed tubular quartz reactor as described in chapter 2. 150 mg of catalyst was used for each test. The samples were diluted with quartz to minimize the pressure drop across the catalyst bed. The catalyst was activated in flowing air (40 ml/min), at 10 K/min to 823 K. It was held at this temperature for one hour. The material was reduced at 823 K in hydrogen flow (35 ml/min) for one hour. After reduction, PtZrMOR was pre-sulfided by exposure to a flow containing 1000 ppm H_2S in helium for 1 hr at 623K and subsequently purged with pure helium for an additional hour. Pre-sulfiding increased the Pt cluster size (Table 3). The reactant gas contained *n*-butane and hydrogen, balanced with helium and/or H_2S . The reactor effluent was collected with an automatic sampling valve system, stored in multi-loop valves and subsequently analyzed by a HP5890 gas chromatograph using a 50 m $\text{Al}_2\text{O}_3/\text{KCl}$ capillary column and equipped with a flame ionisation detector and coupled to a mass selective detector HP 5971A. Carbon deposits on spent catalysts were determined with Simultaneous Elemental Analyzer for CHNS.

6.3 Results

6.3.1 General Characterization

Physicochemical characterization of the samples studied is shown in Table 1 below. The XRD pattern of H-MOR matched very well with that reported in literature [36]. Mordenite modified with Zr and Pt showed essentially the same diffractogram as that observed for the parent H-MOR.

Table 1. Physico-chemical characterization of the catalysts.

Catalysts	Conc. of Acid sites(mmol/g)	S_{BET} (m^2/g)	Micropore vol.(m^3/g)	tetrahedral/ octahedral Al^{a}	Zr (wt%)	Pt ^b (wt%)
H-MOR	1.20	328	0.15	n.d.	-	-
PtMOR	1.15	332	0.15	5	-	0.1
PtZrMOR	0.95	320	0.14	4	1	0.1

n.d.; not determined, a; determined by ^{27}Al -NMR, b; determined by AAS

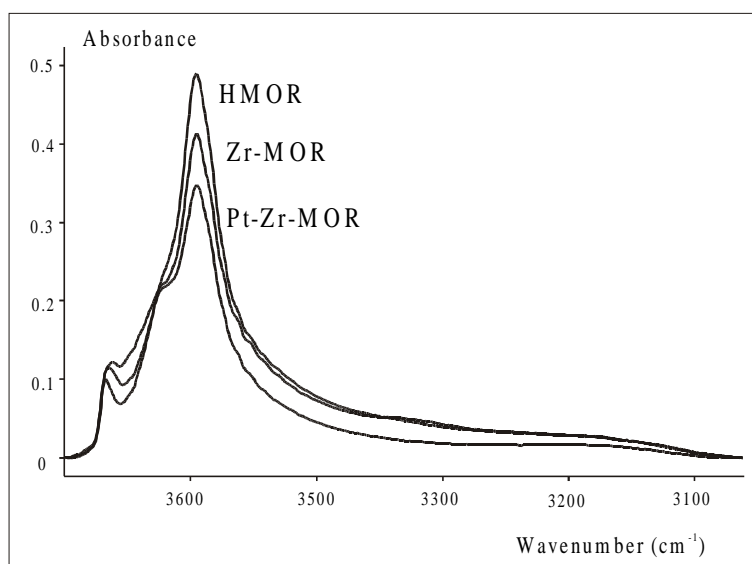


Figure 1. Preparation of PtZrMOR followed by FTIR; spectra recorded at 723 K under Helium flow. Samples were calcined and reduced *ex situ*.

NH₃ sorption by TGA pointed out a loss of 0.25 moles/gram (20 %) acidic sites after the incorporation of zirconium and Pt (Table 1). This result may imply both highly dispersed zirconium in a direct interaction with the acidic sites and blocking of acid sites. Calorimetric analysis of the adsorption of *n*-butane on H-MOR, PtMOR and PtZrMOR gave differential heats of adsorption amounting to 49 kJ/mol in case of H-MOR and 45 kJ/mol for PtMOR and PtZrMOR. Although there is a slight decrease compared to H-MOR, this decrease was independent of the addition of zirconium. The maximum loading at 13 mbar *n*-butane was in all cases 0.64 ± 0.03 mmol/g.

Addition of Zr induced a substantial decrease of intensity of the stretch vibration corresponding to bridged OH at 3590 cm^{-1} , indicating again a direct interaction with the acid sites of mordenite. (Fig.1). The silanol band at 3736 cm^{-1} disappeared under a new band at 3724 cm^{-1} which is attributed to terminal zirconium hydroxide stretch vibrations [12]. Bridged ZrOH groups were also observed, at 3648 cm^{-1} [13]. Additionally, an external Al-OH band around 3660 cm^{-1} could be discerned. The subsequent addition of Pt induced an additional decline in bridged Si-OH-Al groups, which was restored for about 70 % after subsequent reduction. Furthermore, part of zirconium hydroxyl stretch vibrations disappeared after reduction.

6.3.2 Kinetic measurements and extended characterization

Product selectivities at 20 mol% conversion over fresh PtMOR and PtZrMOR are listed in Table 2. The catalyst containing zirconium has the highest selectivity toward isobutane due to a decrease in the formation of C₁-C₃ species. Figures 2, 3 and 4 show the relation between yield and conversion for PtZrMOR, the fresh catalyst, the pre-sulfided PtZrMOR and pre-sulfided catalyst in presence of 1000 ppm H₂S, respectively. As seen, all products are primary until a conversion level of about 12 mol %. The rate of hydrogenolysis (at a given similar conversion), which is for the sake of convenience defined as the sum of the formation rates of methane and ethane (omitting propane that can be formed *via* disproportionation as well) decreased by pre-sulfiding by about 25 % (compared to the fresh PtZrMOR). No further decrease was observed in the presence of 1000 ppm H₂S. Conversion levels for fresh PtMOR and PtZrMOR are presented as a function of the H₂S concentration in figure 5 and 6, respectively.

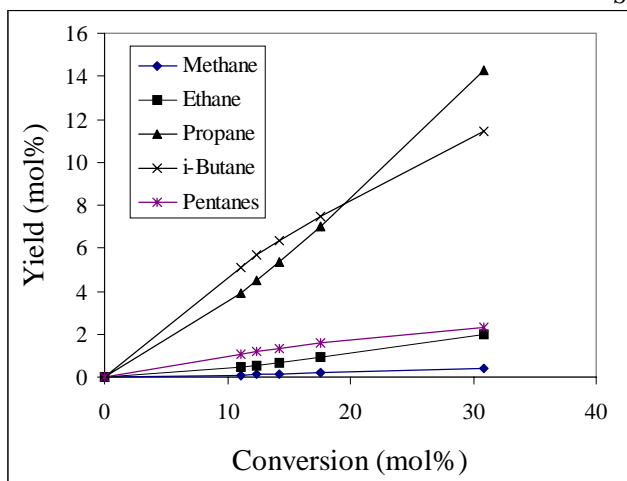


Figure 2. Yield/conversion plot for fresh PtZrMOR; WHSV = 0.05 -0.10 mol/g*h, $P_{n-butane}$ = 81 mbar, P_{H_2} = 320 mbar.

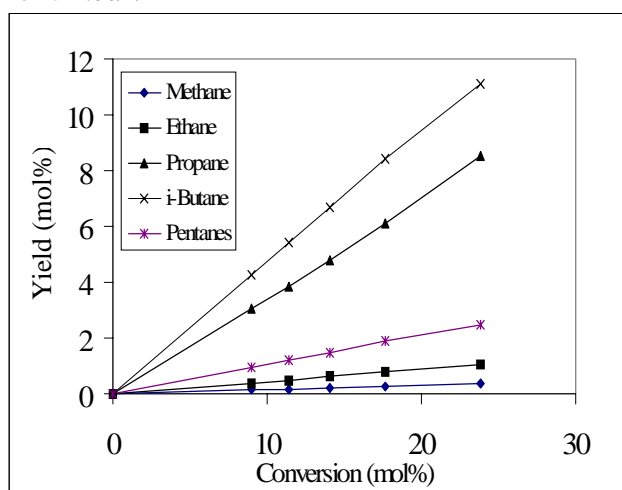


Figure 3. Yield/conversion plot for pre-sulfided PtZrMOR; WHSV = 0.05 -0.10 mol/g*h, $P_{n-butane}$ = 81 mbar, P_{H_2} = 320 mbar, P_{H_2S} = 0 mbar.

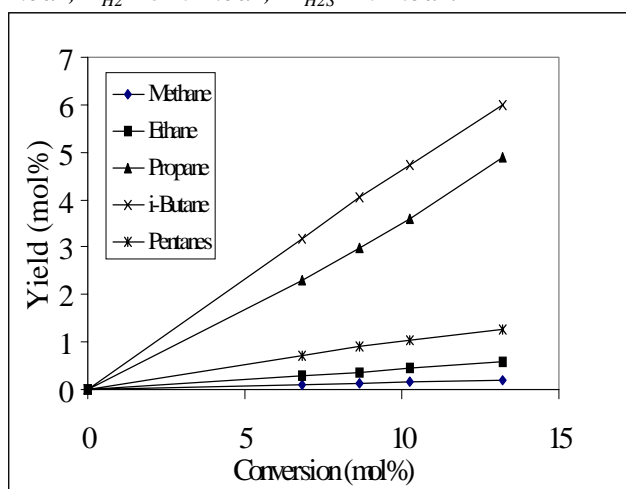


Figure 4. Yield/conversion plot for pre-sulfided PtZrMOR; WHSV = 0.05 -0.10 mol/g*h, $P_{n-butane}$ = 81 mbar, P_{H_2} = 320 mbar, P_{H_2S} = 1000 mbar.

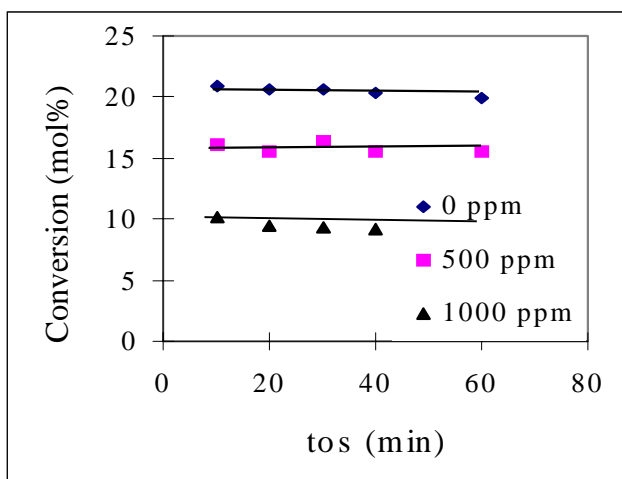


Figure 5. Effect of H_2S on activity and stability of PtMOR. $P_{n-butane}=220$ mbar, $P_{H_2}=880$ mbar, $WHSV=0.08$ mol/g*h.

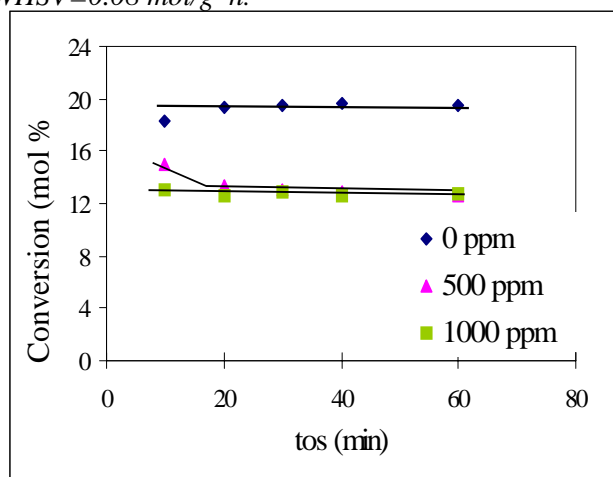


Figure 6. Effect of H_2S on activity and stability of PtZrMOR. $P_{n-butane}=220$ mbar, $P_{H_2}=880$ mbar, $WHSV=0.08$ mol/g*h.

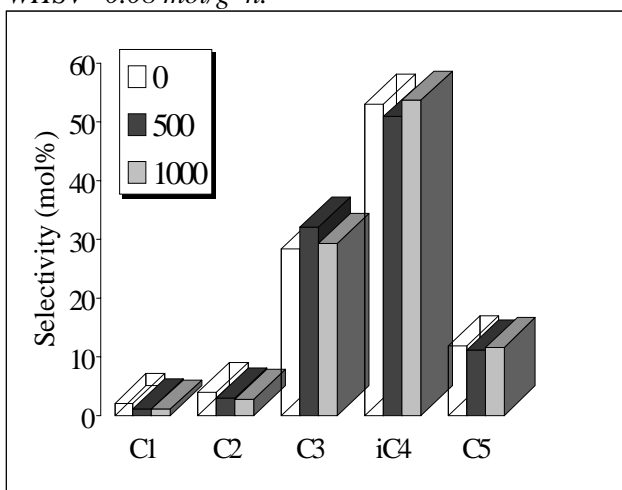


Figure 7. Effect of H_2S on selectivities of PtMOR. $P_{n-butane}=220$ mbar, $P_{H_2}=880$ mbar, $WHSV=0.08$ mol/g*h.

Both catalysts show similar catalytic stability but in both cases a lower activity with increasing H_2S concentration is observed. Figures 7 and 8 show the corresponding product distributions in the presence of 0, 500 and 1000 ppm H_2S in the feed. With both catalysts the only apparent impact of sulfur is the suppression of C_1+C_2 formation. The slightly higher selectivity toward isomerization for PtZrMOR is preserved also when sulfur was present. In order to test the reversibility of the sulfidation process the experiments were repeated employing a regeneration cycle. In between two experiments with H_2S , the catalyst was reactivated by heating in air and reduced in hydrogen at 823 K, both for 1 hour. In case of PtMOR this did not lead to any difference in activity or product distributions.

Table 2. Comparison of PtMOR and PtZrMOR at 20 mol % conversion; $P_{\text{nC}_4} = 220 \text{ mbar}$, $T = 623 \text{ K}$.

Catalysts	PtMOR	PtZrMOR
	Sel. (mol%)	Sel. (mol%)
isobutane	52.5	58.5
propane	28.5	24.6
pentanes	11.6	11
C_1+C_2	6.5	5.2
others	0.9	0.7

However, for PtZrMOR a distinctly different behavior was observed (see Fig. 9). With higher concentrations of sulfur in the feed, the initial activity increased, and this was accompanied with a rapid loss of catalytic stability. After the entire $\text{nC}_4+\text{H}_2+\text{H}_2\text{S}+\text{He}$ sequence the catalyst was heated in air and hydrogen at 823 K for 1 hour and the activity was measured under helium without sulfur. The initial activity and product distribution as found during the very first sequence with the fresh catalyst could be almost completely recovered and also the stability was restored. A similar test for PtMOR revealed the same restorative phenomenon.

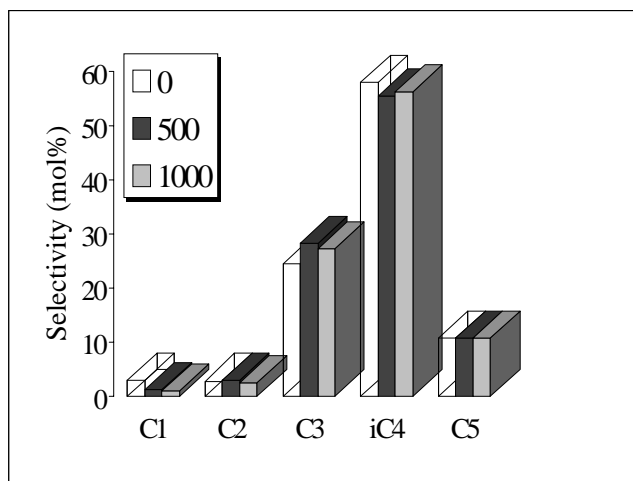


Figure 8. Effect of H_2S on selectivities of PtZrMOR. $P_{n-butane} = 220$ mbar, $P_{H_2} = 880$ mbar, $WHSV = 0.08$ mol/g \cdot h.

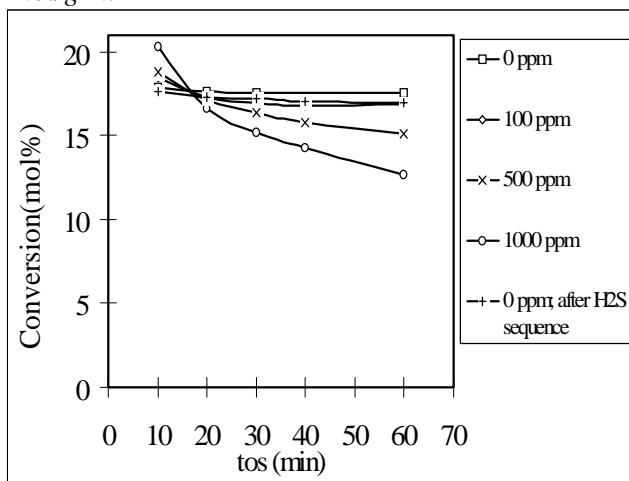


Figure 9. Effect of H_2S on activity and stability of PtZrMOR. $P_{n-butane} = 220$ mbar, $P_{H_2} = 880$ mbar, $WHSV = 0.08$ mol/g \cdot h; with regeneration in between sequences.

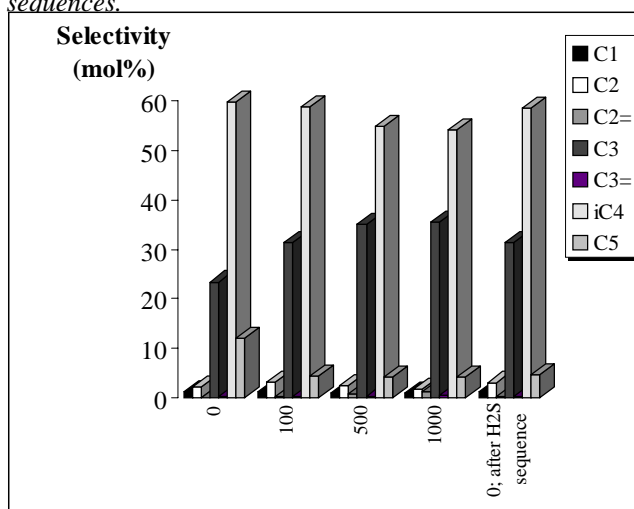
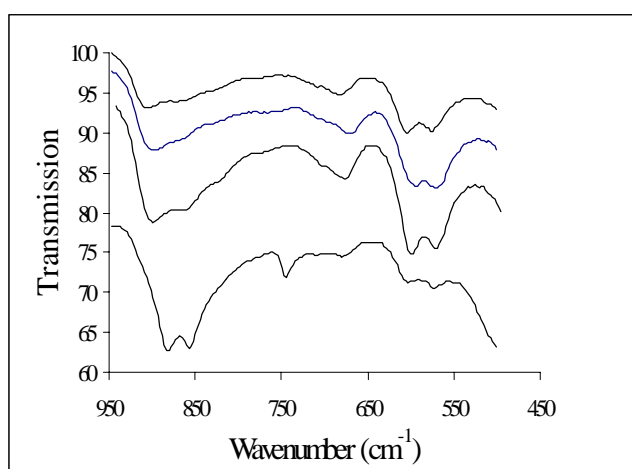
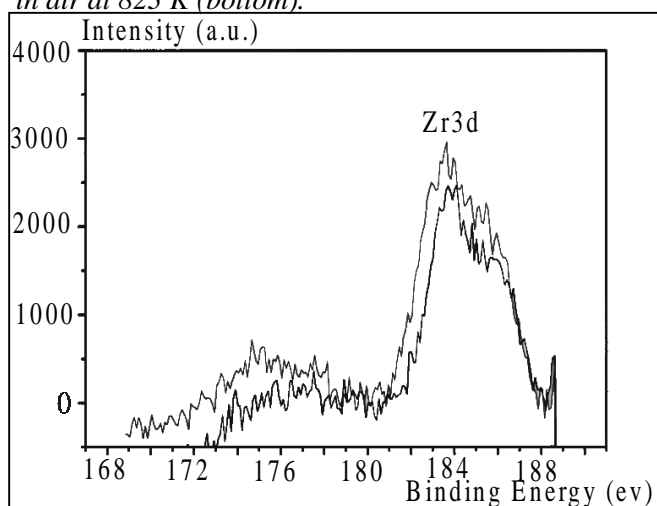


Figure 10. Effect of H_2S on selectivities of PtZrMOR. $P_{n-butane} = 220$ mbar, $P_{H_2} = 880$ mbar, $WHSV = 0.08$ mol/g \cdot h; with regeneration in between sequences.

Table 3. Averaged particle size of fresh and spent catalysts used in reaction with sulfur

Catalysts	Particle size Pt (nm)
PtMOR(fresh)	<i>below detection limit</i>
PtMOR(spent)	10.5
PtZrMOR(fresh)	2
PtZrMOR(spent)	16
PtZrMOR(presulfided)	5.5

**Figure 11.** Ir spectra of Pt-MOR (top), PtZrMOR respectively fresh, poisoned with 1000 ppm H₂S, poisoned with 1000 ppm H₂S and subsequently heated in air at 823 K (bottom).**Figure 12.** XPS spectra of PtZrMOR poisoned with 1000 ppm H₂S (lower), poisoned with 1000 ppm H₂S and subsequently heated in air at 823 K (upper); spectra represent Zr3d bindings energy.

Unlike for PtMOR, product distributions over PtZrMOR differed significantly depending on the oxidative regenerations in between the sulfur sequences. Figure 10 shows the selectivity plots (associated with the activity data shown in figure 9) for PtZrMOR at 0 to 1000 ppm H₂S in the feed with the oxidative regeneration applied. Up to 200 ppm H₂S, the production of propane increased at the expense of pentanes. At higher concentrations of H₂S, however, a further increase in the formation of propane was seen, but then at the expense of iso-butane. This may indicate that there are two different ways of propane formation. Additionally, half of the original hydrogenolysis activity was lost at 1000 ppm.

TEM/EDX analysis showed a sulfur induced Pt sintering process for both catalysts. Particle size distributions for the samples are listed in Table 3. To test the difference in sulfur-induced acidity changes, pyridine was adsorbed at 10⁻² mbar on both fresh PtZrMOR and spent, subsequently regenerated PtZrMOR. For the fresh catalyst pyridine induced bands at 1544 and 1452 cm⁻¹ assigned to Brønsted (PyH⁺) and Lewis acid sites (PyL), respectively. In case of the sulfur treated and oxidative regenerated PtZrMOR the same bands can be observed however the relative intensities has changed. Using the molar extinction coefficients as reported by Lavalley [14], the poisoned catalyst had 25 % more Lewis acidity than the fresh analogue.

Figure 11 shows the IR spectra of fresh PtMOR, fresh PtZrMOR, 1000 ppm H₂S treated PtZrMOR and the latter heated at 823 K in air, respectively. While the first three spectra are essentially similar, the fourth spectrum clearly shows an additional band around 740 cm⁻¹ which is assigned to sulfate in sulfated zirconia [15].

The presence of low quantities of sulfur (sulfate) in the spent catalysts was also seen with XPS. Zr3d intensities of H₂S exposed PtZrMOR with and without the oxidative high temperature treatment indicated that Zr is present in (partially) oxidized state which could be either ZrO_x or Zr(OH)₄ but likely a mixture of both (Fig.12). Only the intensity pattern found for the catalyst with the oxidative high temperature treatment covers the binding energy as expected from zirconium in interaction with sulfur (181.8 eV). Analysis of carbon deposits after 60 minutes time on stream pointed out that PtZrMOR used in reaction with H₂S, subsequently reactivated and again measured under H₂S, contained a similar amount of carbon as spent H-MOR. PtZrMOR treated with 1000 ppm H₂S but not regenerated in between the sequences contained less carbon and had higher H/C ratio than the others (Table 4).

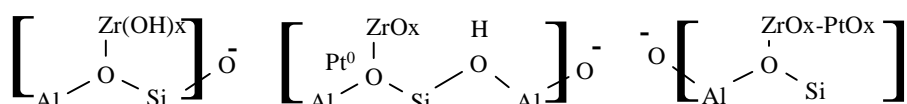
Table 4. Carbon analysis on spent catalysts: 1) HMOR used with nC_4/H_2 2) PtZrMOR used with $nC_4/H_2/H_2S$, regenerated in between the sequences 3) PtZrMOR used with $nC_4/H_2/H_2S$, non-regenerated.

Catalysts	Carbon (Wt%)	Hydrogen (Wt%)	Ratio H/C
1	0.145	0.163	1.11
2	0.11	0.125	1.13
3	0.054	0.072	1.34

6.4 Discussion

6.4.1 The structure of PtZrMOR catalyst

Zirconium has been shown to be present in oxidized form (XRF and XPS). This is in accordance with our expectance of forming $Zr(OH)_4$ and ZrO_2 during calcination which cannot be reduced with hydrogen at 823 K. Zirconia was present uniformly in well-dispersed form in all catalysts as concluded from the constant EDX Zr-intensities while scanning over the entire sample. Infrared spectroscopic analysis as well as NH_3 desorption show that $ZrOx$ remains in interaction with the bridged hydroxyl groups in the zeolite after calcination. Subsequent ion-exchange with Pt-precursor induces an additional loss in bridged Si-OH-Al which implies that Pt,



Scheme 1. Proposed structure of PtZrMOR; representation of three possible coordinations of Zr.

partly, is also exchanged. The loss of free zirconium hydroxyls was also seen (FTIR) which indicates that Pt is also present in interaction with $ZrOx$. Similar sorption capacity for *n*-butane found for PtMOR and PtZrMOR point out that the role of zirconium is rather acid site removal than blocking micropores. Hence, we propose the composition to be as qualitatively depicted in scheme 1.

6.4.2 The influence of Zr and pre-sulfidation on the product distribution

Bifunctional catalysts, such as needed in hydrocracking and hydroisomerization, demand a (de-)hydrogenation function. The incorporation of platinum into mordenite is known to improve the catalytic stability of this catalyst in the presence of hydrogen [9, 16]. This improved stability, however, is reached at the price of a lower activity. This is largely attributed to the high hydrogenation activity that results in a lower concentration of alkenes (and carbocationic intermediates) needed for isomerization *via* the bimolecular mechanism [9]. For optimal performance, the sites catalyzing hydrogenation/dehydrogenation should, therefore, just establish the equilibrium and keep the acid sites clean from olefinic coke precursors. An imbalance in hydrogenation and acid function can alter the apparent reaction network [17,18]. Mostly, an optimum in the hydroisomerization activity as a function of metal loading has been reported [6,7]. At lower loadings the rate of hydrogenation-dehydrogenation is too low, while at higher loading hydrogenolysis gains in significance [9, 19]. Although the impact of Pt loading is well established, the importance of dispersion of this loading is less straightforward. The metal accessibility rather than the amount of metal determine hydrogenation activity. Incorporation of zirconium should improve metal dispersion as claimed by Mobil [8]. The presence of Zr at some bridging OH groups leaves the exchange sites for Pt well separated and hence limits the chance of Pt sintering during reduction. Hence, Pt particles are expected to be smaller. However, the consequence of having smaller Pt particles is not straightforwardly answered. While van Broekhoven *et al.* report hydrogenolysis activity to be less with decreasing metal particle size [20], Nazimec *et al.* [10] report 2 to 4 nm particles to be most active in hydrogenolysis. Others report the hydrogenolysis activity to decrease with a larger Pt particle size [21,22]. TEM studies on the catalysts indicated a less homogeneously dispersed Pt upon introduction of zirconium and a larger mean Pt particle size. Nevertheless, the hydrogenolysis activity was somewhat reduced that is in agreement with the proposals that larger Pt particles are disfavoring hydrogenolysis. Other experiments showed that the addition of Zr to PtMOR is more beneficial for catalysts with higher Pt enrichments [33].

The intrinsic activities for PtMOR and PtZrMOR turned out to be similar although ammonia sorption revealed 25 % less acid sites in the latter case. As the rate determining step is the dimerization on the accessible acid sites in the main channels of MOR, it indicates that ZrO_2 and, likely, also Pt partly are situated in the side pockets of MOR inaccessible to nC_4 [11].

Pre-sulfiding the bifunctional catalysts suppressed hydrogenolysis reactions to a certain extent in agreement with work of Menon *et al.* [28]. The catalytic stability, however, was left unchanged. Thus, we conclude that the bifunctionality of the catalysts and the ability of Pt to hydrogenate coke precursors was entirely retained. A drop in the steady state conversion can be rationalized with the growth of Pt (the average metal cluster size increased from 2 to 5.5 nm after presulfidation (Table 4).

6.4.2 Sulfur tolerance of Pt-(Zr)-MOR

Acid bifunctional zeolite catalysts are claimed to have better resistance to poisons, nevertheless too high a sulfur content in the feed will still deteriorate the catalysts performance [23]. PtMOR is known to maintain significant performance in hydroisomerization of pentane in the presence of moderate amounts of sulfur (500 ppm)[1,23].

Among the most relevant questions to address when dealing with sulfur poisoning is (1) Do metal particles grow on acidic and non-acidic supports in the presence of sulfur ?, (2) Is sulfur reversibly or irreversibly bound ?, (3) Is the surface sulfur coverage lower on acidic supported metal particles ? Using EXAFS and high resolution electron microscopy, it has been shown before that platinum clusters supported on non-acidic LTL zeolite start to grow when exposed to sulfur [25]. This appears to be an important mode of deactivation, reducing the available metal surface area, both by virtue of the lower surface/volume ratio of larger particles and also by filling the zeolite channels and blocking access. Although the growth of Pt clusters is apparently evidenced in case of non-acidic zeolite, the fate of metal particles supported on acidic zeolite like mordenite is still not unequivocally answered [26]. Our HREM work, however, indicates indisputably the growth of Pt particles upon sulfur addition.

The kinetic results obtained with PtMOR and PtZrMOR are essentially similar. The major impact of H₂S was seen to be the loss of steady state activity. This would be rather straightforward explainable as caused by Pt particle growth which led to reduced availability of metal. Additionally, the bigger Pt particles may block the accessibility to the Brønsted acid sites. Moreover, the preservation of catalysts stability indicates that the parallel loss of metal sites and acid sites, both as a possible consequence of the Pt growth, allows the (de-)hydrogenation-acid protolysis equilibrium as desired for a bifunctional mechanism to be preserved.

Testing the reversibility of surface bound sulfur *via* employing a high temperature regeneration shed new light on the mechanism of sulfur poisoning but induced also new mechanistic complexity for PtZrMOR. Once the catalyst is regenerated and measured under helium, activity and stability is retained. Also, hydrogenolysis activity was restored. This implies that suppression of (de-)hydrogenation activity and hydrogenolysis is due to the prior formation of reversibly bound sulfur-species which are released during the high temperature regeneration. In this respect it is worth mentioning that similar behavior was found by Pönitzsch *et al.* [29] and Menon *et al.* [30,31] for Pt/alumina; heating at 873K(773K) in hydrogen led to release of reversibly bound sulfur species thereby restoring hydrogenolysis activity. Moreover, this also means that the significant reduction in accessible Pt surface area does not induce any differences in the performance of the bifunctional catalyst. Thus, in line with other authors [30, 35], we believe that sulfidation enhances the (de-) hydrogenation activity of Pt. Preliminary experiments show that the restorative properties of the sulfur poisoned catalysts are also evident for *n*-pentane hydroisomerization and also with other molecular sieves [34].

For PtZrMOR, the regeneration brought about some characteristics for *n*-butane isomerization that were not found for PtMOR. PtZrMOR started deactivating, this effect being more significant with increasing the concentration sulfur. A carbon analysis on spent catalyst showed that this is due to enhanced coke formation. Additionally, disproportionation gained importance at the expense of isomerization. The initial activity found for PtZrMOR increases with increasing content of sulfur in the feedstream (see Fig. 9). When attempting to explain those differences regarding PtMOR and PtZrMOR we should start with considering the presence of zirconia. This indirectly introduces options for having Pt in a different location, viz., Pt onto a different support (see scheme 1) and additionally, the activity of zirconia should be accounted for. One could think the following to occur in case of PtZrMOR; the H₂S partially interacts with the zirconia while subsequent calcination in air yields sulfated zirconia, known to have high acidity and reasonable isomerization activity [27]. PtZrMOR (1000 ppm), when regenerated beforehand showed exactly the same activity trend as H-MOR and similar quantity of carbon deposits. This may indicate that the hydrogenation functionality of Pt is eliminated during sulfur cofeed, the balance between (de-)hydrogenation and acid protolysis is lost and the catalyst acts similar to an ordinary H-MOR. This is in agreement with earlier findings on Pt supported reforming catalysts

[28] which show that higher loadings of H₂S result in a drastic decrease of the dehydrogenation activity. This phenomenon is, however, in present work only observed when the catalyst was already exposed to sulfur and regenerated at high temperature. This indicates that, strictly under these conditions, some structural changes have occurred. When we now recall the observations found by IR (see Fig. 11), those changes are indeed evidenced. As it is not seen for PtMOR, the answer should be sought for in the introduction of an additional type of acidity by formation of a "SO_x"-zirconia. The increase of the overall acidity by the presence of sulfated-zirconia is also indicated by the increase of the (bimolecular) cracking activity at the expense of isomerization.

6.5 Conclusion

Addition of zirconia and pre-sulfidation were tried for fine-tuning the bifunctional PtMORdenite catalyst toward isomerization selectivity by suppressing hydrogenolysis activity of Pt. Both led indeed to a moderate suppression of hydrogenolysis. The addition of zirconia is shown to be more beneficial for catalysts enriched with higher Pt loadings [33].

PtMOR and PtZrMOR catalysts for hydroisomerization of *n*-butane reveal sulfur tolerance up to 1000 ppm. In both cases, the only impact upon sulfur in the feed was a lower steady state activity; catalytic stability and selectivity were retained. Although a Pt sintering process is evident, the prevailing reason for reduced steady state activity was found to be due to binding of reversible sulfur species. Oxidative regeneration at high temperature is sufficient to remove those species and to restore the initial conversion. Preliminary experiments show that the restorative properties of the sulfur poisoned catalysts can be extended to *n*-pentane hydroisomerization and also to other molecular sieves [34]. Although the total metal area became significantly less after sulfur exposure the stability could be entirely preserved. This suggests that only very little amount of effective Pt area is necessary to sufficiently hydrogenate coke precursors or sulfidation increases the intrinsic (de-) hydrogenation activity of Pt. The combination of zirconia, H₂S and regeneration brought about an additional mechanistic complexity under sulfur cofeed. This has shown to be due to the formation of sulfated-zirconia. The presence of sulfated zirconia increased the overall acidity of the catalysts resulting to higher cracking activity at the expense of isomerization and lowered the catalyst stability.

Acknowledgment

Dr. Patricia.J. Kooyman is kindly acknowledged for the critical reviewing of this chapter.

References

1. Sie, S.T., *Stud. Surf. Sci. Catal.* **85**, 621 (1994).
2. de Agudelo, M. US Patent 5416052.
3. Maxwell, I.E., and Stork, W.J.H., *Stud. Surf. Sci. Catal.* **58**, 571 (1991).
4. Marcewski, H., *J.Chem.Soc.Farad. Trans. 1*, **82**, 1687 (1986).
5. Asuquo, R.A., Eder-Mirth, G., and Lercher, J.A., *J. Catal.* **155**, 376 (1995).
6. Liu, H., Lei, G.D., and Sachtler, W.M.H., *Appl. Catal. A: General* **137**, 167 (1996).
7. Bearez, C., Avendano F., Chevalier, F., and Guisnet, M., *Bull. Soc. Chim.* 346 (1985).
8. Absil, R.P.L., and Huang, Y., US patent No. 4837397 (assigned to Mobil).
9. Asuquo, R.A., Eder-Mirth, G., Pieterse, J.A.Z., Seshan, K. and Lercher, J.A., *J. Catal.* **168**, 92 (1997).
10. Nazimek, D., and Ryczkowski, J., *React. Kinet. Catal. Lett.* **40**, 137 (1989).
11. Eder, F., and Lercher, J.A., *Stud. Surf. Sci. Catal.* **97**, 495 (1995).
12. Yamaguchi, T., Nakano, Y., and Tanabe, K., *Bull. Chem. Soc. jpn.* **21**, 2481, (1978).
13. Kustov, L.M., Kazansky, B., Figureas, F., and Tichit, D., *J. Catal.* **150**, 143 (1994).
14. Khabtou, S., Chevreau, T., and Lavalley, J.C., *Microp. Mater.* **3**, 133, (1994).
15. Nyquist, R.A. and Kagel, R.O., “*Infrared spectra of Inorganic Compounds*”, 461, pg. 279
16. Kouwenhoven, H.W., and Van Zijl Langhout, W.C. *Chem. Eng. Prog. Apr.* 65 (1971).
17. Alvarez, F., Ribeiro, F.R., Gianetto, G., Chevalier, F., Perot, G., and Guisnet, M., *Stud. Surf. Sci. Catal.* **49**, 1339 (1989).
18. Degnan T.F., and Kennedy, C.R., *AIChE journal* **39**(4), 607 (1993).
19. Ribeiro, F., Marcilly, C., and Guisnet, M., *J.Catal.* **78**, 275 (1982).
20. van Broekhoven, E.H., and Ponec, V., in “*Progress in Surface Science*”, Vol.19, No. 4, p385 (1985).
21. Rodriguez-Reinoso, F., Rodriquez-Ramos, I., Morena-Castilla, C., Guerrero-Ruiz, and Lopez-Gonzalez, J.D., *J. Catal.* **107**, 1 (1987).
22. Che, M., and Bennet, C. O., *Adv. Catal.* **136**, 55 (1989).
23. Jao, J R.M. Leu, L.J. and Chang, J.R., *Appl. Catal.* **135**, 301 (1996) and references therein.
24. Sie, S. T., *Stud. in Surf. Sci. Catal.* **85**, 621 (1994).
25. Vaarkamp, M., Miller, J.T., Modica, F.S., Lane, G.S., and Koningsberger, D.C., *J.Catal* **138**, 675 (1993).
26. Ishihara, A., *Chem. letters* 589 (1993).
27. Song, X., and Sayari, A., *Catal.rev.-sci.eng.* **38**(3), 329 (1996) and references therein.
28. Menon, P.G., and Paal, Z., *Ind. Chem. Res.* **36**, 3282 (1997) and references therein.

29. Pönitzsch.L., Wilde, M., Tetenyi, P., Bobrovolszky, M, and Paal, Z., *Appl. Catal.* **86**, 115 (1992).
30. Menon.,P.G., *Ind. Eng.Chem.Prod.Res.Div.* **21**,52 (1982).
31. Menon.P.G., in ' *Advances in Catalysis Science and Technology*', Prasada Rao, T.S.T., Ed., New Delhi, India, 1985, pg.1-15.
32. Meier,W.M and Olson,D.H. *Atlas of zeolite structure types*, Butterworth-Heinemann, London (1992).
33. Asuquo, R.A., *PhD thesis*, ISBN 90-9009570-5, University of Twente, 1996.
34. Kinage, A., Pieterse, J.A.Z., He, Y., and Lercher, J.A., unpublished results.
35. Resasco, D.E., and Haller, G., in "*Catalysis*", **11**, 379 (1994) and references 40 and 69 therein.
36. Meier,W.M. and Olson, D.H., *Atlas of zeolite structure types*, Butterworth-Heinemann, London 1992.

Sorption and Ordering of Dibranched Alkanes on Medium Pore Zeolites Ferrierite and TON

Abstract

The sorption of (methyl substituted) pyridines and 2,2-dimethylalkanes on medium pore zeolites FER and TON has been studied by *in situ* IR spectroscopy, calorimetry and gravimetry in order to describe sorption at the outer surface and the pore mouths of the zeolite crystals. 6 % and 3 % of the Brønsted acid sites (determined by adsorption of 2,4,6 trimethylpyridine) were found to be on the outer surface and the pore mouth of TON and FER, respectively. This agrees fairly well with the fraction of sites that are available for the 2,2-dimethylalkanes which are unable to fully enter the pores of the zeolites studied. Remarkably, at low coverage all three dimethylalkanes adsorb in parallel to the outer surface. As the coverage increases, additional 2,2-dimethylpentane and 2,2-dimethylhexane molecules sorb in such a manner that the propyl- and butyl-group point into the pore. Also, approximately 80 % of the 2,2-dimethylpentane and 2,2-dimethylhexane molecules that initially sorbed parallel to the outer surface rearrange to this sorption structure. This ordering is well documented by the marked increase in the heat of adsorption as the equilibrium pressure increases and by the IR spectra of hydroxy groups in interaction with the alkane during this process.

7.1 Introduction

Ferrierite (FER) and ZSM-22 (TON) in their proton exchanged form are catalysts commercially applied in the skeletal isomerization of alkenes and alkanes [1, 2]. Although the heuristic aspects of the catalytic properties of both molecular sieves are well documented, the mechanistic aspects of the conversions on a molecular level are remarkably controversial.

The pore diameters of TON and FER are similar to the kinetic diameters of singly branched alkanes. Thus, it is difficult to imagine that the total volume of the molecular sieve is utilized for the reaction. The shape of the pores and the molecules suggest that individual molecules cannot pass each other within a channel, i.e. single file diffusion prevails [3]. The severe impact of these constraints upon the microscopic steps of sorption and surface reaction led Martens *et al.* to conclude that skeletal isomerization of hexadecane proceeds only at the pore mouth, and the outer surface of TON crystallites [4]. It was shown that the array of adjacent pore openings acts as a template for the branching of the linear chain. The spacing of the pores in the crystal surface and the chain branching in the hydrocarbon skeletons match closely.

While such a concept is intuitively intriguing, it is mainly based on circumstantial kinetic evidence. Very little is known about the nature and morphology of the outer surface of zeolites. The proposed concept assumes a clean and mesoscopically not corrugated surface allowing the regularity for the linear chain to isomerize in regular intervals. As one synthesizes a microporous material out of a solution containing colloidal or dissolved silica entities, it is unlikely that the surface is not contaminated by amorphous material that forms a macroporous overlayer. This is expected to severely impact the sorption of sterically more demanding alkanes. Moreover, it is frequently found that the distribution of alumina is inhomogeneous over the crystallite and, hence, the concentration of Brønsted acid sites cannot be deduced by extrapolating the bulk chemical composition. Thus, the concentration, strength and accessibility of Brønsted acid sites at the pore entrance must be experimentally assessed in order to allow for a full molecular description of the sorption and eventually catalyzed reactions.

In this contribution we describe the unique sorption behavior of dibranched alkanes on FER and TON serving as a model, how sterically demanding molecules might sorb on the surface of microporous materials. Additionally, the quantitative determination of the concentration of acid sites in FER and TON accessible to reactants of various sizes is discussed.

7.2 Experimental

7.2.1 Materials

Silica (Aerosil 200) was obtained from Degussa. For activation, the material was heated in vacuum with 10K/min to 873 K and held there for one hour. NH_4^+ -ZSM22 with a Si/Al ratio of 52 was received from Dr. M. Derewinski of the Polish Academy of Science. Na/K-FER was obtained from Tosoh Co (Si/Al 9). The samples were completely transferred into NH_4^+ -form by ion exchanging them three times with 1 molar NH_4NO_3 . The NH_4^+ -form was transferred to the H^+ -form by heating in vacuum to 673K with 10K/min. Pyridine and 2,4,6-trimethylpyridine (TMP) were obtained from Fluka (>99 % purity). 2,2-dimethylbutane (DMB), 2,2-dimethylpentane (DMP) and 2,2-dimethylhexane (DMH) were obtained from Sigma Aldrich (>99.95 % purity).

7.2.2 IR spectroscopy

The adsorption studies were performed in a vacuum infrared cell, which was placed in a BRUKER IFS88 IR spectrometer. The cell was evacuated to a base pressure of 10^{-7} mbar. The samples were pressed into self-supporting wafers of approximately 5 mg and activated *in situ* at 673 K. The probe molecules were introduced *via* a differentially pumped dosing valve. The partial pressure was increased stepwise from 10^{-4} to 10^{-1} mbar. The integrated intensities of a band characteristic for pyridinium ions and the decrease in the intensity of the hydroxyl bands were used to determine the fraction of Brønsted acid sites accessible. Comparative measurements on silica were used to assign the bands for the substituted pyridines. Detailed information on the experimental procedures can be found in refs. [5, 22].

7.2.3 Microcalorimetry and gravimetry

The gravimetric and calorimetric measurements were performed in a modified SETARAM TG-DSC 111 instrument [5]. The system consists of four main parts, i.e. the balance, the calorimeter, the vacuum system and the mass spectrometer to analyze the gas composition. For the sorption experiments the samples were pressed into thin wafers that were subsequently broken into small platelets. As described above, the NH_4^+ -form of the samples was transformed

into the H^+ -form by heating in vacuum to 673K with an increment of 10K/min and holding that temperature for two hours. After activation, the system was cooled down to the sorption temperature. The adsorption of dibranched alkanes was studied at 343 K between 10^{-2} and 13 mbar equilibrium pressure. The hydrocarbons were admitted in doses and were allowed to equilibrate with the zeolite. Equilibration was assumed being reached when the heat signal reached the initial, constant value and changes in the gravimetric signal were not observed. NH_3 sorption measurements were performed in order to determine the total acid site concentration.

7.3. Results and discussions

7.3.1. Structural information and general characterization

FER contains two perpendicularly intersecting channel systems [6,7]. One consists of 10 membered rings with a dimension of 0.42 x 0.54 nm, the other of 8 membered rings with a dimension of 0.35 x 0.48 nm (see Figure 1a). The unit cell was reported to contain 5 non-equivalent T-atoms [7]. The density of T-atoms is reported to be 17.7 per 1000 \AA^3 [6].

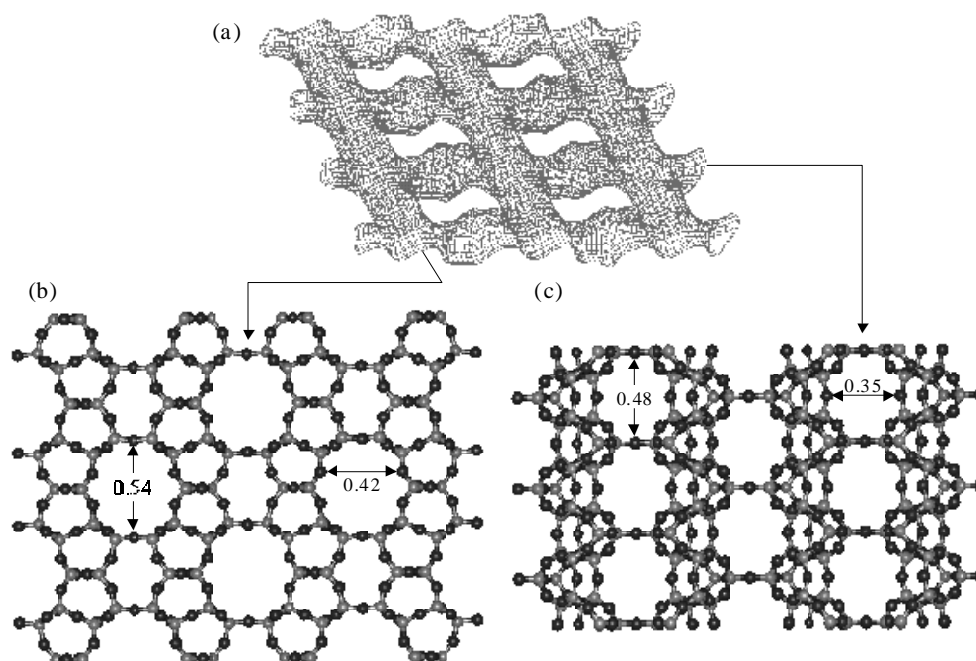


Figure 1a. Schematic representation of FER, (a) pore system, (b) viewed along the 10 ring channels and (c) viewed along the 8 ring channels).

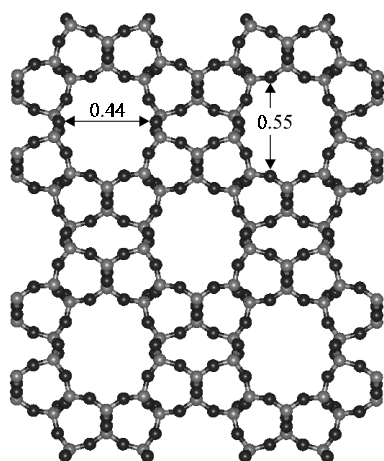


Figure 1b. TON (viewed along the 10 ring channels).

The TON structure has a unidimensional elliptical pore system. The channels consist of 10 membered rings and are of the dimension 0.44 x 0.55 nm (see Figure 1b). The density of T-atoms is reported to be 19.7 per 1000 Å³ [6].

Scanning electron microscopy (SEM) showed small platelike particles for FER, sizing (1 -2) x 1 µm. For TON a needle like structure was observed, sizing (2-4) x 1 µm. By means of ammonia and pyridine sorption ($\gamma(1455) = 1.5 \mu\text{mol}^{-1}.\text{cm}$ and $\gamma(1545) = 1.8 \mu\text{mol}^{-1}.\text{cm}$ [8]) the Brønsted acid site concentrations of FER and TON were determined to be 1.9 mmol/g Brønsted and 0.36 mmol/g, respectively. The Lewis acid site concentration was estimated to be 0.07 mmol/g and 0.05 mmol/g, respectively. The heat of ammonia sorption was in both cases 140 kJ/mol indicating a similar strength of interaction between the acid sites of the materials and the sorbed ammonia.

7.3.2 Adsorption of pyridine homologues

The probe molecules used in this study were pyridine and 2,4,6-trimethylpyridine(TMP). The size of TMP, 6.2*5.6 Å, clearly suggests that the sorption of TMP allows to calibrate the concentration of the acid sites at the external surface / in the micropore mouth. Sorption of the pyridines on Brønsted acid sites lead to the formation of pyridinium ions and to hydrogen bonded pyridine [8-11]. The interaction of the nitrogen lone pair with accessible Al³⁺ cations leads to an electron pair donor - electron pair acceptor type of interaction (interaction with Lewis sites). The basicity of pyridines increases with methyl substitution due to inductive effects, however, it is known that the substitution in positions 2 and 6 induces steric constraints at the nitrogen lone pair weakening the coordination compared to pyridine [10]. This prompted Benesi *et al.* to propose the use of 2,6,-dimethyl-pyridine as a specific probe for protonic sites [12]. While the molecule was used subsequently for selectively poisoning Brønsted acid sites [13], Knözinger *et al.* showed that TMP is able to form coordinative bonds with exposed aluminum cations on a γ -alumina surface [10].

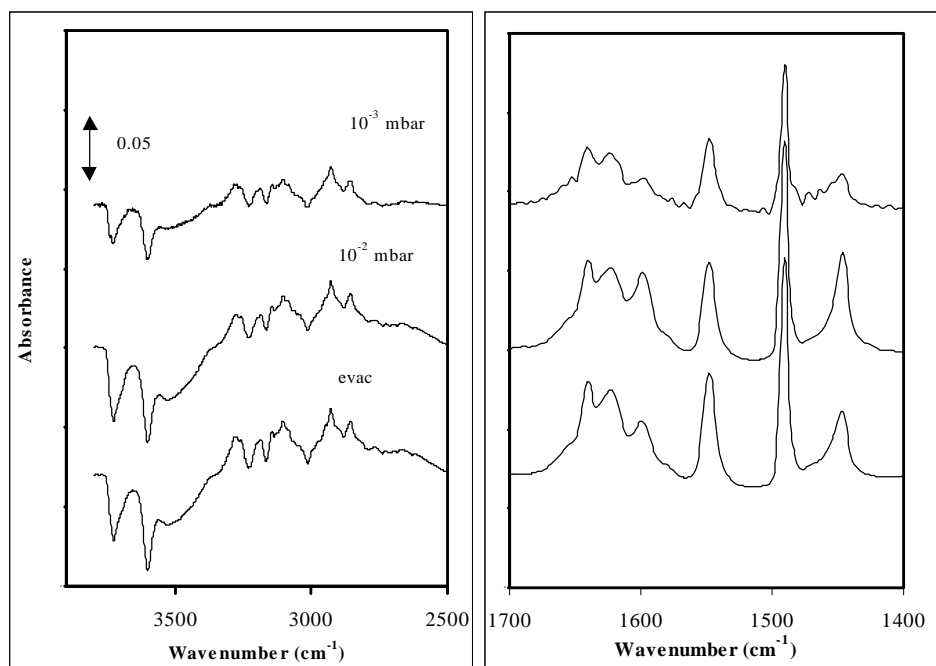


Figure 2. Sorption of pyridine on TON at RT and 10^{-3} and 10^{-2} mbar equilibrium loading.

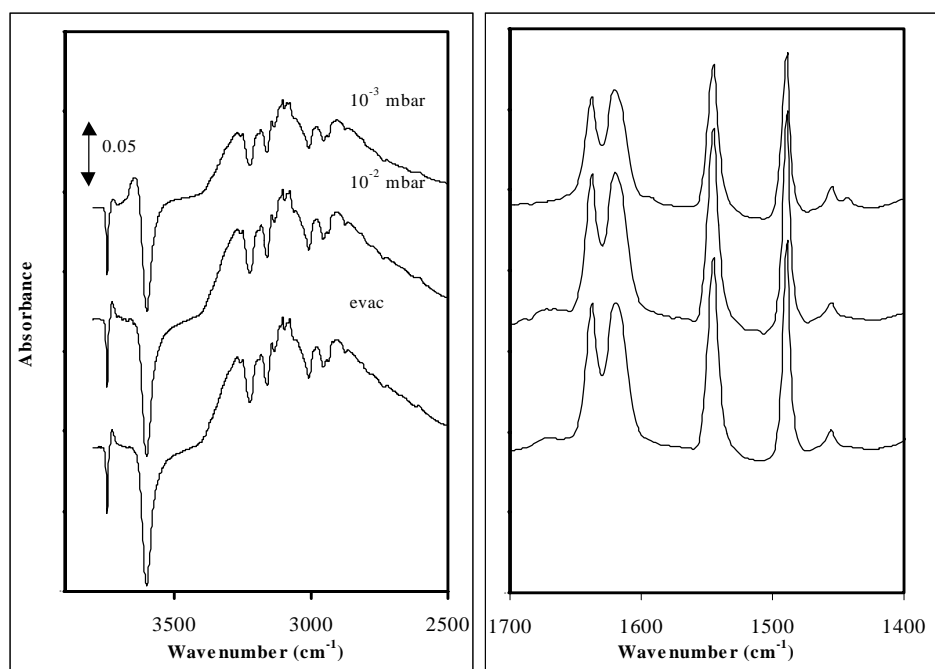


Figure 3. Sorption of pyridine on FER at RT and 10^{-3} and 10^{-2} mbar equilibrium loading.

7.3.3 Adsorption on TON

For TON, sorption studies were carried out at 298K with pyridine and TMP. Typically, the compounds were sorbed at 10^{-4} mbar, allowed to equilibrate, and stepwise exposed to 10^{-3} mbar

and 10^{-2} mbar. The maximum fraction of Brønsted acid sites consumed after equilibration at the different partial pressures of pyridine and TMP are compiled in Table 1. The maximum loading was 6 % for TMP and 92 % for pyridine. Figure 2 shows the difference IR spectra obtained for pyridine after equilibration for the loadings studied. Upon admittance of pyridine, the band at 3740 cm^{-1} disappeared (all SiOH are fully accessible) while the band of bridging OH groups at 3603 cm^{-1} disappeared only in part. The strong and broad absorption band between 3300 and 2000 cm^{-1} indicates moderately strong hydrogen bonding of pyridine to Si-OH groups and of pyridinium ions with the bridging oxygen at the aluminum framework sites. Upon increasing the partial pressure of pyridine, the interaction with the zeolite framework (conjugated weak base) is partly replaced by the interaction with excess pyridine as concluded from the additional perturbations of the N-H stretching vibrations of the pyridinium ions. The skeletal combination modes (overtone of the lattice vibrations) shifted to slightly lower wavenumber upon exposure to pyridine. Ring vibration bands were observed at $1640, 1623, 1600, 1547, 1494, 1456$ and 1446 cm^{-1} . Comparing these bands with the wavenumbers reported by Glazunov *et al.* [14] they were assigned to ring stretching modes ($1640, 1623, 1547\text{ cm}^{-1}$ (PyH^+), 1600 and 1491 cm^{-1} (PyL)). The band at 1547 cm^{-1} served as characteristic band for quantifying pyridinium ions (PyH^+). To quantify pyridine adsorbed coordinatively to accessible Al^{3+} cations (PyL) the band at 1456 cm^{-1} , for physisorbed pyridine the band at 1446 cm^{-1} was used. Detailed assignments on basis of refs.[10,11,14, 15, 16,17,18] are compiled in Table 2.

The equilibrium coverage of TMP was significantly lower than that of pyridine. All Si-OH groups interacted with TMP. However, only 6 % of the strong Brønsted acid sites (3604 cm^{-1}) disappeared after equilibration at 10^{-2} mbar. In parallel, a band at 1637 cm^{-1} corresponding to TMPH^+ appeared. The low uptake indicates that only the outer surface and the pore mouths are accessible for TMP.

Table 1. maximum uptake with pyridine and TMP at 298 K and 573 K.

Probe molecule	Coverage at 10^{-4}		Coverage at 10^{-3} mbar (%)		Coverage at 10^{-2} mbar (%)		Coverage at 10^{-1} mbar (%)	
	mbar (%)							
	TON	FER	TON	FER			TON	FER
2,4,6-trimethylpyridine	3	1	5	2.5	6	3	-	-
Pyridine	43	27	59	40	92	45(69) ¹	100 ¹	100 ¹

¹-at 573 K

Table 2. Assignment of vibrational modes of Py and TMP adsorbed on FER and TON (between brackets).

Vibrational modes	Py liquid	PyH ⁺	PyL	TMP on γ -alumina ¹⁰	TMPyH ⁺	TMPyL
8a;Vcc(N)A ₁	1579 s	1638 s (1640 s)	(1600 m)	1634	1639 vs (1637 m)	-
8b;Vcc(N) B ₁	1572 m	1619s (1623 s)	(1575 m)	1566	1572 w (1574 m)	-
19a;Vcc(N)A ₁	1478 s	1489 vs (1491 vs)	-	1500	1488 w	-
∂ asCH ₃	-	-	-	1455	-	1452 w
19b;Vcc(N)B ₁	1439 vs	1545 s (1547s)	1455 w (1456m)	1415	1547 w	1411 w
∂ sCH ₃	-	-	-	1383	1390 w	1380 w

Note, between brackets represent TON

vs, very strong; s, strong m, medium; w, weak

In accordance with ref. [8] the sole presence of TMPH⁺ is attributed to the steric constraints around the nitrogen atom. To test the accessibility of acid sites under relevant catalytic conditions, pyridine was sorbed at 573 K and 10⁻¹ mbar. Despite the large differences at low temperatures, pyridine covered nearly 100 % of the strong Brønsted acid sites as concluded from the complete disappearance of the band of the SiOHAl groups (Table 1).

7.4.4 Adsorption on FER

Table 1 shows the uptake of pyridine and TMP after 21 hours of contact with 10⁻⁴, 10⁻³ and 10⁻² mbar of the sorbate at room temperature. It was not possible to reach equilibrium coverage with pyridine at the low pressures despite the extended equilibration time (21 hours). Therefore, coverages are compared at 10⁻² mbar after 21 hour. In the case of pyridine, 45 % of all Brønsted acid sites were concluded to interact after 21 hours equilibration time. The slow equilibration is

affiliated with higher acid site density and slightly smaller 10 membered ring openings of FER in comparison to TON. TMP reached only 3 % of all Brønsted acid sites. In case of TMP sorption the band corresponding to TMPH^+ appeared at 1638 cm^{-1} and persisted upon evacuation at ambient temperature. Other bands at 1617 and 1570 cm^{-1} (TMP coordinated to a Lewis acid site) disappeared upon evacuation indicating that coordinatively bound TMP is not stable at 10^{-7}

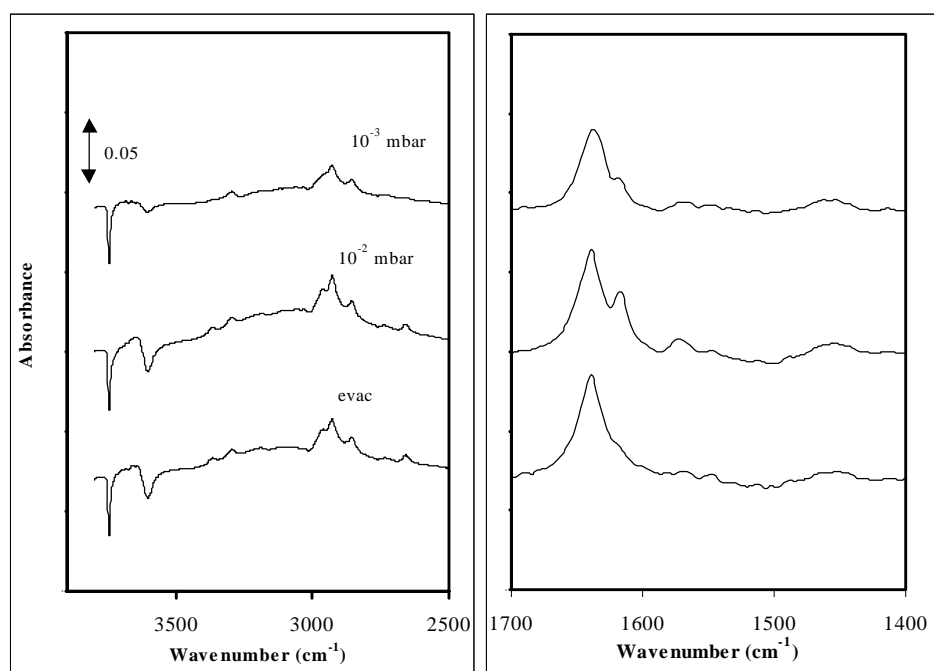


Figure 4. Sorption of TMP on FER at RT and 10^{-3} and 10^{-2} mbar equilibrium loading.

mbar at ambient temperature.

Figure 3 shows the (difference) IR spectra for pyridine at 298 K, after 21 hours of exposure. In accordance with its chemical composition a higher intensity of the bands at 1619 and 1545 cm^{-1} , the smaller band at 1455 cm^{-1} , indicate that FER has a higher concentration of Brønsted acid sites than TON. Upon contact with (substituted) pyridine (see also Figure 4 for TMP) the band of the Si-OH groups is shifted downwards by approximately 100 cm^{-1} , which is attributed to a weak hydrogen bonding *via* π electrons of the aromatic ring [8]. As this is the weaker basic function it should be emphasized that only steric constraints can force pyridine not to interact *via* its lone electron pair at the nitrogen.

With increasing exposure to pyridine, the intensities for the bands characteristic for pyridinium ions and coordinatively adsorbed pyridine increased, however, their relative ratio

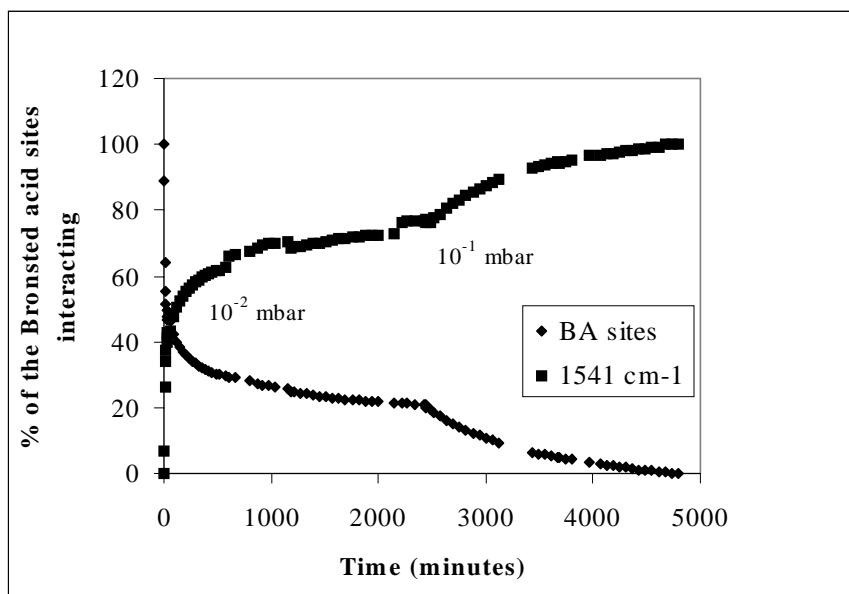


Figure 5. Uptake of pyridine on FER at 573 K and 10^{-2} , 10^{-1} mbar.

remained the same. At the lowest loading a substantially higher fraction of pyridine is bound to acid sites at the outer surface of the crystallites, thus, the monotonous change of relative intensities of the bands suggests an even distribution of Brønsted and Lewis acid sites throughout the material.

To probe the role of the temperature upon the accessibility of the pore structure, pyridine was sorbed at 10^{-2} mbar and 573 K. Even at this higher temperature equilibrium does not seem to be reached completely. After 42 hours 70 % of the Brønsted acid sites interacted with the base, which is, however, substantially higher than the 45 % found after exposure for 21 hours at ambient temperature. In order to probe whether or not the limited coverage is related to constraints in accessibility or to constraints in the transport of pyridine in FER, the sample was exposed to 10^{-1} mbar pyridine at 573K. In this case, full coverage was achieved after 73 hours of exposure (Fig.5).

7.4.5 Sorption of dibranched alkanes

Interactions based on London dispersion forces and localized induced dipole acid-base hydrogen bonding will contribute to the sorption of an alkane in a zeolite pore and on the outer surface of the crystallite [20]. The induced dipole acid-base hydrogen bonding with alkanes has been shown to contribute only 6 kJ/mol for FAU and 10 kJ/mol for H-ZSM5 independent of the size of the n-alkane. This should be compared with the overall heat of adsorption of n-

hexane on H- FAU and H-ZSM5, which were 53 kJ/mol and 82 kJ/mol, respectively. This indicates that for non polar and weakly polarizable molecules the energy of interaction and the heat of sorption are energetically fairly well described with non localized bonding.

The bonding forces involved are mostly determined by the geometry of the environment around the sorbed molecule. As these forces are additive, the strong interaction of weakly polar molecules in microporous materials has been explained by the optimized interactions through the curved surface (see, e.g. the formulation of the “confinement effect” by Derouane [21]). Previous own work has shown that the concept agrees very well with experimental observations [5,22,23]. The heat of sorption depends subtly on the fit between the size of the molecule and the size of the zeolite pores. For light alkanes (ethane to *n*-hexane) the sorption enthalpy increases in the sequence FAU<MOR<MFI<TON. Usually, with FER a 1-2

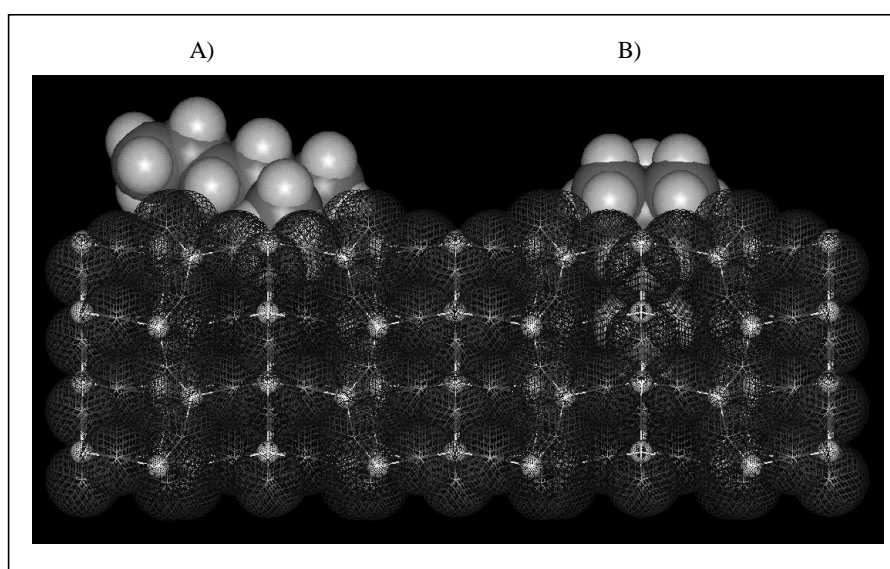


Figure 6. Optimized sorption structure of 2,2-dimethylhexane.

kJ/mol lower sorption enthalpy was found than with TON. This has been attributed to increasing repulsive forces, as the pore diameter passes an optimum value [5]. It should be noted that TON and FER exert constraints upon sorption of single branched alkanes leading to a lower uptake compared to *n*-alkanes. Therefore, sorption of dibranched alkanes allows to probe selectively sorption characteristics of the outer surface and pore entrance of TON and FER.

Model visualizations using the MSI Insight II software support this conclusion [27]. A rigid fragment of SiO₂ polymorph with TON topology was generated using the crystallographic data from reference [6]. Geometry optimization of 2,2-dimethylhexane was performed in a

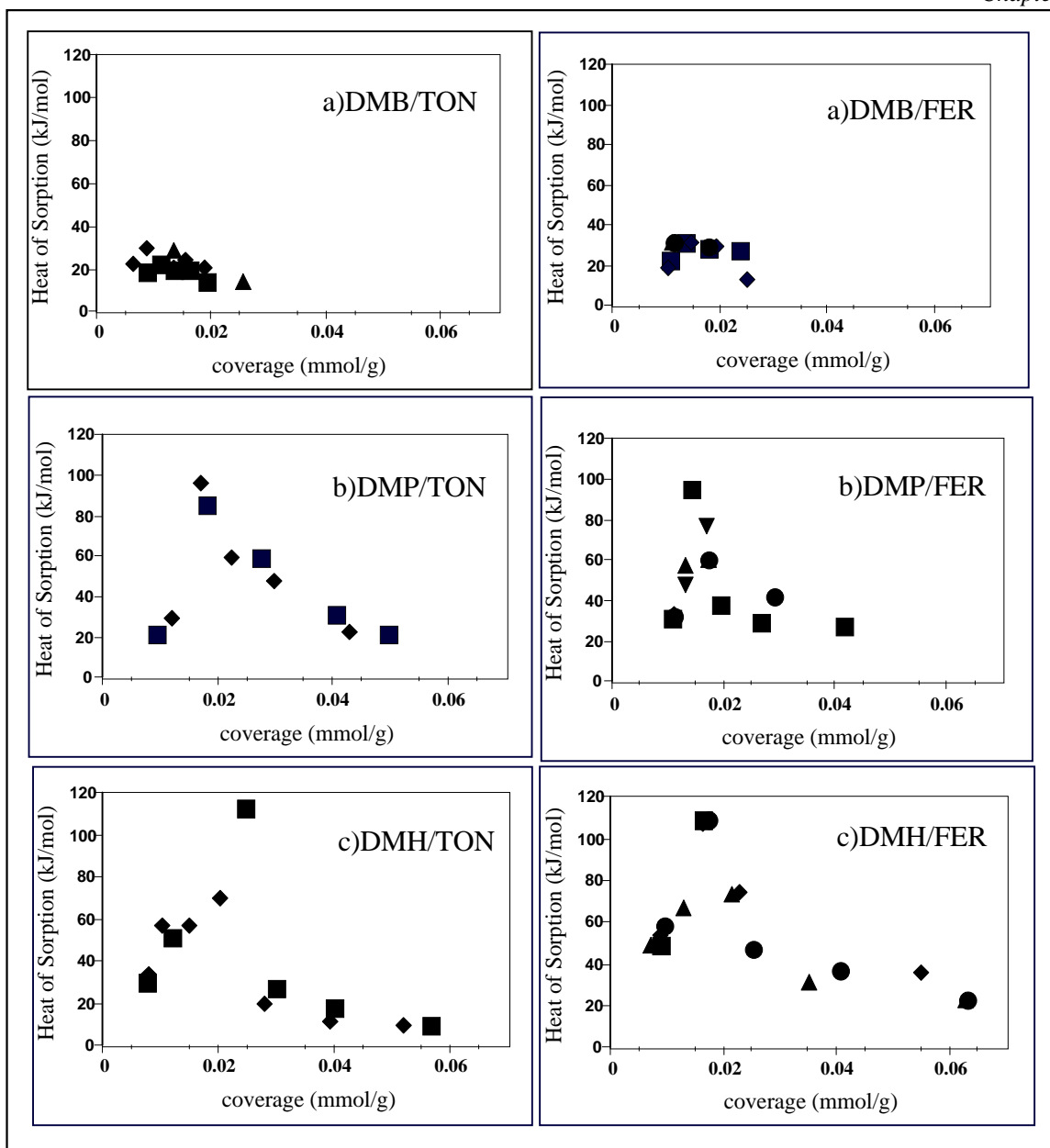


Figure 7. Differential heat of sorption on TON and FER as function of the coverage at 343 K; a) 2,2-dimethylbutane b) 2,2-dimethylpentane c) 2,2-dimethylhexane.

CVFF-aug force field, representative for the Lennard-Jones adsorption potential, in vacuum until a RMS gradient (total energy gradient calculated as a root-mean-square gradient) of 10^{-4} kJ/mol was reached. The docking results suggest that the sorption structure of the molecule can be optimized at the outer surface in such way that the methyl group of the neopentane unit points into the pore mouth and the rest of the molecule is stretched along the surface (Fig. 6a.). Additionally, the molecule may pin the neopentane unit into the pore mouth having his butane tail pointing upwards (not shown). Both sorption structures reveal similar adsorption potentials

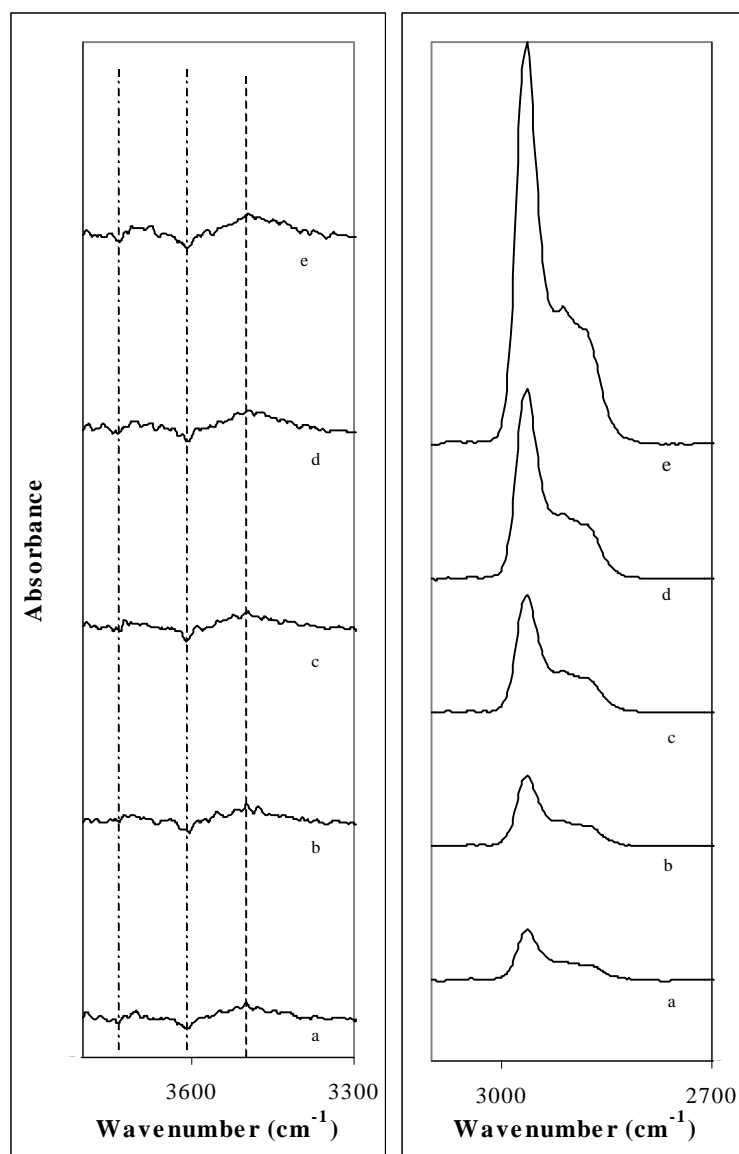


Figure 8. I.r. spectra of TON during sorption of DMB (343K). The lines correspond to increasing (a, b,...e) equilibrium pressures between 0.01 and 13 mbar of DMB.

heat flux to be monitored by the calorimetric measurements.

Upon exposing TON to DMP the initial heat of sorption was about 25 kJ/mol. This value rapidly increased with coverage and reached 97 kJ/mol at a coverage of approximately 0.017 mmol/g. With further increase in the coverage the heat of adsorption dropped again to approximately 20 kJ/mol at a coverage of 0.05 mmol/g. A similar trend was found for DMH. The initial heat of adsorption was about 27 kJ/mol and the maximum value of 113 kJ/mol was reached at approximately 0.025 mmol/g. For FER, very similar trends were observed as a function of coverage. The heat of sorption of DMB was again much lower than the other analogues. The highest value observed was 30 kJ/mol, but as with TON a distinct maximum in

Sorption and ordering.....

(18-24 kJ/mol). Finally, the molecule may enter the pore mouth with the longer hydrocarbon chain part, favorably in his most open (symmetric) conformation with part of the neopentane unit remaining externally (Fig. 6b.). This results in an adsorption potential amounting to approximately 65 kJ/mol.

Figure 7 depicts the heat of sorption of DMB, DMP and DMH on TON, as a function of the sorbate loading 343 K. For DMB, the heat of sorption was about 30 kJ/mol until a coverage of approximately 0.015 mmol/g. At the higher coverages the very slow uptake at longer equilibration indicates rearrangement of molecules that produces a too low

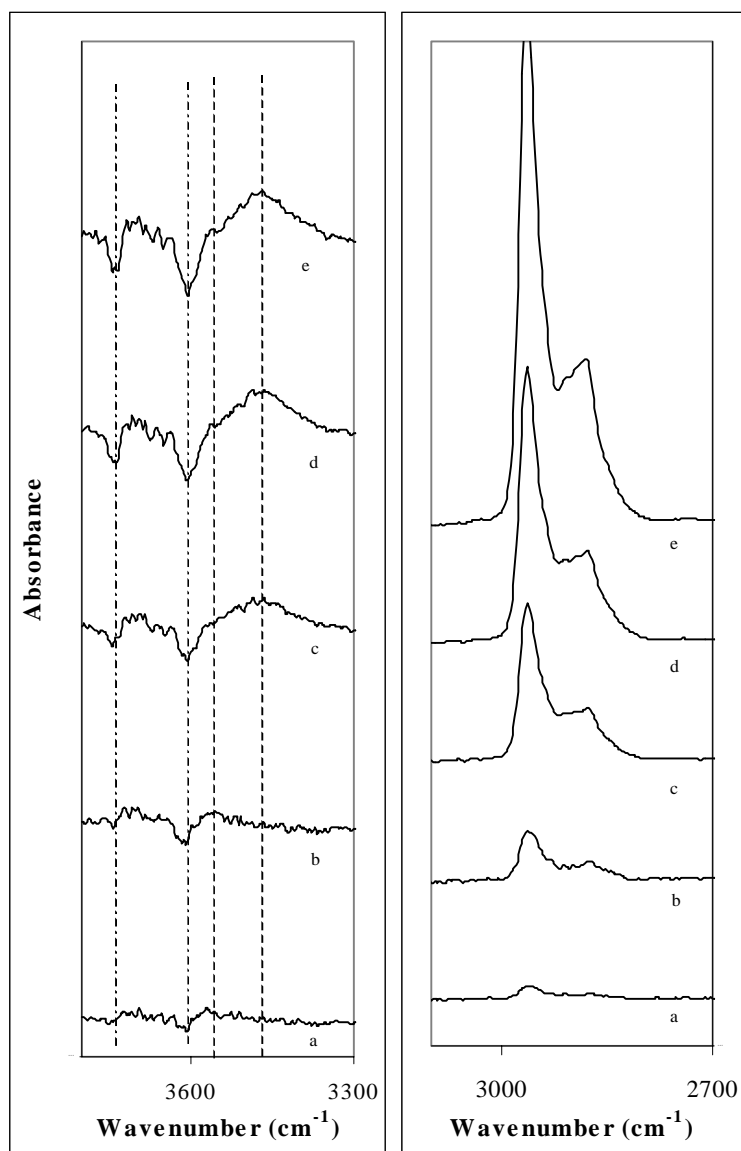


Figure 9. I.r. spectra of TON during sorption of DMP (343K). The lines correspond to increasing (a, b,...e) equilibrium pressures between 0.01 and 13 mbar of DMP.

the heat of adsorption was not observed. However, for DMP and DMH, the heat of adsorption increased again rapidly with coverage to maximum values of 95 and 108 kJ/mol, reached at 0.018 and 0.02 mmol/g, respectively (see Fig.7). If we assume that the uptake corresponds only to localized adsorption at the Brønsted acid sites, the maximum concentrations of acid sites involved in the local adsorption with DMB, DMP and DMH can be estimated to be approximately 3, 5 and 5.5 % for TON and 1, 2 and 2.5 % for FER, respectively.

It should be emphasized at this point that the sharp increase of heat of sorption for DMP and DMH as a function of coverage has not been observed in other

molecular sieves. While intermolecular attractions induce an increase in the heat of adsorption with coverage for wide pore zeolites, such increase never exceeded the heat of condensation of the alkanes sorbed [24]. In the present case the difference between the heat of adsorption at low and moderate coverage exceeds this by far. The very low heat of adsorption at the initial stages suggests that the adsorption takes place completely at the outside of the zeolite crystallite. This is strongly supported by the fact that the isosteric heat of adsorption of hexane on macroporous materials as γ -alumina is approximately 25 kJ/mol [25]. Apparently, it is thermodynamically favorable to adsorb the longer hydrocarbon part parallel to the crystallite surface. This parallel sorption structure would account for about $6 \cdot 10^{18}$ molecule /g which corresponds to about 0.5

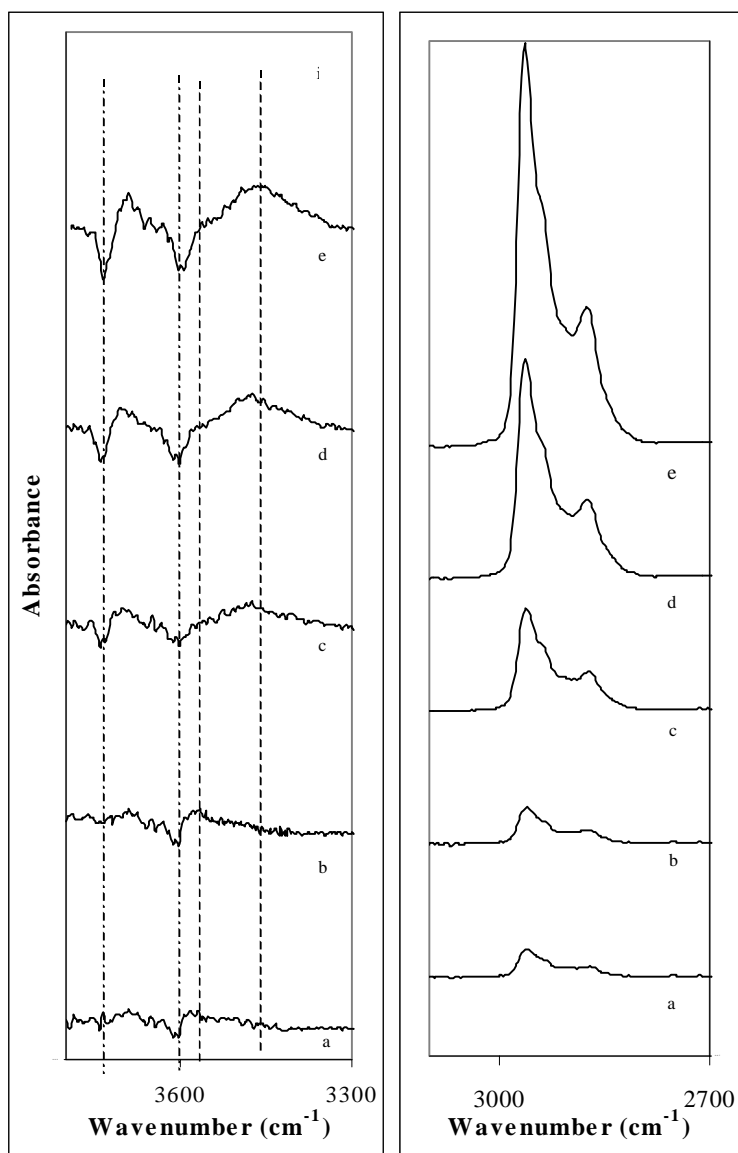


Figure 10. I.r. spectra of TON during sorption of DMH (343K). The lines correspond to increasing (a, b,...e) equilibrium pressures between 0.01 and 13 mbar of DMH.

molecule/ pore mouth acid site. The coverage revealing the highest heat of sorption corresponds to roughly $1.2 \cdot 10^{19}$ molecules/g corresponding to about 1 molecule/poremouth acid site. Thus, as the coverage increases, additional molecules DMP and DMH sorb in a way that a much higher heat of adsorption is generated. In order to account for this we suggest that additional molecules do not longer sorb parallel to the surface but rather protrude into the TON channels which would indeed lead to a much higher heat of sorption. However, this still is inappropriate to account for the total gain in sorption energy at a coverage that is only twice as much as the initial coverage with low energy.

The increase brought about by additional molecules having their sorption structure changed from parallel to the direction of the pore would amount to approximately the enthalpy that the *n*-alkane tail generates after adsorption in TON and FER corresponding to the contribution by four CH_3/CH_2 groups, i.e. by 48-60 kJ/mol [5]. The fact the observed increase exceeds this value is explained with the contribution of direct bonding to a Brønsted acidic hydroxyl group (estimated contribution 10 kJ/mol) and by the fact that the majority of the molecules initially sorbed with the parallel sorption structure rearrange their sorption structure from being adsorbed parallel to the surface to point into the pore mouths, i.e. adopting the sorption structure of the later adsorbed alkanes.

The *in situ* IR (difference) spectra during the adsorption confirm these conclusions. The IR spectrum of activated TON shows bands at 3740 cm^{-1} and at 3603 cm^{-1} which are attributed to the terminal and bridging OH groups, respectively. Upon sorption of DMB (Fig.8) at increasing equilibrium pressure the intensities of both bands decreased simultaneously and a single broad band characteristic of hydrogen bridge bonding the alkane appeared at lower wavenumbers. In contrast to DMB, the spectra during sorption of DMP (Fig. 9) and DMH clearly show a distinct difference between low and at high coverages. At the lowest loadings a small shift towards lower wavenumber of the band of bridging hydroxyl groups ($40 - 60\text{ cm}^{-1}$) was observed indicating weak interactions with a methyl group.

At higher coverage a larger downward shift of the bridging hydroxyl groups is seen, i.e. 140 cm^{-1} for DMP and 145 cm^{-1} for DMH. Note that the wavenumber of the perturbed OH group indicates the strength of the interaction [26] and, hence, the increasing shift points to a higher strength. The shift of the free Si-OH-Al group was in case of DMB only 95 cm^{-1} and this non-proportional lower value confirms the strikingly lower heat of sorption in comparison with the other alkanes.

At low coverage, the uptake of hydrocarbons corresponded fairly well to the decrease of the band of the free hydroxyl groups. When more than about 3 % (DMB) to 6 % (DMP, DMH) of the total Brønsted acid sites interacted with hydrocarbons, the concentration of sorbed alkanes exceeded the stoichiometry of 1 molecule per 1 pore mouth acid site indicating that the additional molecules adsorbed outside the pore mouth. Therefore, it seems plausible to suggest that the branched alkanes sorb first on the surface of the zeolite crystals in such a manner that one of the methyl group points into the pore mouth, while the rest of the molecule is sorbed in parallel to the external crystal face. With DMB, the difference between the methyl and the ethyl group is so small that it is hardly noticeable. Most likely, there is rapid redistribution between the two forms of adsorption. Moreover, it should be kept in mind that the adsorption form parallel to the surface will have a higher entropy in the adsorbed state and might, therefore, be preferred. For DMP and DMH the gain in enthalpy at higher loadings clearly outweighs the loss of entropy and a strict ordering of the longer alkane chain into the pore mouth occurs. The differences in the maximum heats of adsorption for DMP and DMH ($13\text{--}16\text{ kJ/mol}$) are in the range of the values found for the adsorption of linear and single branched alkanes [6,23], i.e. one additional methylene group will contribute about 12 kJ/mol to the overall heat of sorption. Therefore, the

arrangement of the longer part of the dibranched alkane appears to be very similar to the arrangement of the linear alkane in the optimized conformation.

7.5 Conclusions

The sorption of dibranched alkanes and methyl substituted pyridines in medium pore zeolites FER and TON has been investigated by means of *in situ* IR spectroscopy and combined calorimetry and gravimetry. The accessibility of Brønsted acid sites for dibranched alkanes is established by probing the acid sites with (substituted) pyridine. For both zeolites the uptake of the dibranched alkanes was small compared to the linear molecules. The orientation of the sorbate seems to depend subtly upon the size of the molecule. At low coverage all three dimethylalkanes are adsorbed in parallel to the outer surface of the zeolite. As the coverage increases, additional molecules sorb in such a manner that the propyl- and butyl-group point into the pore. Also, it is very interesting to note that approximately 80 % of the 2,2-dimethylpentane and 2,2-dimethylhexane molecules that initially sorbed parallel to the outer surface rearrange to this sorption structure. With 2,2-dimethylbutane a clear differentiation is not possible with the present data. The adsorption at the pore mouth involves strong Brønsted acid sites as shown directly by *in situ* IR measurements that also allow to follow the rearrangement of the dibranched molecules. The strong Brønsted acid sites (sufficient strong to convert alkanes and alkenes in skeletal isomerization) are therefore concluded to be located in the pore mouth rather than on the outside of the zeolite crystal.

Acknowledgment The fruitful discussions and the providing of the dibranched alkanes by J. Martens, P. Jacobs, University of Leuven, were highly appreciated. Drs. László Domokos is kindly acknowledged for assistance concerning the MSI software. I am grateful to Dr. M. Derewinski for providing the TON sample.

References

1. Mooiweer, H.H., de Jong, K.P., Kraushaar-Czarnetzki, B., Stork, W.H.J., and Krutzen, B.C.H., *Stud. Surf. Sci. Catal.* **84**, 2327 (1996).

2. Houzvicka, J, and Ponec, V., *Catal. Rev.,-Sci. Eng.* **39** (4), 319 (1997).
3. Kärger, J., Petzold, M., Pfeifer, H., Ernst, S., and Weitkamp, J., *J. Catal.* **136**, 283 (1992).
4. Martens, J.A., Souverijns, W., Verrelst, W., Parton, R., Froment, G.F. and Jacobs, P.A., *Angew. Chem. Int. Ed. Engl.* **107**, 2726 (1995).
5. Eder, F., and Lercher, J.A., *J. Phys.Chem. B* **101**,1273 (1997).
6. Meier,W.M. and Olson, D.H. *Atlas of zeolite structure types*, Butterworth-Heinemann, London 1992.
7. Morris, R.E., Weigel, S.J., Henson, N.J., Bull, L.M., Janicke, M.T., Chmelka, B.F., and Cheetman, A. K., *J. Am. Chem. Soc.* **116**,11854 (1994).
8. Knözinger, H., in “*Elementary Reaction steps in Heterogeneous Catalysis*“, eds., R.W. Joyner and R. v. Santen, Kluwer Academic Publishers, pg. 267 1993.
9. Khabtou, S., Chevreau, T., and Lavalley, J.C., *Micr. Mat.* **3**,133 (1994).
10. Knözinger, H., Krietenbrink, P., and Ratnasamy, V., *J. Catal.* **48**, 436 (1977).
11. Buzzoni, R., Bordiga, S., Ricchiardi, G., Lamberti, C., and Zecchina, A., *Langmuir* **12**, 930 (1996).
12. Benesi, H.A., *J. Catal.* **28**,176 (1973).
13. Jolly, S., Saussey, J., Lavelley, J.C., Zanier, N., Benazzi, E., and Joly, J.F., *Ber. Bunsenges. Phys. Chem.* **97**, 3 (1993).
14. Glazunov, V.P., and Odinokov, S.E. *Spectrochim. Acta* **38A**, 399 (1982).
15. Dewing, J., Monks, G.T., and Youll, B., *J. Catal.* **44**, 2 (1976).
16. Matulewicz, E. R. A., Kerkhof, F.P.J.M., Moulijn J.A., and Reitsma, H. J., *J. Colloid Interface Sci.* **77**, 110 (1980).
17. Corma, A., Rodellas, C., and Fornes, V., *J. Catal.* **88**, 374 (1984).
18. Jacobs, P.A., Heylen, C.F., *J. Catal.* **34**, 267 (1974).
19. Deka, R., and Vetrivel, R., *J.Catal.* **174**, 88 (1998) (and references therein).
20. Barrer, R.M., *J.Colloid Interface Sci.* **31**, 415 (1966).
21. Derouane, E.G., Andre, J.M., and Lucas, A.A., *J. Catal.* **110**, 58 (1988).
22. Eder, F., Stockenhuber, M., and Lercher, J.A., *Stud. Surf. Sci. Catal.* **97**, 495 (1995).
23. Van Well, W.J.M., Cottin, X., de Haan, J.W., Smit, B., Nivarthi, G.S., Lercher, J.A., van Hooff, J.H.C., and van Santen, R.A., *J. Phys. Chem.* **102**, 3945 (1998).
24. Eder, F., and Lercher, J.A., *Zeolites* **18**, 75 (1997).
25. Baumgarten, E., Weinstrauch, F., and Höffkes, H., *J. Chromatography* **138**, 347 (1977).
26. Hair, M.L., and Ertl, W. *J. Phys. Chem.* **74**, 91 (1970).
27. Insight II program, MSI Technologies Inc. 1998.

*Structure-activity correlations for TON, FER and MOR in the hydro- isomerization of *n*-Butane*

Abstract

n-Butane hydro-conversion was studied over (Pt loaded) molecular sieves with TON, FER and MOR morphology. The conversion occurs *via* a complex interplay of mono- and bimolecular bifunctional acid mechanism and monofunctional platinum catalyzed hydrogenolysis. Hydroisomerization was concluded to occur bimolecularly at low temperatures. This is evident from the reaction order in *n*-butane of 2 for isobutane formation and the presence of 2,2,4-trimethylpentane among the products. Intracrystalline diffusion limitations of the reaction rates seem to be important for TON. Due to diffusion controlled reaction rates for TON, the presence of Pt in TON was detrimental for the isomerization selectivity. As the ratio of utilized acid sites to accessible Pt becomes low, diffusion of the feed molecules to the acid sites is too slow to prevent Pt hydrogenolysis of *n*-butane. Reactions on H-FER occur predominantly on the outer surface and the pore mouth of the molecular sieve, presumably owing to rapid pore filling following a transient period of single-file diffusion. Due to high intrinsic activity toward (hydro)cracking this does not lead to high selectivity toward isobutane. Addition of Pt (bifunctionality) was in this case beneficial. Reaction at the external surface is not diffusion limited, allowing bifunctional *n*C₄-isomerization to occur. Although PtFER was found to approach selectivity levels as found for PtMOR, the latter has a significant advantage as the larger concentration of accessible acid sites lead to much higher activity.

8.1 Introduction

Brønsted acidic H-mordenite as component of commercial isomerization catalysts has received a lot of attention [1-8]. *n*-Butane isomerization over mordenite was shown to occur *via* a bimolecular reaction pathway (involving dimerisation, isomerisation *via* methyl/hydride shifts and cracking) which overcomes the need for the formation of a primary carbocation which constitutes an intermediate in the skeletal monomolecular isomerization [7,8]. Pt in mordenite has also been suggested to contribute to the isomerization of butane *via* a parallel bifunctional route involving dehydrogenation of the alkane on the metal site [5 - 7].

It is interesting to rationalize the steric requirements for the bimolecular mechanism in the one-dimensional pores of mordenite. The kinetic diameters of branched alkanes (e.g. *i*-butane) approaches the pore size of mordenite, implying that the individual molecules cannot pass each other within one channel. This type of motion is referred to as *single file* diffusion [9]. Generally, concentration gradients inside the pores are the driving force for the directed motion of the molecules. However, in *single file* diffusion, a displaced molecule is more likely to return to its original position than to proceed further, since the latter would stipulate a further concentration of the molecules ahead [9] which seems to be highly constrained because of the space limitations in one dimensional pores.

This becomes even more important when considering TON as catalyst for *n*-butane isomerization. The pores of TON are straight unidirectional channels which have a significantly smaller diameter and coincide with the kinetic diameter of a singly branched alkane. In line with this, recent work by Martens *et al.* [10] describing the selective isomerization of long-chain alkanes over TON introduced the concept of shape-selective isomerization at crystal terminating faces, termed pore mouth catalysis. Although there is solid kinetic evidence supporting this, several questions still remain unanswered as already pointed out by Ernst [11]. For instance, it is not clear whether the concept can be transferred to other reactants and other zeolite structures and what role the active sites at the external surface of the zeolite crystals play. In a recent paper [12] it was shown by us that the acid sites in HFER and HTON are in principal sufficiently strong to polarize dibranched alkanes but these sites are located in the poremouth rather than fully at the external surface.

Intuitively, the concept of pore mouth catalysis and single file diffusion seem to be related

as, at least for well back mixing, a concentration gradient across a zeolite particle does not exist. For the current example, the use of differential conditions lets us expect that the reaction will be controlled by sites at the outer surface of crystals of TON and FER.

The current contribution presents a kinetic study of *n*-butane conversion over zeolites with effectively unidirectional pores, i.e. TON, FER and MOR under differential conditions and at low temperature which favor bimolecular reaction pathway. Unlike the higher linear analogues, the disfavored energetics for the formation of the primary carbenium ion intermediates favor *n*-butane (hydro-)isomerization to occur exclusively *via* the bimolecular pathway demanding the formation of bulky branched C₈ intermediates. The choice of the zeolite, i.e. MOR, TON and FER with different pore sizes, provides understanding on the ease of the bimolecular mechanism and how the steric constraints affect the place where the reaction takes place. The unidirectional MOR structure has cross sections with so-called side pockets allowing (small) molecules to pass each other. Next to its smaller pore size TON does not have this structural feature. FER has a two dimensional structure with 10MR channels comparable to TON. The 8 membered apertures of FER are expected to exclude any contribution to the reactions due to severe geometrical constraints [13,14].

8.2 Experimental

8.2.1 Catalysts

Na/K-FER and Na-MOR (obtained from TOSOH) with a Si/Al ratio of 9 and 10, respectively, were used for the present investigation. Ion exchange of the samples in Na⁺ form was performed with 1 M NH₄NO₃ (Merck Co., 101188.1000) at neutral pH conditions at a temperature of 365K, using approximately 7 ml liquid per gram solid. The procedure was repeated three times to ensure complete ion exchange. Finally, the sample was washed with distilled water. NH₄-TON was kindly donated by Exxon with a Si/Al ratio of 18 (TON-18) and Shell (SRTCA), Si/Al 20 (TON-20). 0.1 wt % Pt was incorporated by ion exchange from a solution of Pt(NH₃)₄ (OH)₂. The catalysts were calcined at 623 K (823 K for MOR) *ex situ* and reduced *in situ* at 623 K (823 K for MOR) for 1 hr (MOR) and 2 hrs (TON and FER) in hydrogen flow (35 ml/min) before being used.

8.2.2 Characterization

The morphology and size of the crystallites was investigated using a JEOL-JSM-35 CT Scanning Electron Microscope. EDAX spectroscopy to determine total Si/Al ratios was performed on a S800 Scanning Electron Microscope from Hitachi Co. equipped with a Kevex Quantum detector Energy Dispersive X-ray system allowing elemental compositions to be determined within an accuracy of 5% (relative). The instrument had a resolution at 5.9 keV of 109 eV. In order to ensure that the data collected were representative of the whole sample, scans were made at more than one location. Calibration with a standard sample of known Si/Al ratio was performed prior to the measurements.

The NH_3 sorption measurements to determine acid site concentration and strength were performed on a modified SETARAM TG-DSC 111 apparatus equipped with a BALZERS QMS420 mass spectrometer to detect the concentration of desorbed substances from Temperature Programmed Desorption (see for more details ref. 13, 15). The same system was used to record isotherms of nC_4 to explore the sorption capacity together with the heat of sorption.

FTIR measurements were performed with a BRUKER IFS-88 spectrometer with a spectral resolution of 4 cm^{-1} and equipped with a BALZERS QMS420 mass spectrometer, a vacuum cell and a flow cell. The cells consisted of a stainless steel chamber equipped with CaF_2 windows and a resistance-heated furnace, in which a golden sample holder is placed. A self-supporting wafer was pressed and activated with 5 K/minute to 823 K (673 K in case of TON and FER) in either a stream of He or a base pressure of 10^{-7} mbar and the spectra were recorded with time-resolution of approximately 30 seconds. A spectrum of the empty IR cell was used as reference (I_0) to convert the single beam spectra (I) into absorbance spectra ($\log I_0/I$).

The Pt particle size was determined using high resolution transmission electron microscopy (HREM). A Philips CM 30 T electron microscope with a LaB_6 filament as the source of electrons was used, operated at 300 kV. Samples were mounted on a carbon polymer microgrid supported on a copper grid by placing a few droplets of a suspension of a ground sample in ethanol on the grid, followed by drying at ambient conditions.

8.2.3 Kinetic experiments

The catalytic tests were performed in a fixed bed tubular quartz reactor with an inner diameter of 5 mm and operated in continuous flow mode. 75 to 150 mg of catalyst were used for each test. The catalyst was activated in flowing air (40 ml/min), at 5 K/min to 823 K in case of MOR and 673 K in case of FER and TON. In case of Pt containing catalysts, the stream of air was subsequently switched to a stream of 50 mol% hydrogen in helium for another hour. Finally, the catalysts were purged *in situ* at 673 K in flowing He. The reactor was then cooled down to the reaction temperature, typically between 523 and 623 K. The reactant stream contained typically *n*-butane (Praxair, 99.95 % purity, 0.02% iC_4 and 0.03% C_3 impurities), hydrogen and helium. The reactor effluent was collected with an automatic sampling valve system, stored in multi-loop valves and subsequently analyzed by a HP5890 gas chromatograph using a 50 m Al_2O_3/KCl capillary column equipped with a flame ionization detector and coupled to a mass selective detector HP 5971A. The set up allowed for transient and steady state experiments. Yields and selectivities were calculated on a carbon basis in mol % with corrections for the impurities in the feed. Kinetic analysis was carried out after 1 to 3 hours of ageing after which no apparent changes in conversions could be observed. External mass transfer limitation was checked for by changing the flow rate at constant space time and found to be absent under the present conditions.

8.3 Results

8.3.1 Characterization

The physico-chemical properties of the materials are listed in Table 1. The dispersion of Pt diminished in the order $PtMOR \gg PtTON \approx PtFER$ as deduced from TEM/EDX analysis. While for Pt-MOR Pt particle size was homogeneous below 0.5 nm, larger Pt particles were found in case of Pt-TON and Pt-FER (0.5-3 nm). Therefore, considering the pore sizes, a significant fraction of Pt was located on the outer surface for FER and TON. Note, however, we cannot exclude the possibility of having Pt clusters below 0.5 nm also present inside the micro pores (below the detection limit).

Table 1. Physico-chemical properties of the materials.

Catalysts	Si/Al total	Crystal size (001) (μm)	Acid sites (mmol/g) ¹	Brønsted acid sites (mmol/g) ²	Lewis acid sites (mmol/g) ²	$\Delta H \text{NH}_3$ (kJ/mol)	$\Delta H \text{nC}_4$ (kJ/mol)
HMOR	10	1.5	1.25	1.2	0.05	148	49
PtMOR	10	1.5	1.2	1.13	0.07	n.d	48
HTON	20	2	0.49	0.43	0.07	140	59
HTON	18	4	0.65	0.50	0.15	n.d	57
PtTON	18	4	0.63	0.57	0.06	n.d	59.5
HFER	9	1.5	1.95	1.9	0.05	140	59
PtFER	9	1.5	1.90	n.d	n.d	n.d	63.5

1 - determined by ammonia sorption, 2- determined by ammonia and pyridine sorption

In the case of MOR, EDX analysis showed that Pt was distributed uniformly throughout the material. Ammonia calorimetry indicated that the strength of the interaction with sorbed ammonia and the zeolite framework is very similar for all zeolites. This may indicate a similar acid strength assuming that contribution of physisorption is similar for the zeolites. Gravimetric analysis of the adsorption of *n*-butane on the H-form and Pt-form of the zeolites showed that in the case of MOR the maximum loading at 13 mbar *n*-butane was the same for both cases. These observations indicate that the accessibility of the micropores in MOR did not change upon the presence of platinum particles. A 10 % lower sorption capacity for *n*-butane was evident in the case of PtTON compared to HTON, but not for PtFER. Note also, the number of acid sites gravimetrically determined with ammonia in case of TON and FER were very similar irrespective of the presence of platinum (see Table 1).

8.3.2 Kinetic measurements

In the next paragraphs, the influence of various system variables are described.

8.3.2.1 Influence of temperature

All Pt containing catalysts showed stable activity with time on stream. The H-form of the zeolites showed stable activity with time-on-stream at temperatures below 573 K and typical conversion levels below 3 %. At temperatures above 573 K, approximately 2 hours time-on-stream were necessary to obtain stable catalyst operation.

Figure 1 shows the influence of temperature on the product distributions obtained with HTON. The main products were methane, ethane, propane, isobutane, butenes, pentanes. Also a trace amount of 2,2,4TMP was detected. Although the selectivity toward isomerization was rather high (about 75 %) at 548 K, it decreased rapidly with temperature. Mainly methane, ethane and propane (monomolecular cracking route) as well as butenes gained in importance with temperature at the cost of the selectivity to isomerization. Loading HTON-18 with 0.1 wt% Pt (at hydrogen to *n*-butane ratio of 4) increased the formation of methane and ethane dramatically, which was attributed to metal (hydrogenolysis) activity (Fig.2). Isomerization and disproportionation became less significant.

In Table 2, the apparent activation energies are compiled for (Pt)TON. For HTON, very low activation energies for the formation of branched products (*i*C₄ and *i*C₅) were found. For PtTON, the activation energy (86.5 kJ/mol) compares well with the value found for *n*-hexane (hydro-) conversion [16].

The main product found over HFER (Fig.3) was ethane. Also, at temperatures above 560 K, C₁ and C₃ were abundant and in equimolar amounts indicating intrinsic activity for (hydro)cracking of feed butane. At lower temperatures, a clear excess of C₃ exist indicating an important additional (bimolecular) reaction route. Also the level of unsaturated products appeared higher than in the case of HTON. *i*C₄ production was only marginal. Addition of Pt to HFER increased the selectivity toward *i*C₄ appreciably. With increasing the temperature, the selectivity slightly decreased mainly due to the increased metal activity (Fig. 4).

Table 2. Apparent activation energies (in kJ/mol) as deduced from the Arrhenius correlations between 523 and 623 K.

Catalyst	HTON	PtTON	HFER	PtFER	HMOR	PtMOR
	$E_{act,app}$	$E_{act,app}$	$E_{act,app}$	$E_{act,app}$	$E_{act,app}$	$E_{act,app}$
Total	79±2	86±2	112±5	118±4	105±4	120±3
Methane	95	85	145	135	100	65
Ethane	118	81	120	125	105	75
Propane	119	84	130	131	135	143
i-Butane	53	130	111	112	100	135
Pentanes	63	115	-	-	115	150

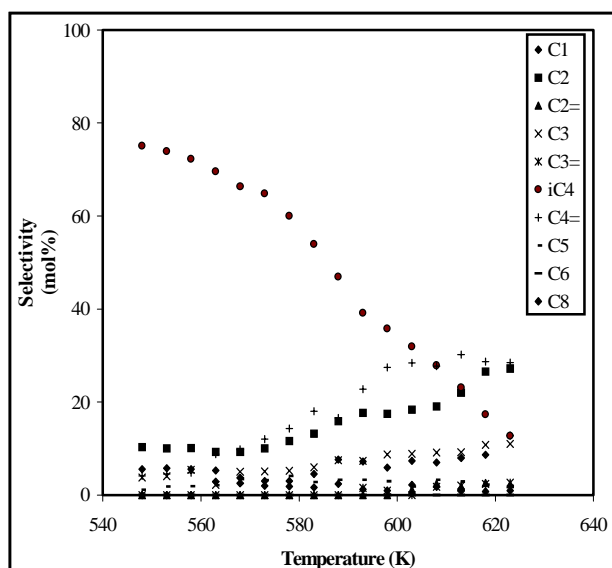


Figure 1. Influence of temperature on the product distribution over HTON-18, $H_2/nC_4=4$, 280 mbar nC_4 .

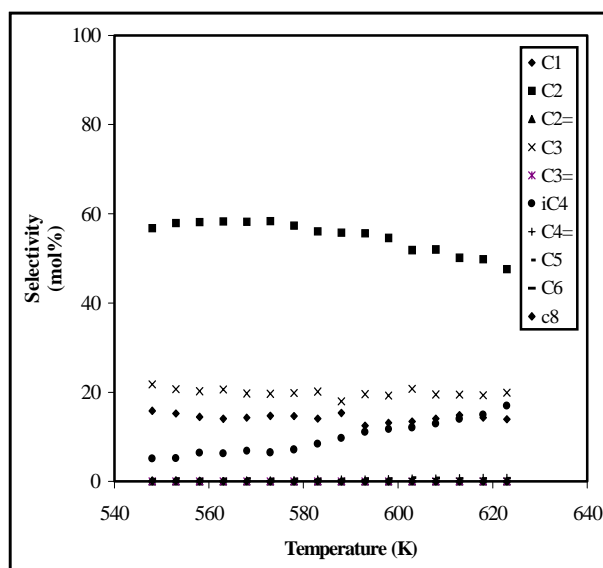


Figure 2. Influence of temperature on the product distribution over PtTON-18, $H_2/nC_4=4$, 280 mbar nC_4 .

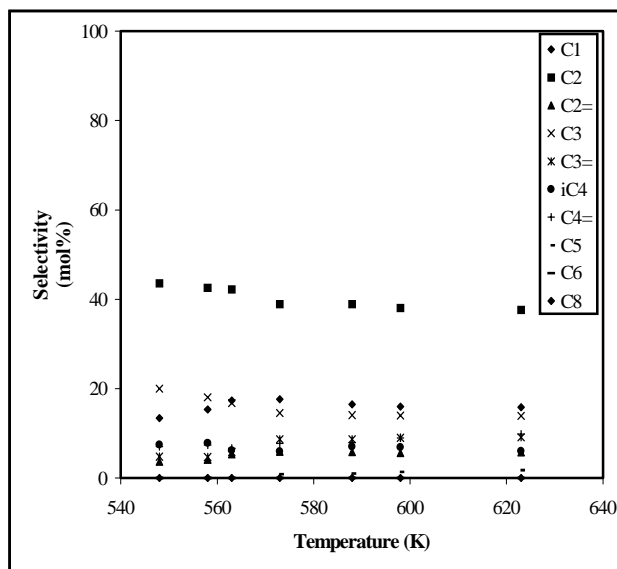


Figure 3. Influence of temperature on the product distribution over HFER, $H_2/nC_4=4$, 280 mbar nC_4 .

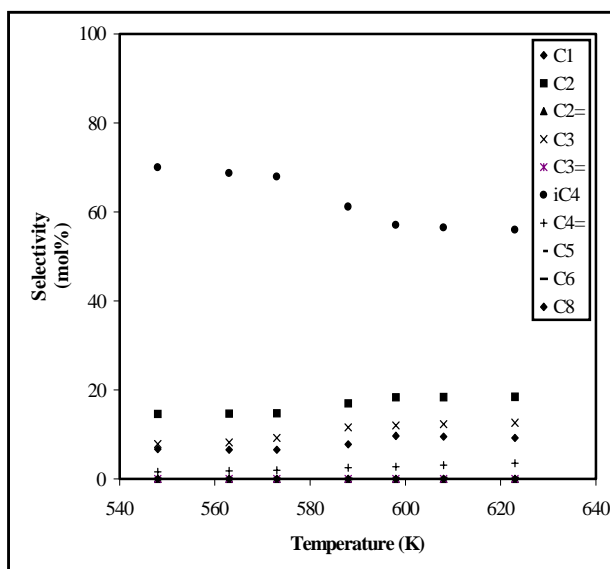


Figure 4. Influence of temperature on the product distribution over PtFER, $H_2/nC_4=4$, 280 mbar nC_4 .

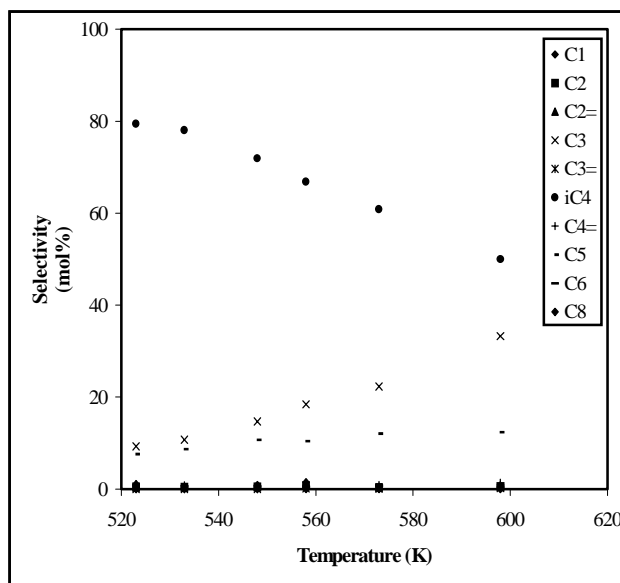


Figure 5. Influence of temperature on the product distribution over HMOR, $H_2/nC_4=4$, 280 mbar nC_4 .

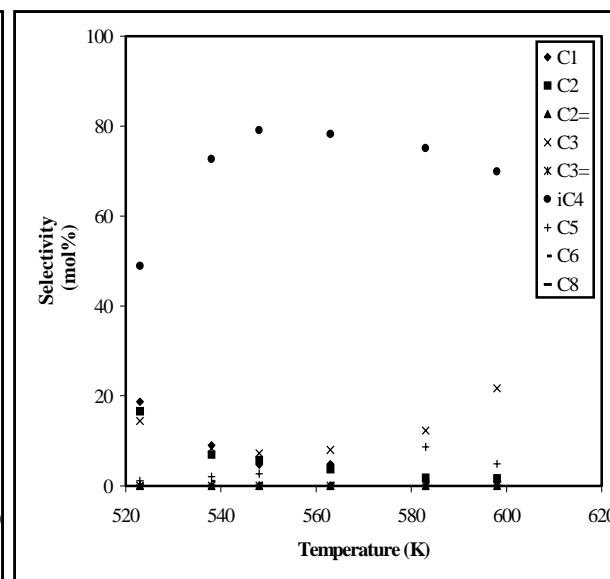


Figure 6. Influence of temperature on the product distribution over PtMOR, $H_2/nC_4=4$, 280 mbar nC_4 .

The activation energies for *n*-butane conversion were also higher than that found with TON. As in the case of TON, the presence of Pt in FER gave rise to slightly higher activation energy for *n*-butane conversion.

Product distribution found over mordenite are depicted in Figures 5 and 6. The trends were

in perfect agreement with those reported earlier [7]. The isomerization selectivity for HMOR was the highest at the lower temperatures (about 80 %) but decreased significantly with increasing temperature. Unlike for HTON and HFER, where the cracking activity (C_1+C_3) was remarkable, the loss in selectivity with temperature was mainly due to enhanced activity for disproportionation (C_3+C_5). PtMOR shows the highest selectivity towards isomerization between 548 and 563 K. Below this temperature hydro-cracking seemed an important side reaction, while at higher temperatures disproportionation gained importance at the expense of isomerization. As already seen for TON and FER, the activation energy for *n*-butane conversion were slightly higher in the presence of Pt.

8.3.2.2 Influence of variation of the space velocity

The WHSV was varied in order to vary the conversion. The main products formed (C_1 - C_5) were concluded to be primary as indicated by the linear yield-conversion correlations.

Table 3. TOF based activities for the catalysts at 548 K and $H_2/nC_4=4$.

Catalyst	TOF (hr ⁻¹)
HTON	0.133
PTON	1.525
HFER	0.065
PFER	0.122
HMOR	6.9 (13.8)
PMOR	0.9 (1.8)

The product distributions are compared in Table 4 at a total conversion of 0.9 %. As described above, MOR was significantly more active than TON and FER. This cannot be explained on the basis of the acid site concentration. For MOR, it was argued that only 1/3 to 2/3 of the acid sites is accessible to alkanes without achieving a clear consensus [17-21]. These accessible sites were suggested to be located in the 12MR main channels. Our sorption studies show that the heat of sorption of nC_4 remains constant up to a coverage of at least 50 % of the total amount of acid sites derived with ammonia sorption. Therefore, we conclude that at least 50 % of the acid sites

are accessible to *n*-butane. In this case, the TOF (see Table 3) of MOR exceeds the activity of TON and FER significantly indicating that a much larger fraction of the acid sites of MOR was used for the reaction than with TON and FER (in Table 3 the TOF values calculated with 50 % of the total concentration of acid sites are displayed in brackets).

8.3.2.3 Influence of partial pressure *n*-Butane

The logarithmic form of the power rate law

$$r = k.p(nC_4H_{10})^m .p(H_2)^n \quad (1)$$

was used to compute the reaction orders in *n*-butane and product formation with *n*-butane pressure at hydrogen pressure of 730 mbar. The results are compiled in Table 5 with *n*-butane partial pressures varying between 280 and 100 mbar. The rates of *n*-butane conversion and product formation increased with *n*-butane partial pressure. This, however, becomes less significant at higher temperatures as shown here for TON. The same effect was reported earlier in the case of MOR [3]. The orders are smaller in case of Pt comprising zeolites than found for the H-form parent materials. The reaction order in *n*-butane for the formation of isobutane as well as for the formation of pentanes was, as found before for MOR, close to two at 548 K. It was slightly lower at higher temperature.

8.3.2.4 Influence of hydrogen partial pressure

The partial pressure hydrogen was varied between 180 mbar and 800 mbar at a constant partial pressure *n*-butane of 200 mbar. The power rate law was applied to calculate the reaction orders in hydrogen. TON and FER show negative order in hydrogen with respect to the total conversion. The order becomes more negative when Pt is present. The same effect was found before for mordenite catalysts [3]. Over HMOR, the selectivity to isobutane and isopentane increased slightly while propane, ethane and methane became less abundant with increasing the hydrogen partial pressure. For PtMOR, increasing the partial pressure hydrogen decreased isomerization activity at the benefit of mainly disproportionation and hydrogenolysis at 548 K.

However, at higher temperatures the selectivity toward isomerization benefits from the increasing H_2/nC_4 ratio. A similar effect was found for PtTON. At 548 K the isomerization selectivity continued to decrease with increasing partial pressure hydrogen due to significant hydrogenolysis while at 598K selectivity increased until a H_2/nC_4 ratio of 1.9. A similar situation was found in case of HTON at 598 K. In case of PtFER at 598 K clearly a substantial increase in hydrogenolysis with increasing partial pressure hydrogen was observed, diminishing the isomerization selectivity.

Table 4. Comparison of selectivities (mol%) of catalysts at 0.9 % conversion; $H_2/nC_4=4$, $P_{C_4}=220$ mbar, T 548 K.

Catalyst	Methane	Ethane	Ethene	Propane	Propene	<i>i</i> - Butane	Butenes	Pentanes	Hexanes	2,2,4- TMP
HTON	0	12.6	0	3.8	0	72.8	4.1	1.2	0	5.5
PtTON	15.8	56	0	22	0	5.1	0	0.9	0	0.2
HFER	13.4	43.4	3.5	20	4.6	7.5	7	0.4	0	0.2
PtFER	6.7	13.7	0	7.8	0	70	1.6	0.2	0	0
HMOR	0.4	1	0.1	14.7	0.3	71.9	1.6	9.6	0.5	0
PtMOR	4	4.1	0	6.8	0	81	0.6	3.2	0.3	0

Table 5. Orders (*n*) of the reaction for *n*-butane, hydrogen and products.

Catalyst	HTON	PTON	HFER	PFER	(P)HMOR ^a
	<i>n</i> (548K, 573K, 598K)	<i>n</i> (573K, 598K)	<i>n</i> (598K)	<i>n</i> (598K)	<i>n</i> (543K, 573K, 623K)
Total	1.7, 0.9, 0.8	0.6, 0.3	0.8	1	1.5, 1, 0.5
Methane	0.3	0.5, 0.3	1	1.1	nd
Ethane	1, 0.6, 0.6	0.2, -0.3	1.1	1	nd
Propane	1.6, 1.5, 1.5	0.6, -0.2	2	1.1	nd
i-Butane	1.9, 1.9, 1.6	1.2, 1.1	2	1.2	1.3, 0.7, 0
Pentanes	2, 1.6, 1.6	1.6, 1.3	nd	nd	nd
2,2,4TMP	-0.9, -1.2, -1.2	nd	-1.2	-0.9	nd
Hydrogen	-0.3	-0.5, -0.9	-0.3	-0.8	-0.2 (-0.4) ^b

a; taken from reference 3, *b*; taken from reference 7, nd.; not determined

8.4 Discussion

The conversion of *n*-butane over mordenite based catalysts in the presence of hydrogen was investigated before at reaction temperatures between 523 K and 623 K [Chapter 5]. Special attention was paid to the influence of Pt upon catalytic activity, selectivity and stability. With H-form mordenite the catalytic activity for *n*-butane conversion decreased markedly after a short time on stream. However, deactivation could be minimized by hydrogen in the presence of Pt. This was explained by a reduction of the concentration of intermediate olefins in the zeolite pores. The best results with respect to selective conversion of *n*-butane to isobutane were obtained for 0.05 to 0.25 wt % Pt on mordenite in the presence of hydrogen. Higher concentrations of Pt in the catalyst are shown to be detrimental for *n*-butane isomerization because of increasing selectivity to hydrogenolysis. *n*-Butane conversion was concluded to occur *via* a bimolecular mechanism involving a complex network of hydrogen transfer, oligomerization/cracking, isomerization, dehydrogenation and hydrogenolysis [chapter 5, 7].

On bifunctional catalysts three modes of alkane isomerization can (co)exist; monofunctional acid, monofunctional metallic and bifunctional isomerization. These mechanisms are

characterized by substantially different reaction kinetics and characteristic selectivities [24]. The monofunctional acid mechanism *via* cyclopropyl carbenium ion [26] is characterized by a low activation energy (42-50 kJ/mol) and low reaction order in hydrogen (0) while the monofunctional metallic mechanism is distinguished by its high activation energy (230-293 kJ/mol) and highly negative reaction order in hydrogen (2 - 3.4). These values are related, however, to *n*-heptane, for which the isomerization on the acid sites does not occur *via* the much more demanding primary carbenium ion (which is claimed to have 100 kJ/mol higher true energy of activation [25]). The activation energies and reaction orders in hydrogen found for a bifunctional mechanism are reported to have intermediate values between those for the monofunctional catalysts. Typical values for $E_{\text{act,app}}$ for bifunctional isomerization of *n*-hexane [16] were 100-120 kJ/mol and orders between 1 and 0 for *n*-hexane conversion, and between -1 and 0 for the total order in hydrogen.

In the experiments, negative orders in hydrogen were found among all the samples indicating in all cases a significant contribution of the classical bifunctional mechanism. The reaction kinetics follow a negative order in hydrogen, because dehydrogenation-hydrogenation steps are equilibrated and the equilibrium concentrations of alkene intermediates decrease with increasing hydrogen pressure. The H-form zeolites contained an iron impurity of about 0.02-0.04 wt% that can also have (de)hydrogenation functionality. However, Guisnet and co-workers pointed out that hydrogen may react with carbenium ions limiting their concentration [22]. Over HMOR, hydrogen inhibited *n*-butane isomerization that occurs through a bimolecular pathway, but had practically no effect on *n*-hexane isomerization (monomolecular [16]). The bimolecular pathway requires the presence of neighboring alkoxyde species making this reaction more sensitive to concentration of alkoxyde species on the surface. Indeed, the apparent activation energies for Pt comprising zeolites were in all cases higher than the value found for the H-form of the zeolites. For Pt containing zeolites also larger negative orders in hydrogen were found. Therefore, the higher $E_{\text{act,app}}$ is explained with Langmuir-Hinshelwood rate equations (assuming the surface reaction to be rate determining) that account for the inhibition of the reaction by hydrogen to some extend [23].

The presence of 2,2,4-trimethylpentane in the products and the positive order of about 2 for

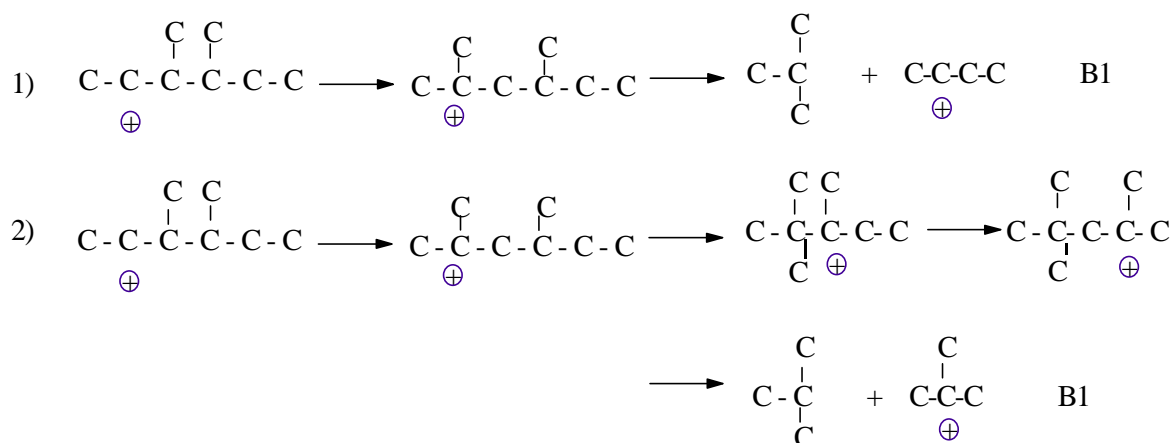


Figure 7. Proposed mechanism for the formation of isobutane [26].

isobutane formation indicates indeed that isomerization occurred *via* a bimolecular mechanism. This reaction path avoids the formation of primary carbenium ion and is in general accordance with reaction conditions (high partial pressure and low temperatures).

Brouwer [26] proposed that trimethylpentane cations can rapidly equilibrate with all other trimethylpentane cations in liquid superacids, and the preferred cleavage pathway proceeds through the 2,2,4-trimethylpentane cation to form a tertiary isobutane cation and isobutene (isobutoxy group). The formation of this species in the zeolite can be rationalized as follows: the C₈ intermediate that is initially formed from two *n*-butane surface species is most likely a secondary carbenium ion, i.e. 3,4-dimethylhexane, which can rapidly form a tertiary carbenium ion (2,4-dimethylhexane) *via* nonbranching methyl and hydride shifts. This species can undergo type B₁ cracking to form a secondary *n*-butyl carbenium ion and an isobutyl species (see Fig. 7, route 1). Alternatively, 2,4-dimethylhexane can form a secondary carbenium ion (2,2,3-trimethylpentane) *via* a branching rearrangement involving cyclopropyl ring formation and hydride shift. Subsequently, 2,2,3-trimethylpentane can form a tertiary carbenium ion, 2,2,4-trimethylpentane through nonbranching methyl and hydride shifts. Finally, 2,2,4-trimethylpentane cracks *via* the type B₁ (sec - ter) scission mechanism to yield isobutoxy and isobutyl species, eventually desorbing as isobutane *via* hydride transfer (see Fig. 7, route 2).

Type C cracking (sec - sec) of 2-methylheptane toward propane and pentene is suggested to cause part of the propane formed and pentene.

Another important route for the formation of propane in case of HFER seems to be

monomolecular cracking of feed butane to methane and propene, the latter being desorbed as propane due to fast hydride transfer. Lower apparent activation energies for the formation of C₁-C₃ over H-form zeolites than found over Pt comprising zeolites indicate that hydrogenolysis is of minor importance in comparison to the cracking mode in case of the H-form. However, also this reaction route cannot satisfactorily explain the (still) non-stoichiometric formation of propane compared to methane.

A bimolecular reaction route is proposed to account for this, likely *via* the disproportionation of dimerized *n*-butane toward propane and *n*-pentane. Pentanes are, however, only present in trace amounts in the gas phase obtained with FER, which suggests their cracking toward ethane and propane. In accordance with such a proposal the excessive formation of propane compared to pentanes was reported previously in literature for the conversion of *n*-butane over 12MR MOR and in particular for 10MR ZSM5 zeolites [7,27]. Guisnet *et al.* [27] report that for HMFI, propane is formed in significant amounts, while practically no pentanes were observed. ¹³C labelling experiments showed that this propane is formed *via* a bimolecular reaction pathway. The excessive propane formation was explained to be caused by limitations in desorption of branched products and steric constraints in the formation of the C₈ intermediates in the narrow pores of MFI [27]. It can be suggested that a similar situation exist on comparing FER and TON (10MR like in the case of MFI) with 12 MR MOR explaining excessive formation of propane over the 10MR zeolites in present study.

The most likely bimolecular route for the formation of propane is independently reported by two groups to follow formation of C₉ alkoxy species, priorily formed by the reaction between butene and C₅ alkoxy species [7,27]. C₉ alkoxy species undergo β-scission forming hexene and propoxyde species, which latter consume hydride from feed butane and desorb as propane. Additionally, hexene is protonated and undergoes cracking toward C₃ species that will again desorb as propane provided hydride transfer is sufficiently fast.

The exceptionally low apparent activation energy for the formation of isobutane and isopentane for HTON-18 might be due to internal diffusion limitations. In order to investigate this, TON-18 was compared with TON-20. The samples had comparable acid site densities but different crystal sizes. The crystallite sizes in the 001 direction were 4 ± 1 μm and 2 ± 0.5 μm

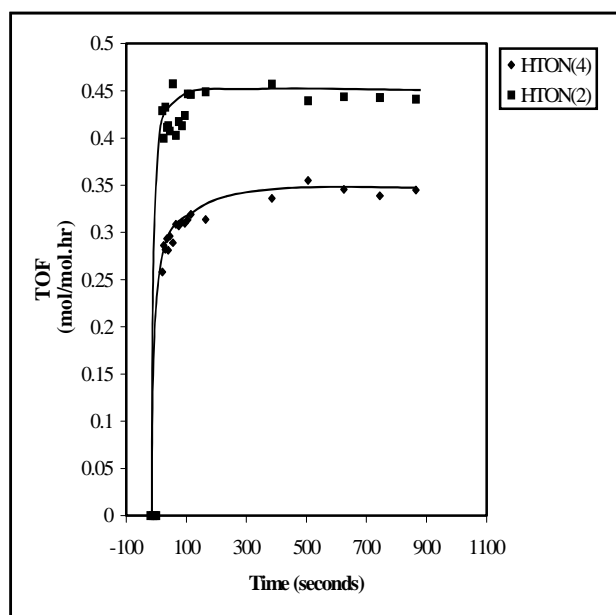


Figure 8. Influence of crystal size on the activity over HTON, 220 mbar nC_4 , $P_{tot} = 2$ bar.

respectively. The reaction was carried out without hydrogen in order to exclude a possible difference due to different negative orders in hydrogen. The smaller crystallites (TON-20) showed on a TOF basis (normalized on the amount of Brønsted acid sites deduced from ammonia and pyridine sorption) about 1.5 times higher activity supporting an internal diffusion limited reaction sequence for HTON-18 (see Figure 8). It is noteworthy that van der Runstraat *et al.* came to the same conclusion for hydro-conversion of n -hexane over TON with crystallites sizing $4\mu\text{m}$ [16].

PtTON shows an $E_{act,app.}$ of only 86.5 kJ/mol. This value matches well with the value found by van den Runstraat *et al.* for the hydroisomerization of n -hexane. As the $E_{act,app.}$ for iC_4 and C_5 is respectively 130 and 112 kJ/mol the low total activation energy for transformation of nC_4 is mainly caused by low $E_{act,app.}$ for monomolecular cracking and hydrogenolysis. We conclude, therefore, that this catalyst does not comprise optimal bifunctionality following the Weisz intimacy criterium [30]. The reaction of nC_4 on the Pt sites might cause the hydrogenation-dehydrogenation reaction to be not equilibrated. For PtTON, the much lower order for propane formation than for pentane indicates that propane is predominantly formed *via* hydrogenolysis and monomolecular cracking.

It was reported in the literature [28] that creating larger metal particles in MOR might locally destroy the zeolite, thus creating three-dimensionality of the pore structure and, thus, increasing accessibility to acid sites. Especially in the case of TON and FER a good confinement of the Pt salt precursor might have implemented a local rupture of the micropore system by metallic Pt during reduction. Part of the enhanced total activity might in this situation be assigned to thus created higher accessibility of the acid sites. However, this is not directly supported by the nC_4 sorption studies, which show slightly less sorption capacity in case of PtTON and no

effect for FER. Also, the larger Pt particles are located on the outer surface as concluded from TEM analysis. Therefore, we do not believe that the accessibility of acid sites increased for the Pt containing catalysts.

The decrease in the total order with increasing temperature and with the incorporation of Pt conceptually implies that the zeolite gets more covered. However, the temperature effect in the order of isobutane formation could also be reconciled by suggesting a change of the mechanism of isomerization from a bimolecular pathway at 548 K toward a more important role of the monomolecular pathway with increase of the temperature. The thermodynamics of the monomolecular pathway become more favorable at higher temperature. The presence of the monomolecular route has also been proposed by Tran *et al.* for nC_4 hydroisomerization over HMOR [29]. However, lower reaction orders with increase of the temperature were also found for formation of pentanes, which can occur only *via* the bimolecular reaction route (see Table 5). Thus, the decrease in the order with temperature is due to the formation of more carbenium ions at the higher temperature.

Similarly, the decrease in the order of reaction in *n*-butane with the presence of Pt is explained by an enhanced formation of carbenium ions *via* butenes formed through dehydrogenation of *n*-butane on Pt. The same phenomenon can also explain the increase in the apparent activation energy [23]. The increase of the coverage with temperature is interesting from the point of view of *single file* diffusion. When the micropores are filled, a product molecule formed deep inside a pore cannot escape to the gas phase. In that case only sites near the pore mouths contribute to the conversion. This concept seems especially useful to explain the reactions over FER. HTON is found to be about 10 times less active than HMOR. Additionally, the TOF for HFER is about a factor of two lower than the one found with HTON. This suggests that HMOR utilizes much more acid sites than HTON which in turn utilizes more acid sites than HFER. In the case of FER, unlike for TON, indications for internal diffusion limitations could not be found. The $E_{act,app}$ is much higher than the one found for HTON and a deviation from linear for the Arrhenius plot was not observed. Therefore, the most plausible explanation to explain the trends found for FER is to suggest that reactions are restricted to the pore mouths. Owing to the high intrinsic cracking activity of HFER, this does not lead to high selectivity to isomerized

products. The incorporation of Pt is in this case beneficial. Hydro-conversion at the outer surface is not diffusion limited and transport of butene and/or isobutene between the Pt clusters located at the exterior and the adjacent pore mouths is fast enough resulting to bifunctional catalysis at the outer surface. The suggestion that TON and especially FER utilize acid sites near the pore entrances is also supported by the presence of 2,2,4-trimethylpentane in the gas phase. The fact that this precursor for isobutane could never be observed in case of MOR may find origin in the fact that this species inside the micropore structure will not be able to escape in the gas phase. However, the formation of this species at the pore mouth acid site allows desorption.

8.5 Conclusions

n-Butane hydro-conversion was studied over (Pt loaded) molecular sieves with TON, FER and MOR morphology. The conversion occurs *via* a complex interplay of mono- and bimolecular bifunctional acid mechanism and monofunctional platinum catalyzed hydrogenolysis. Hydroisomerization was concluded to occur (bifunctional) bimolecularly at low temperatures. This is evident from the reaction order in *n*-butane of 2 for isobutane formation and the presence of 2,2,4-trimethylpentane in the products. Intracrystalline diffusion limitations of the reaction rates seem to be important for TON. Due to diffusion controlled reaction rates for TON, the presence of Pt in TON was detrimental for isomerization selectivity as diffusion of the feed molecules to the acid sites is too slow to prevent Pt from hydrogenolysis of *n*-butane. Reactions on HFER occur predominantly on the outer surface and the pore mouth of the molecular sieve, presumably owing to rapid pore filling following a single-file diffusion mechanism. Due to high intrinsic activity toward (hydro)cracking this does not lead to high selectivity toward isobutane. Addition of Pt (bifunctionality) was in this case beneficial. The reaction at the external surface is not diffusion limited, allowing bifunctional nC_4 -isomerization to occur. Although PtFER was found to approach selectivity levels as found for PtMOR, the latter has a major advantage as the larger accessibility of acid sites leads to a much higher activity.

Acknowledgment

Dr. M.J.G. Janssen (Exxon Chemical) is kindly acknowledged for donating the TON samples.

Dr. G.P. Pirngruber is kindly acknowledged for the critical reviewing of this chapter.

References

1. Tonks, G. V., and Verstappen, A.E.L.M.M., *US Patent* No. 5073667 (1991).
2. Mitsce, R. T., and Pollitzer, E. L., *U.S Patent* No. 3544,451 (1970).
3. Asuquo, R. A., Eder-Mirth, G and Lercher, J. A., *J Catal*, **155**, 376 (1995).
4. Tie, S.T. in Jansen, J.C. Stocker, M. and Weitkamp, J. (Eds), in “*Advanced Zeolite Science and Applications, Studies in Surface Science and Catalysis*”, vol. **85**, 587 (1994).
5. Liu, H., Lei, G.D., and Sachtler, W.M.H., *Appl. Catal. A:General* **137**, 167 (1996).
6. Chao, K., Hung-chung, W., and Leu, L., *J. Catal.* **157**, 289, (1995).
7. Asuquo, R.A., Eder-mirth, G., Pieterse, J.A.Z., Seshan, K., and Lercher, J.A., *J. Catal.* **168**, 292 (1997).
8. Bearez, C., Chevalier, F and Guisnet, M., *React. Kinet. Catal. Lett.* **22**, 405 (1983).
9. Kärger, J., Petzold, M., Pfeifer, H., Ernst, S., and Weitkamp, J., *J. Catal.* **136**, 283 (1992).
10. Martens, J.A., Souverijns, W., Verrelst, W., Parton, R., Froment, G.F., Jacobs, P.A., *Angew. Chem.* **107**, 2726 (1995).
11. Ernst, S., *Angew. Chem. Int. Ed. Engl.* **35**, 63 (1996).
12. Pieterse, J.A.Z., Veefkind-Reyes, S., Seshan, K., and Lercher, J.A., *submitted for publication*.
13. Eder, F., and Lercher, J.A., *J. Phys.Chem. B* **101**,1273 (1997).
14. Van Well, W.J.M., Cottin, X., de Haan, J.W., van Hooff, J.H.C., Nivarthi, G., Lercher, J.A., Smit, B., and van Santen, R.A., *J. Phys. Chem.* **102**, 3945 (1998).
15. Eder, F., Stockenhuber, M., and Lercher, J.A., *Stud. Surf. Sci. Catal.* **97** 495 (1995).
16. Van de Runstraat, A, Kamp, J.A., Stobbelaar, P.J., van Grondelle, J., Krijnen, S., and van Santen, R.A., *J. Catal*, **171**, 77, (1997).
17. Zholobenko, V.L., Makarova, M.A., and Dwyer, J., *J. Phys. Chem.* **97**, 5962 (1993).
18. Maache, M., Janin, A., Lavalley, J.C., and Benazzi, E., *Zeolites* **15**, 507 (1995).

19. Makarova, M.A., Wilson, A.E., van Liemt, B.J., Mesters, C.M.A.M., de Winter, A.W., and Williams, C., *J. Catal.* **172**, 170, (1997).
20. Datka, J., Gil, B., and Kubacka, A., *Zeolites* **17**, 428 (1996).
21. Eder, F., Stockenhuber, M., and Lercher, J.A., in “*Zeolites: A Refined Tool for Designing Catalytic Sites*”, Bonneviot, L., Kaliaguine S. (editors), Elsevier, Amsterdam, 1995, 495.
22. Tran, M.-Trung, Gnep, N.S., Guisnet, M., and Nascimento, O., *Catal. Lett.* **47**, 57 (1997).
23. Van Santen, R., in “*Catalysis; An Integrated Approach to Homogeneous, Heterogeneous and Industrial Catalysis*”, Moulijn, J.A., van Leeuwen, P.W.N.M., Van Santen, R.A., (Editors), Elsevier, Amsterdam, 1993.
24. Belloum, M., Travers. Ch., and Bournonville, J.P.; *Revue de l'Institut Français du Pétrole*, **46**, 89 (1991).
25. Brouwer, D.M., and Hogeveen, H., *Prog. Phys. Org. Chem.* **9**, 192 (1972).
26. Brouwer, D.M., in “*Chemistry and chemical engineering of catalytic processes*”, R. Prins and G.C.A. Schuit, Eds., Vol. 137. Sijthoff & Noordhof, Alphen a/d Rijn, 1980.
27. Guisnet, M., and Gnep, N.S., *Appl. Catal. A:General* **146**, 33, (1996).
28. Carvill, B. T., Lerner, B.A., Adelman, B.J., Tomczak, D.C., and Sachtler, W.M.H., *J. Catal.*, **144**, 1 (1994).
29. Tran, M.-Trung, Gnep, N.S., Szabo, G., and Guisnet, M., *J. Catal.* **174**, 185 (1998).
30. Weisz, P.B., in “*Advances in Catalysis and Related Subjects, Vol. 13*”, D.D. Eley, P.W. Selwood, and P.B. Weisz, Eds., p.157. Academic Press, London, 1963.

Summary/Samenvatting

The use of a catalyst, a material that selectively accelerates a chemical reaction by providing a new reaction path way (without being consumed itself), is of major importance in chemical industry. In a heterogeneously catalyzed reaction, at least one of the reactants must be adsorbed on the solid surface. Due to the interaction of the reactants and the surface of the catalyst, specific bonds in the molecules can be more easily formed or broken. For a monomolecular reaction, the action of the catalyst is to decrease the energy barrier in the rate determining step (i.e. energy of activation) or to increase the transition entropy (i.e. the entropy difference between the ground state prior to the rate determining step and the activated complex). For bimolecular reactions, the higher concentration of the reactants on the surface of the solid in comparison to the gas phase may also enhance the rate of reaction. The consequence of the use of a catalyst is that the chemical reaction can proceed under milder conditions so that less restraints have to be put on the design of reactors and less energy is consumed.

The catalysts used in this thesis are zeolites which are widely employed in industrial catalysts. Their lattice consists of tetrahedrally, to oxygen coordinated Si and Al atoms. The latter introduce a negative charge to the crystalline structure, which is compensated by metal cations or protons. Compensation of this charge by protons generates Brønsted acid sites. Their location and their acid strength, and therefore their impact on catalytic reactions largely depends on the structure of the various zeolites. Because the pore dimensions of the channel structure in zeolites fall in the range of the kinetic radii of many hydrocarbons, these materials were also denoted as *molecular sieves*. The idea of molecular sieving lead to the concept of shape selectivity, which

is one of the striking advantages zeolites offer.

The work presented in this thesis describes the catalytic conversion of light alkanes over a variety of zeolites. Alkanes are the main component of crude oil and form the base of valuable fuel fractions obtained from crude oil. Crude oil refining processes aim at meeting the constantly changing requirements on fuels with respect to environmental legislation. The heterogeneity of industrial catalysts with respect to the variety of components involved, e.g. matrix, catalytically active components and additives, requires to study the reaction of light alkanes over well defined model (zeolite) catalysts.

A measure of the (commercial) value of alkanes for fuel is their Relative Octane Number (RON). At present, the most important processes involved in the production of high octane number gasoline are the alkylation of isobutane with olefins and the etherification of isobutene with methanol to produce methyl tertiary butyl ether (MTBE). In both cases, the starting material is obtained directly from *n*-butane by isomerization and dehydrogenation. A great deal of the research described in this thesis (*chapter 5, 6 and 8*) is therefore devoted to *n*-butane (hydro-) isomerization.

In *chapter 5* the performance of H-Mordenite (MOR) was improved by means of the introduction of a noble metal, platinum. The thus obtained catalyst operates bifunctional: the noble metal part (platinum) hydrogenates coke precursors that otherwise block the Brønsted acid sites and progressively deactivate the catalyst performance with time on stream. Mordenite (MOR) was compared with Ferrierite (FER) and ZSM-22 (TON) for *n*-butane (hydro-) isomerization in *chapter 8*, of which the latter two have proven to be promising in isomerization of *n*-butene to isobutene. MOR was, however, found to be much more active compared to the others due to the much larger concentration of the acid sites being utilized in the reaction. In all cases the actual isomerization step was concluded to occur bimolecular. For TON and FER the majority of the reactions take place at the outer surface and poremouths of the zeolites, a characteristic having familiarity with a relative new concept in the literature of shape selective catalysis at the outer surface of molecular sieves.

From a commercial point of view, the catalysts should be highly active, selective, stable and not cause corrosion problems. Corrosion is the problem with the current technology for *n*-butane isomerization with chlorided platinum alumina as the catalyst. In that respect the use of

Pt-loaded Mordenite (or other large pore zeolites, e.g. BEA) could be an attractive alternative. Moreover, crude oil contains some sulfur containing compounds. These compounds are known to deactivate noble metals and are therefore a serious threat for the bifunctionality of the catalysts. As separation of the various crude oil fractions is expensive and should be avoided the demand for highly sulfur tolerant catalysts can be understood. In *chapter 6* it is shown that catalysts based on Mordenite are very sulfur tolerant. Although the presence of sulfur reduces the activity the catalysts remain selective and stable. The reason for reduced activity was found to be reversible bounded sulfur species that could be removed applying a high temperature oxidative regeneration cycle after which the original activity could be restored.

The other chapters in this thesis aim at the understanding of the underlying processes for catalysts activity and selectivity. In *chapter 3* the primary activation of isobutane in the zeolite pore was studied with hydrogen-deuterium exchange in order to study the underlying reactions for the formation of the electron-deficient carbocations responsible for the catalytic reaction cycle. It was concluded that mainly hydride abstraction from the alkane is responsible for the formation of carbenium ions (in the transition state). Although zeolites inherently comprise Brønsted acidity, Lewis acid sites can be generated by e.g. steam induced breaking of labile bonds that dealuminate the frame work and form coordinatively unsaturated aluminium species out the frame work rendering acidity. These sites were found to be active in hydride abstraction and this may be at the origin of their role in reactions over metal-free zeolites. The Lewis acid sites do not have any other apparent role in the course of the catalytic cycle: stabilization of the carbenium ions as well as the propagation and termination steps occur at Brønsted acid sites.

The role of dealumination for catalytic activity was also dealt with in *chapter 4*. A series of dealuminated Mordenite catalysts was extensively characterized and their activity and selectivity was studied in *n*-hexane hydroisomerization and *n*-butane monomolecular cracking. It was concluded that dealumination, although reduces the concentration of Brønsted acid sites, eases the accessibility of the remaining acid sites. Importantly, it increases the accessibility of the Brønsted acid sites of higher acid site strength located in the side pockets. This results in a higher catalytic activity in alkane conversion reactions.

Chapter 7 deals with FER and TON medium size pore zeolites respective the accessibility of their acid sites to probe molecules of various size and the sorption characteristics of bulky

branched alkanes which are possible intermediates in alkane isomerization reactions. It was found that dibranched alkanes sorb only at the pore mouth of FER and TON. This makes these isomers unlikely to be formed inside the pores of the molecular sieve or their formation provide explanation for the often reported diffusion determined activity and selectivity in hydrocarbon isomerization. In particular, it explains the low activity of TON and FER in the bimolecular (hydro-) isomerization of *n*-butane as discussed in *chapter 8*. The accessibility of the Brønsted acid sites is less for 2,2-dimethylbutane than for 2,2-dimethylpentane and 2,2-dimethylhexane. This suggests that the Brønsted acid sites playing a role in alkane skeletal isomerization are located in the pore mouth rather than on the outer surface of TON and FER. The adsorption structure of dibranched alkanes in the pore mouth is dependent on the size of the largest linear part of the alkane and the coverage.

Samenvatting

Het gebruik van een katalysator, een materiaal dat selectief een bepaalde reactie versneld zonder daarbij zelf geconsumeerd bij te worden, heeft een belangrijke rol in de chemische industrie. In een heterogeen gekatalyseerde reactie is tenminste een van de reactanten geadsorbeerd aan de vast stof. De reactanten kunnen reageren met het oppervlakte van de katalysator waardoor specifieke bindingen makkelijker worden gevormd of gebroken. Voor een monomoleculaire reactie betekent het gebruik van een katalysator dat de energie barriere verlaagd wordt in de snelheids bepalende stap (de aktiverings energie) danwel het verhogen van de overgangs entropie (het verschil tussen de grond toestand voorafgaande aan de snelheids bepalende stap en het geactiveerde complex). Voor een bimoleculaire reaktie kan de hogere concentratie van reactanten op het oppervlak ten opzichte van de gas fase de reaktie snelheid ook verhogen. De consequentie van het gebruik van een katalysator is dat de chemische reactie onder mildere condities plaats kan vinden zodat minder eissen aan het ontwerp van reactoren hoeven gesteld te worden en minder energie wordt verbruikt.

De katalysatoren gebruikt in dit proefschrift zijn zeolieten die veelvuldig gebruikt worden in industriële katalysatoren. Zeolieten zijn opgebouwd uit tetrahedrale, aan zuurstof gecoördineerde silicium en aliminium atomen. De laatsten introduceren een negatieve lading in de kristallijne structuur die gecompenseerd wordt door metal kationen of protonen. De compensering van de negatieve ladings overschot door protonen genereert Brønsted zure plaatsen. De lokatie en de zuursterkte van deze Brønsted zure plaatsen en daardoor hun direkte invloed op katalytische reakties hangt samen met de specifieke structuur van verschillende zeolieten. Ten gevolge van het feit dat de porië dimensies van de kanalen samen vallen met de diameter van vele koolwaterstoffen worden zeolieten ook wel moleculaire zeven genoemd. Het idee van moleculair zeven resulteerde in het concept van vorm selectiviteit welke een van de meest typerende voordelen is die het gebruik van zeolieten opleverd.

Het werk dat in dit proefschrift is beschreven is the katalytische conversie van lichte alkanen over diverse zeolieten. Alkanen zijn de hoofd componenten van ruwe olie en staan aan de basis van de waardevolle brandstof frakties verkregen uit ruwe olie. De raffinage processen

van ruwe olie zijn erop gebaseerd voortdurend aan de steeds scherpere milieu-eisen van brandstoffen te voldoen. De heterogeniteit van industriële katalysatoren met betrekking tot de diversiteit van de componenten aanwezig zoals de matrix, katalytisch actief component en additieven noodzaakt de bestudering van reacties van lichte alkanen over goed gedefinieerde model (zeoliet) katalysatoren.

Een maat voor de (commerciële) waarde van alkanen in brandstof is hun relatieve oktaan getal (RON). De meest gebruikte processen voor de productie van brandstoffen met een hoog octaan getal zijn de alkylering van isobutaan met olefinen en de etherificatie van isobuteen met methanol voor productie van methyl tertiary butyl ether (MTBE). In beide gevallen wordt het start materiaal direct verkregen uit *n*-butane middels isomerisatie en dehydrogenering. Een groot gedeelte van het onderzoek beschreven in dit proefschrift (*hoofdstuk 5, 6 and 8*) is daarom gericht op *n*-butane (hydro-)isomerisatie.

In *hoofdstuk 5* is onderzoek beschreven die er op gericht was de prestatie van H-Mordenite (MOR) te verbeteren door de introductie van een edel metaal, platina. De op deze manier verkregen katalysator opereerde bifunctioneel: het edel metaal hydrogeneerde coke (katalysator vergif) intermediëren welke zonder Pt de toegankelijk van Brønsted zure plaatsen blokkeerden, resulterende in een afname van de activiteit met verloop van de tijd. (Pt-)Mordenite (MOR) was ook vergeleken met (Pt-)Ferrierite (FER) en (Pt-)ZSM-22 (TON) zeolieten in *hoofdstuk 8*, van welke de laatste twee zeolieten bewezen veelbelovende katalysatoren voor de isomerisatie van *n*-butene naar isobutene te zijn. MOR bleek echter veel actiever te zijn dan FER en TON daar in MOR een veel groter deel van de zure plaatsen beschikbaar zijn voor de reactie. De eigenlijke isomerisatie reactie bleek voornamelijk bimoleculair te zijn voor alle drie zeolieten. In het geval van FER en TON vinden alle reacties plaats aan de uiteinden van de poriën, iets dat veel overeenstemming heeft met een relatief nieuw concept in de literatuur van vorm selectiviteit op het buiten oppervlak van moleculaire zeven.

In commercieel opzicht moeten katalysatoren actief, selectief en stabiel zijn maar ook zeker geen corrosie problemen geven. Corrosie is het probleem met de huidige technologie voor *n*-butaan isomerisatie met gechlorideerd platinum op alumina als katalysator. In dit opzicht is het gebruik van Pt-Mordeniet (of andere grote poriën zeolieten zoals BEA) een aantrekkelijk alternatief.

Ruwe olie bevat ook zwavel houdende verbindingen. Deze zijn bekend dat ze de edel metalen deaktiveren en zijn daarom een serieuze bedreiging voor de bifunktionaliteit van de katalysatoren. Gezien het feit dat het scheiden van de zwavel houdende frakties een dure optie is, is het belang om katalysatoren te ontwikkelen met een hoge mate van zwavel tolerantie begrijpelijk. In *hoofdstuk 6* is laten zien dat de bifunktionele katalysatoren gebaseerd op MOR heel zwavel tolerant zijn. Hoewel de aanwezigheid van zwavel de activiteit van de katalysatoren reduceerde bleven de katalysatoren verder stabiel met verloop van de tijd en ook de selektiviteit kon worden behouden. De reden voor de lagere activiteit is geconcludeerd samen te hangen met de aanwezigheid van omkeerbare zwavel vergiftiging van het edel metaal. Deze zwavel fragmenten konden verwijderd worden door het toe passen van een oxidatieve regeneratie procedure waardoor de originele activiteit hersteld wordt.

De rest van de hoofdstukken beschreven in dit proefschrift hebben als doelstelling het begrip van de onderliggende chemische reacties van alkanen in zeolieten die bepalend zijn voor de katalytische activiteit en selektiviteit te verbeteren. In *hoofdstuk 3* wordt de chemische activering van isobutaan in de zeoliet porië bestudeerd met waterstof-deuterium uitwisseling met als doelstelling de achtergrond voor de vorming van de elektron arme carbokationen verantwoordelijk voor de katalytische reacties te doorgronden. Het was geconcludeerd dat voornamelijk de abstraktie van een waterstof hydride verantwoordelijk is voor de vorming van carbenium ionen (in de overgangs toestand). Hoewel zeolieten in de waterstof vorm Brønsted zuur zijn kunnen ook Lewis zure plaatsen worden gevormd door bijvoorbeeld een voorbehandeling met stoom bij hogere temperaturen. De stoom behandeling dealumineert het zeoliet maar laat de geëxtraheerde aluminium achter op posities buiten het rooster die Lewis zure plaatsen kunnen vormen. Deze Lewis zure plaatsen waren aantoonbaar actief in de hydride abstraktie van isobutaan en zijn daarom belangrijk voor de vorming van carbenium ionen in metaal vrije zeolieten. Lewis zure plaatsen hebben verder geen aantoonbare rol in het verloop van de katalytische reactie cycli: de stabilisatie van carbenium ionen vindt plaats op Brønsted zure plaatsen alsmede de propagatie en terminatie stappen.

De invloed van zeoliet dealuminatie is ook behandeld in *hoofdstuk 4*. Een serie gedealumineerde MOR katalysatoren waren zorgvuldig gekarakteriseerd en hun activiteit was bestudeerd in *n*-hexaan (hydro-)isomerizatie en *n*-butane monomoleculair kraken. Het was

geconcludeerd dat dealuminering, hoewel het de concentratie van Brønsted zure plaatsen verminderd, de bereikbaarheid van de overgebleven Brønsted zure plaatsen vereenvoudigd. Het verhoogd voornamelijk de bereikbaarheid van de Brønsted zure plaatsen in de zij-holten welke een hogere zuur sterkte hebben. Dit leidt tot een hogere activiteit voor alkaan conversie reacties.

Hoofdstuk 7 gaat over de bereikbaarheid van zure plaatsen in FER and TON zeolieten voor moleculen van verschillende omvang en de adsorptie karakteristieken van omvangrijke dubbel vertakte alkanen, potentiële intermediären in alkaan isomerizatie reacties. De belangrijkste vondst was dat dubbel vertakte alkanen alleen aan de porië mond van FER en TON adsorberen. Daardoor kunnen deze alkanen niet worden gevormd in de poriën van FER en TON ofwel hun vorming zou een mogelijke verklaring kunnen zijn voor produkt diffusie bepaalde selectiviteit zoals wel wordt beweerd voor *n*-buteen isomerizatie. Het geeft ook een verklaring waarom TON en FER zoveel minder actief zijn voor de (hydro-)isomerizatie van *n*-butaan als is besproken in *hoofdstuk 8*. De bereikbaarheid van de Brønsted zure plaatsen is slechter voor 2,2,-dimethylbutaan dan voor 2,2,-dimethylpentaan en 2,2,-dimethylhexaan. Dit suggereerd dat de Brønsted zure plaatsen die een rol spelen in skelet isomerizatie van alkanen zich voornamelijk in de porië mond bevinden en niet volledig op het buiten oppervlak van de zeolieten. De adsorptie structuur van dubbel vertakte alkanen in de porië mond is afhankelijk van de lengte van het lineaire gedeelte van het alkaan en van de bedekking.

Curriculum Vitae

Johannis A. Z. (Jean-Pierre) Pieterse werd geboren op 7 februari 1970 te Oude Tonge (Oostflakkee). Na het afsluiten van de MAVO te Oude Tonge in 1986 vervolgde hij zijn studie met drie jaar MLO aan de Laboratorium school Zeeland te Goes en stapte vervolgens over naar de HLO, Hogeschool Rotterdam en omstreken, om zo in 1993, met een afstudeer periode bij Unilever Research Laboratorium in Vlaardingen, het HLO diploma te behalen. Aansluitend studeerde hij Scheikunde aan de Rijks Universiteit Leiden. Een verkiezing tot RUL vertegenwoordiger stelde hem in staat 4 maanden onderzoek te verrichten aan Grinnell college, Iowa, Verenigde Staten, aan fotoluminescentie eigenschappen van chemische sensoren. In 1995 studeerde hij af bij de vakgroep Heterogene Katalyse en Oppervlakte Chemie onder leiding van prof.dr. V. Ponc op een onderzoek naar de selectieve reductie van azijnzuur naar aceetaldehyde. Vervolgens begon hij in december 1995 een promotieonderzoek bij de vakgroep Katalytische Processen en Materialen binnen de faculteit Chemische Technologie van de Universiteit Twente onder leiding van prof.dr. J.A. Lercher. De resultaten van dit onderzoek aan activering van alkanen over zeolieten bij lage temperaturen staan beschreven in dit proefschrift.

Publications

- **The formation of ketones and aldehydes from carboxylic acids, structure-activity relationship for two competitive reactions*, R. Pestman, A. van Duijne, J.A.Z. Pieterse, and V. Ponec, *J. Mol. Cat.* 103(3), 175 (1996).
- **Reactions of carboxylic acids on oxides. 1. Selective hydrogenation of acetic acid to acetaldehyde*, R. Pestman, R.M. Koster, J.A.Z. Pieterse, and V. Ponec, *J. Catal.* 168, 255 (1997).
- **Reactions of carboxylic acids on oxides. 2. Bimolecular reaction of aliphatic acids to ketones*, R. Pestman, R.M. Koster, A. van Duijne, J.A.Z. Pieterse, and V. Ponec, *J. Catal.* 168, 265 (1997).
- **Selective hydrogenation of aliphatic acids to aldehydes*, R. Pestman, R.M. Koster, J.A.Z. Pieterse, and V. Ponec, *Proc. 14th NAM, Snowbird*, 1995.
- *Improving H-Mordenite for the isomerization of n-butane*, R.A. Asuquo, K. Seshan, J.A.Z. Pieterse, and J.A. Lercher, *J. Catal.* 168, 292 (1997).
- *On the accessibility of the acid sites of FER for pyridine*, J.A.Z. Pieterse, K. Seshan, S. Veefkind-Reyes, L. Domokos, and J.A. Lercher, *J. Catal.* 187, 518 (1999).
- *Mechanistic routes of low temperature alkane activation over zeolites*, J.A.Z. Pieterse, K. Seshan, and J.A. Lercher, *Stud. Surf. Sci. Catal.* in press.
- *Sorption and ordering of dibranched alkanes on TON and FER*, J.A.Z. Pieterse, K. Seshan, S. Veefkind-Reyes, and J.A. Lercher, *submitted to J. Phys. Chem.*
- *Brønsted and Lewis acid initiated H/D exchange over zeolites MFI and BEA*, J.A.Z. Pieterse, K. Seshan, and J.A. Lercher, *submitted to J. Phys. Chem.*
- *Structure-activity relations for the hydroisomerization of n-butane over TON, FER and MOR zeolites*, J.A.Z. Pieterse, K. Seshan, and J.A. Lercher, *submitted to J. Catal.*
- *On the role of adsorption effects for the enhanced activity of dealuminated Mordenite catalysts for the conversion of light alkanes*, J.A.Z. Pieterse, J.A. van Bokhoven, M. Tromp, D.C. Koningsberger, K. Seshan, and J.A. Lercher, *in preparation*.
- *Sulfur tolerant catalysts based on Mordenite for the isomerization of n-butane*, J.A.Z. Pieterse, K. Seshan, and J.A. Lercher, *in preparation*.

* not included in this thesis